ON RESILIENT CONTROL FOR SECURE CONNECTED VEHICLES: A HYBRID SYSTEMS APPROACH

A Dissertation
Presented to
the Graduate School of
Clemson University

In Partial Fulfillment
of the Requirements for the Degree
Doctor of Philosophy
Automotive Engineering

---

by
Roberto Merco
December 2019

Accepted by:
Dr. Pierluigi Pisu, Committee Chair
Dr. Richard Brooks
Dr. Francesco Ferrante
Dr. Yunyi Jia
Dr. James Martin

This page is intentionally left blank.

Abstract

According to the “Internet of Things Forecast” conducted by Ericsson, connected devices will be around 29 billion by 2022. This technological revolution enables the concept of Cyber-Physical Systems (CPSs) that will transform many applications, including power-grid, transportation, smart buildings, and manufacturing. Manufacturers and institutions are relying on technologies related to CPSs to improve the efficiency and performances of their products and services. However, the higher the number of connected devices, the higher the exposure to cybersecurity threats. In the case of CPSs, successful cyber-attacks can potentially hamper the economy and endanger human lives. Therefore, it is of paramount importance to develop and adopt resilient technologies that can complement the existing security tools to make CPSs more resilient to cyber-attacks.

By exploiting the intrinsically present physical characteristics of CPSs, this dissertation employs dynamical and control systems theory to improve the CPS resiliency to cyber-attacks. In particular, we consider CPSs as Networked Control Systems (NCSs), which are control systems where plant and controller share sensing and actuating information through networks. This dissertation proposes novel design procedures that maximize the resiliency of NCSs to network imperfections (i.e., sampling, packet dropping, and network delays) and denial of service (DoS) attacks.

We model CPSs from a general point of view to generate design procedures that have a vast spectrum of applicability while creating computationally affordable algorithms capable of real-time performances. Indeed, the findings of this research aspire to be easily applied to several CPSs applications, e.g., power grid, transportation systems, and remote

surgery. However, this dissertation focuses on applying its theoretical outcomes to connected and automated vehicle (CAV) systems where vehicles are capable of sharing information via a wireless communication network.

In the first part of the dissertation, we propose a set of LMI-based constructive Lyapunov-based tools for the analysis of the resiliency of NCSs, and we propose a design approach that maximizes the resiliency.

In the second part of the thesis, we deal with the design of DOS-resilient control systems for connected vehicle applications. In particular, we focus on the Cooperative Adaptive Cruise Control (CACC), which is one of the most popular and promising applications involving CAVs.

Dedication

To my partner, Andrea, my brother, Daniele, and my parents, Lia e Giuseppe.

This page is intentionally left blank.

Acknowledgments

My greatest gratitude goes to Dr. Pisu. He believed in me since the first interview, and he gave me the great opportunity to pursue a PhD in the USA. With his guidance, patience, wisdom, and assistance, Dr. Pisu supported me in the way I needed it. Under his supervision, I could achieve the best quality of work in both courses and research during my PhD studies.

I want to express my special gratitude to my mentor and friend, Dr. Ferrante. He made himself available to a long-distance collaboration. He shared with me his skills and love for research that made the path of learning hybrid dynamical systems easier than I expected. Despite the considerable difference in timezone, I always felt his support and his effort in teaching and advising me. He also made me appreciate the beauty of methodological research.

I want to thank Dr. Brooks, Dr. Jia, and Dr. Martin for being in my committee and giving me precious feedback to improve my research work.

Special acknowledgments are for the people who enriched these years as a PhD student with love and friendship: Andrea, Jasprit, Ashley, Kelly, Marco, Drew, Adhiti, Hazim, Bhavya, Sidharth, Tommy, Liz, John, Roghieh, Zoleikha, Rakan, and Nancy. They became my family away from home.

My final acknowledgments are for the Office of the Vice President for Research and the Graduate School of Clemson University for providing me financial support to improve the quality of this thesis through the Dissertation Completion Grant.

The material presented in this dissertation is based upon work supported by the

National Science Foundation (NSF) under grant No. CNS-1544910. Any opinions, findings, and conclusions or recommendations expressed in this material are those of the authors and do not necessarily reflect the views of the National Science Foundation.

Curriculum Vitae of the Author

Education

- from August 2016 to December 2019, Ph.D. in Automotive Engineering at Clemson University, USA. GPA: 4.0/4.0.
- from September 2007 to October 2010, Master of Science in Control Engineering at the University of Rome “Tor Vergata”. 110/110 Summa Cum Laude.
- from September 2004 to August 2007, Bachelor of Science in Control Engineering at the University of Rome “Tor Vergata”. 110/110 Summa Cum Laude.

Post-Graduate Education and Summer Schools

- July 2017. Summer school: “A Systems and Control Perspective on Privacy, Safety, and Security in large-scale Cyber-Physical Systems”. Organizer: Research school DISC, TU Delft.
- June 2017. Summer school: “oCPS PhD School on Cyber-Physical Systems“. Organizers: IMT Institute for Advanced Studies Lucca, Technische Universiteit Eindhoven, TU München.
- November 2012. Project Manager Certification: ISIPM-Base. From Italian Institution of Project Management.

Honors

- July 2019. Dissertation Completion Grant Award from Clemson University.
- September 2018. Best Presentation award at the Doctorate Symposium of Prognostics and Health Management (PHM).
- September 2018. Accepted at the Doctorate Symposium of Prognostics and Health Management (PHM).
- August 2017. Accepted at the SAE Battle Cyber Auto Challenge.
- February 2011. "Sebastiano e Rita Raeli" outstanding student award, from the University of Rome "Tor Vergata".

List of Publications

Journal Articles

1. R. Merco, F. Ferrante, P. Pisu, "A Hybrid Controller for DoS-Resilient String-Stable Vehicle Platoons", IEEE Transactions on Intelligent Transportation Systems, under review.
2. R. Merco, F. Ferrante, P. Pisu, "On DoS Resiliency Analysis of Networked Control Systems: Trade-off between Jamming Actions and Network Delays", IEEE Control Systems Letters, vol. 3, no. 3, pp. 559–564, July 2019.

Peer-reviewed Conference Articles

1. R. Merco, F. Ferrante, R. Sanfelice, P. Pisu, "LMI-Based Output Feedback Control Design in the Presence of Sporadic Measurements", submitted to American Control Conference (ACC), 2020.
2. R. Merco, F. Ferrante, P. Pisu, "DoS-Resilient Hybrid Controller for String-Stable Connected Vehicles", IEEE Intelligent Vehicles Symposium (IV), pp. 1639-1644, 2019.

3. R. Merco, F. Ferrante, P. Pisu, "Network Aware Control Design for String Stabilization in Vehicle Platoons: An LMI Approach", IEEE American Control Conference (ACC), pp. 539-544, 2019.

4. V. Rastogi, R. Merco, M. Kaur, A. Rayamajhi, M. Gavelli, G. Papa, P. Pisu, S. Babu, A. Robb, J. Martin, "An Immersive Vehicle-in-the-Loop VR Platform for Evaluating Human-to-Autonomous Vehicle Interactions", SAE Technical Paper, No. 2019-01-0143, 2019.

5. R. Merco, Z. Biron, P. Pisu, "Replay Attack Detection in a Platoon of Connected Vehicles with Cooperative Adaptive Cruise Control", IEEE American Control Conference (ACC18), pp. 5582-5587, 2018.

6. A. Rayamajhi, Z. Biron, R. Merco, P. Pisu, J. M. Westall, J. Martin, "The Impact of Dedicated Short Range Communication on Cooperative Adaptive Cruise Control", IEEE International Conference on Communications, pp. 1-7, 2018.

White papers

1. R. Merco, "Nuclear Physics Experimentation Supervision", Automazione Oggi - n. 382 June 2015 (English version available at `http://www.movicon.info/articoli/INFN_AutomateENG.pdf`).

2. R. Merco, "Cleanroom controlled using Movicon", Automazione Oggi - n. 378 January/February 2015 (English version available at `http://www.movicon.info/articoli/Simav_Camere_bianche_Eng.pdf`).

Invited Talks

- June 2019. "DoS-Resilient Control Design for Vehicle Platooning: A Hybrid Systems Approach", University of Grenoble Alpes, GIPSA-lab, Grenoble, France.

- May 2016. "Introduction to Industrial Automation Techniques", Engineering Association of Ascoli Piceno, Ascoli Piceno, Italy.

Academic Experience

- from August 2016 to December 2019, Controls Research Engineer at Clemson University International Center for Automotive Research, USA.
- from April 2010 to September 2010, Visiting Scholar at Institute for Design and Control of Mechatronical Systems, Linz, Austria.

Teaching Experience

- Fall 2019. Teaching assistant for the graduate course "Vehicle Diagnostics", Automotive Engineering Department, Clemson University.
- From August 2018 to August 2019. Teaching assistant for the graduate course "Automotive system integration (Deep Orange 10)", Automotive Engineering Department, Clemson University.
- March 2015. Invited lecturer for the professional short course, "Introduction to PLC and SCADA systems", Istituto Nazionale di Fisica Nucleare (INFN), Frascati, Italy.

Service to the Community

- Reviewer for the journal IEEE Transactions on Intelligent Transportation Systems.
- Reviewer for the 58th Conference on Decision and Control (CDC).
- Reviewer for the 2019 European Control Conference (ECC).
- Reviewer for the 2019 American Control Conference (ACC).

Industrial Experience

- from September 2013 to June 2016, Technical Leader at Automate s.r.l., Italy.
- from November 2010 to September 2013, Automation Engineer at Automate s.r.l., Italy.

Professional Memberships

- Student member, Institute of Electrical and Electronics Engineers (IEEE).
- Student member, IEEE Control Systems Society.

Language

- English, full professional proficiency.
- Italian, native proficiency.

This page is intentionally left blank.

Table of Contents

This page is intentionally left blank.

List of Figures

This page is intentionally left blank.

Chapter 1

General Introduction

The number of connected devices is growing with a rate that increases year after year. Accordingly to [1], the number of connected devices is expected to reach a value of around 29 billion by 2022. The interconnection between devices leads to an increase in the efficiency of complex systems and to enable a carbon dioxide reduction of 15% without employing significant changes in the architectures [110]. Besides the environmental benefits, easy installation, flexibility, and reduced maintenance characterize connected devices [44]. In particular, the most significant advantage in connected devices is due to the enabling of wireless communication that allows overcoming the physical limitation of wired connections.

The systems that will be beneficial for this technological transformation are, to cite a few, power grid, transportation systems, building, and industry [110]. In particular, some of these connected applications (e.g., Intelligent Transportation Systems (ITS) and remote surgery) not only enable data exchange but also allows to remotely control connected actuators to modify the physical environment. These kinds of systems are known as Cyber-Physical Systems (CPS).

As shown in Fig. 1.1, CPSs contain three parts: the physical system, where the physical system along with actuators and sensors are; the cyberspace, where the decision-making algorithm resides; the network, which connects the two spaces. The complexity of CPSs enables novelties in the field of control theory, which aims at exploiting the shared

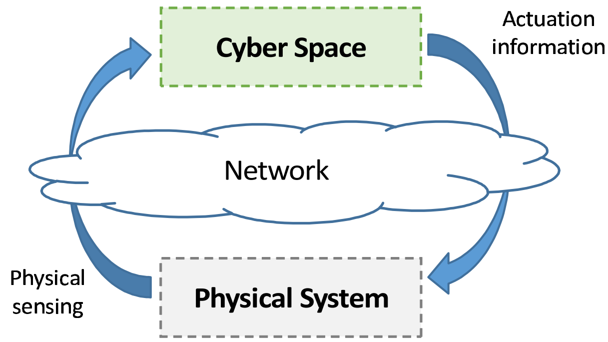

Figure 1.1: Schematic representation of a cyber physical system.

network to develop new control applications with a significant impact on the society [52, 72]. However, there is a strong need for analysis and synthesis of control systems employing shared networks and wireless communication channels. This kind of control systems is often referred to as Networked Control Systems (NCSs), which, in the last decade, have been attracting a significant amount of interest as witnessed by recent surveys [44, 112, 117, 120].

1.1 Challenges for Control System Design

The introduction of the network in control systems leads to network-induced imperfections that can compromise the performance and stability of the networked control system. These network imperfections are inevitable, and can be divided into the following categories [43]:

i) **Sampled data:** Due to the digital nature of the communication channel, the network is packet-based, and signals can be sent only at discrete instants in time.

ii) **Packet losses:** Excessive usage of the communication channel leads to packet collisions and, therefore, packet losses. In the case of wireless communication, packet losses are also due to corrupted data provoked by physical imperfections of the communication channel.

iii) **Variable transmission delay:** Computation and communication resources are limited and shared. Therefore, information can not be sent through the communication channel and instantaneously be received. Furthermore, uncertainties on the communication channel make transmission delays variable over time.

In addition to these network-induced imperfections, another significant concern for CPSs is cyber-security. The use of communication networks exposes networked control systems to malicious deception and denial-of-service (DoS) attacks. Deception attacks aim at manipulating the information of the transmitted packets by injecting false data [84]. In contrast, DoS attacks aim at interfering with the communication channel to generate periods in which the communication is compromised, and no information is exchanged [113]. It is worth noticing that the DoS attacks can be a source of packet losses, which can also occur as natural phenomena of the network channel.

Network-induced imperfections and cyber-attacks are critical phenomena that affect the performance and the stability of networked control systems. Therefore, they need to be taken into account during the design of the controller. However, the nature of CPSs is complicated to be modeled. Indeed, continuous dynamics of the physical system and the discrete behavior of the communication channel and controller (cyberspace) coexist in CPSs. This class of systems can be classified as impulsive dynamical systems, which are, in general, difficult to analyze from the closed-loop stability and performance point of view. In this dissertation, this combination of continuous and discrete behaviors is modeled as hybrid dynamical systems by following the framework in [37].

While designing a networked control system, it is essential to consider that also its architecture influences and affects the quality and reliability of the network. In particular, the way that the transmission intervals are scheduled can significantly influence the number of packet losses, the size of network transmission delays, and the resiliency and performance of the networked control system. Therefore, a strong correlation between cyberspace and physical system emerges, which suggests that the design of NCSs characterized by resiliency and performance needs an integrated approach involving the control, and the information and communication technology communities.

1.2 Opportunities for Intelligent Transportation Systems

The demand for mobility is growing year after year. At the same time, the traffic infrastructure needs to be modified to cope with traffic growth while decreasing its cost and improving efficiency and safety. Dealing with all these aspects is not simple and requires the development of new solutions. Connected and Automated Vehicles (CAVs) are expected to improve traffic throughput, safety, and fuel economy by employing Dedicated Short Range Communication (DSRC) [2, 42, 62, 105]. For such a reason, inter-vehicular low-latency communications standards have been created in the United States (Wireless Access in Vehicular Environment) [58] and in Europe (ITS-G5) [31]. These new standards enhanced the concepts of Vehicle to Vehicle (V2V) and Vehicle to Infrastructure (V2I) communications.

Probably the most famous application involving connected vehicles is the Cooperative Adaptive Cruise Control (CACC). The CACC allows the involved cars to follow the preceding vehicle by keeping the desired relative distance by exploiting the wireless communication and the onboard sensors, e.g., radar, lidar, and cameras. By keeping a short inter-vehicle distance, the string of vehicles controlled by CACC forms a platoon that leads to an increased traffic throughput. The reduced distance between vehicles and attenuation of disturbance and shock waves throughout the string of cars are some of the enhancements of the CACC compared to Adaptive Cruise Control (ACC). Moreover, significant fuel savings are possible due to the reduction in aerodynamic drag, mainly when the CACC is applied to heavy-duty vehicles.

Despite the benefits, exchanging data among vehicles exposes them to network imperfections and network vulnerabilities, such as cyber-attacks. Hence, one of the main challenges in connected vehicle applications is the design of control systems that can deal with an unreliable and a compromised network while guaranteeing stability, safety, and reliability of the vehicles during their collaborative tasks. If the control systems are not reliable to network imperfections and network vulnerabilities, cyber-attacks might cause loss of performance, collisions, and hence, loss of lives.

1.3 Intellectual Merit

This dissertation focuses on improving the resiliency of CPSs. Sampled data, packet losses, and variable network delays are taken into account as network imperfections that are naturally in networked control systems and that are influenced and accentuated by the presence of cyber-attacks.

In particular, the contributions of this thesis are as follows:

- New methodologies for the analysis of the stability of NCSs are introduced. We identify a metric to evaluate the resiliency of the NCS to network imperfections and propose a Lyapunov-based approach to estimate such a metric.

- We propose a procedure based on linear matrix inequalities for the design of linear dynamic output-feedback controllers capable of maximizing the resiliency of the NCS to packet dropouts.

- The vehicle platooning application is considered as a case study employed to validate our theoretical contributions. In particular, we propose new design approaches capable of making Cooperative Adaptive Cruise Controls more resilient to packet dropouts, variable network delays, and Denial-of-Service attacks.

This dissertation aspires to provide valuable contributions to the field of control theory. The theoretical results and outcomes aim at being control algorithms with a complexity that is suitable for real-time applications. To this end, the developed control algorithms are evaluated on vehicle platooning application. Therefore, the outcomes of this dissertation further contribute to advance intelligent transportation systems with new control algorithms for improved resiliency for CAV.

1.4 Broader Impacts

This dissertation is expected to impact the security and reliability of CPSs by helping accelerate the adoption of resilient controllers. Given the general-purpose nature of the control theory, the contributions developed in this research will have a vast spectrum of applications. Indeed, these results are not specific to a particular application and can be easily applied and extended to many CPSs, especially those with limited computational and communication capabilities. This makes our research highly modular and transferable to many different systems. In particular, the specific application to connected and automated vehicles should lead to future market acceptance of these vehicle technologies with a potential improvement in traffic conditions, vehicle and personal safety, and energy consumption.

1.5 Dissertation Organization

The next chapter introduces some preliminaries on hybrid dynamical systems in the framework [37], which is employed to model NCS in this dissertation. The rest of the thesis is divided into two parts, which are introduced as follows.

The first part of the dissertation tackles the problem of resilient NCS from a general perspective. It provides tools for the stability analysis capable of estimating a metric employed to evaluate the resiliency of NCS with respect to network imperfections. Moreover, the first part describes a novel approach to design output-feedback controllers capable of maximizing the resiliency to variable transmission intervals. In particular, the first part of the dissertation is organized as follows:

- Chapter 3 introduces the modeling framework for one-channel output feedback NCSs considered in this dissertation.
- Chapter 4 deals with the problem of estimating maximum allowable transmission interval (MATI) and maximum allowable delay (MAD). Some of the results presented in this chapter can be found in [68].
- Chapter 5 proposes the tools for designing NCSs resilient to variable transmission intervals.

The second part of this thesis is related to a resilient controller design for vehicle platooning. In particular, we propose tuning approaches to increase resiliency to network imperfection of the CACC controller. Moreover, the second part of the dissertation deals with the problem of designing CACC controllers resilient to DoS attacks. This part of the dissertation is organized as follows:

- Chapter 6 introduces the design of network-resilient CACC. Some of the results presented in this chapter can be found in [67].
- Chapter 7 describes the design approach for DoS-resilient CACC. Some of the results presented in this chapter are published in [66].

This page is intentionally left blank.

Chapter 2

Notation and Preliminaries on Hybrid Dynamical Systems

2.1 Notation

In the remainder of the dissertation, the following notation is employed. The set $\mathfrak{N}_{>0}$ is the set of the strictly positive integers, $\mathfrak{N} = \mathfrak{N}_{>0} \cup \{0\}$, $\mathfrak{R}$ is the set of real numbers, $\mathfrak{R}_{\geq 0}$ ($\mathfrak{R}_{>0}$) ($\mathfrak{R}_{<0}$) is the set of nonnegative (positive) (negative) real numbers, $\mathbb{C}$ is the set of complex numbers. Given $z \in \mathbb{C}$, $\mathfrak{Re}(z)$ and $\mathfrak{Im}(z)$ denote, respectively, the real and the imaginary part of z. For any given real polynomial ρ, $\Lambda_{\max}(\rho) = \max_{s\colon \rho(s)=0} \mathfrak{Re}(s)$ and $\mathfrak{Im}(\rho) = \{\omega \in \mathfrak{R}\colon \exists \alpha \in \mathfrak{R} \text{ s.t. } \rho(\alpha + j\omega) = 0\}$ (the set of the imaginary parts of the roots of ρ). With a slight abuse of notation, given a real polynomial $\rho(s) = s^2 + as + b$, with $a, b \in \mathfrak{R}_{>0}$, we denote the damping ratio of the roots of ρ as $\zeta(\rho) = \frac{a}{2\sqrt{b}}$. The symbol $\mathfrak{R}^n$ represents the Euclidean space of dimension n, $\mathfrak{R}^{n\times m}$ is the set of $n \times m$ real matrices. Give any $A \in \mathfrak{R}^{n\times m}$, $A^\top$ denotes the transpose of A, $A^{-\top} = (A^\top)^{-1}$ (when A is nonsingular), $\mathrm{He}(A) = A + A^\top$, $\mathrm{spec}(A)$ denotes the spectrum of A, $\Lambda_{\max}(A) := \max \mathfrak{Re}(\mathrm{spec}(A))$, and $\zeta_{\min}(A) := \min \zeta(\mathrm{spec}(A))$. The identity matrix is denoted by $\mathbf{I}$. For a symmetric matrix A, $A \succ 0$ and $A \succeq 0$ ($A \prec 0$ and $A \preceq 0$) means that A ($-A$) is, respectively, positive definite and positive semidefinite. The symbol $\mathcal{S}_+^n$ represents the set of $n \times n$ symmetric positive definite matrices, $\lambda_{\min}$ and $\lambda_{\max}$ denote respectively the smallest and the largest eigenvalue of the symmetric matrix A. In partitioned symmetric matrices, the symbol $\bullet$ represent a symmetric block. For a vector $x \in \mathfrak{R}^n$, $|x|$ denotes the Euclidean norm. Given two vectors x and y, we denote $(x, y) = [x^\top, y^\top]^\top$. Given a vector $x \in \mathfrak{R}^n$ and a closed set $\mathcal{A}$, the distance of x to $\mathcal{A}$ is defined as $|x|_\mathcal{A} = \inf_{y \in \mathcal{A}} |x - y|$. For any function $z : \mathfrak{R} \to \mathfrak{R}^n$, we denote $z(t^+) := \lim_{s \to t^+} z(s)$ when it exists. By $\vee$ and $\wedge$ we denote, respectively, the logical "or" and "and". A function $\alpha \colon \mathfrak{R}_{\geq 0} \to \mathfrak{R}_{\geq 0}$ is said to be of class $\mathcal{K}$ if it is continuous, $\alpha(0) = 0$ and strictly increasing.

2.2 Preliminaries on Hybrid Dynamical Systems

2.2.1 Introduction

In this section, we provide the main notions and definitions concerning the hybrid dynamical system framework in [37]. Notice that the list of notions given in this section is not exhaustive. Here, we provide only the basic concepts needed to follow the results presented in the remainder of this dissertation. Refer to [37] for a complete presentation of hybrid dynamical systems.

2.2.2 Basic notions

We consider hybrid systems with state $x \in \mathfrak{R}^n$ of the form

$$\mathcal{H} \begin{cases} \dot{x} &= f(x) \qquad x \in C \\ x^+ &\in G(x) \qquad x \in D \end{cases} \tag{2.1}$$

where $\dot{x}$ stands for the velocity of the state and x^+ indicates the value of the state after an instantaneous change. The set where the continuous evolution (flow) of the state occurs is indicated by C. Such an evolution follows the differential equation $\dot{x} = f(x)$. The set wherein discrete evolution (jumps) are allowed to take place is indicate by D. Instantaneous jumps follows the differential inclusion $x^+ \in G(x)$. In the rest of this dissertation, the objects defining the general hybrid system in (2.1) are named as in [37]:

- C is the flow set.
- D is the jump set.
- f is the flow map.
- G is the jump map.

The four data (C, f, D, G) univocally define a hybrid system as in (2.1). For this reason, we represent (2.1) by the shorthand notation $\mathcal{H} = (C, f, D, G)$. The data of the hybrid system in (2.1) with state $\Re^n$ are defined as follows:

- $C \subset \Re^n$
- $f : \Re^n \mapsto \Re^n \,\text{with}\, C \subset \operatorname{dom} f$
- $D \subset \Re^n$
- $G : \Re^n \rightrightarrows \Re^n \,\text{with}\, D \subset \operatorname{dom} G$

2.2.3 Hybrid Time Domains

Since the co-existence of continuous-time and discrete-time behavior, solutions to hybrid dynamical systems are characterized by two variables. To represent the time elapsed, $t \in \Re_{\geq 0}$ is employed, whereas, $j \in \mathfrak{N}$ is used to keep track of the number of jumps occurred. A set $E \subset \Re_{\geq 0} \times \mathfrak{N}$ is a hybrid time domain if it is the union of a finite or infinite sequence of intervals $[t_j, t_{j+1}] \times \{j\}$, with the last interval (if existent) of the form $[t_j, T)$ with T finite or $T = \infty$.

2.2.4 Solution Concept

A function $\phi : \operatorname{dom} \phi \mapsto \Re^n$ is a hybrid arc if $\operatorname{dom} \phi$ is a hybrid time domain and if $\phi(\cdot, j)$ is locally absolutely continuous for each j.

A solution to $\mathcal{H}$ is any hybrid arc defined over a subset of $\Re_{\geq 0} \times \mathfrak{N}$ that satisfies the dynamics of $\mathcal{H}$.

A solution to a hybrid system is said to be *complete* if its domain is unbounded and *maximal*, and if it is not the truncation of another solution. Given a set S, we denote $\mathcal{S}_{\mathcal{H}}(S)$ the set of all maximal solutions ϕ to $\mathcal{H}$ with $\phi(0,0) \in S$.

Assumption 2.2.1. *Given $\mathcal{H} = (C, f, D, G)$, we say that $\mathcal{H}$ satisfies the* hybrid basic conditions *([37]) if: C and D are closed in $\Re^n$; $f \colon \Re^n \to \Re^n$ is continuous on C, and $G \colon \Re^n \rightrightarrows \Re^n$ is locally bounded, nonempty, and outer semicontinuous relatively on*[1] *D.*

2.2.5 Example of Hybrid Systems Modeling: the Bouncing Ball

Mechanical systems with impacts fall into the category of hybrid dynamical systems. The bouncing ball, represented in Fig. 2.1, is the simplest example of this kind of physical phenomenon. In the following, we showcase how to employ the hybrid system framework introduced above to model the bouncing ball.

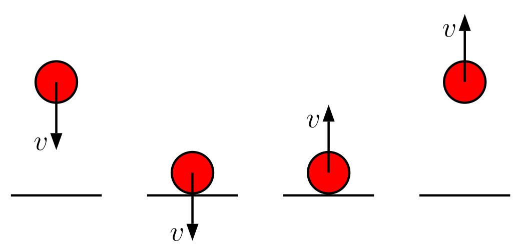

Figure 2.1: Overview of bouncing ball dynamics.

We assume the ball to bounce vertically and be of unitary mass. The vertical position of the ball is denoted by x_1, whereas its vertical speed is denoted by x_2; see Fig. 2.2. We consider $x = (x_1, x_2)$ the state of the ball.

The dynamics of the ball is governed by continuous-time law (flow) whenever the ball is above the surface or whenever, after an impact, it is on the surface with velocity vector that points upward. Impacts (jumps) occur whenever the ball is on the surface with

[1]Let $F \colon \operatorname{dom} F \rightrightarrows \Re^n$ be given and $S \subset \operatorname{dom} F$. We say that F is outer semicontinuous relatively to S if graph F is relatively closed in $S \times \Re^n$.

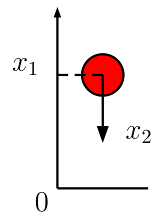

Figure 2.2: Bouncing ball modeling notation.

negative speed. These conditions can be formalized through flow set C and jump set D as follows:

$$C = \{x \in \Re^2 : x_1 > 0 \vee (x_1 = 0 \wedge x_2 \geq 0)\}, \quad D = \{x \in \Re^2 : x_1 = 0 \wedge x_2 < 0\} \tag{2.2}$$

To define the flow map, consider the continuous-time dynamics of the bouncing ball defined as

$$\begin{aligned} \dot{x}_1 &= x_2 \\ \dot{x}_2 &= -\gamma \end{aligned} \tag{2.3}$$

where γ is the acceleration due to gravity. Therefore, the flow map f can be formalized as

$$f(x) = \begin{bmatrix} x_2 \\ -\gamma \end{bmatrix} \tag{2.4}$$

To obtain a consistent model, one needs to set $f(0) = 0$.

When impacts occur, x_1 does not change, whereas x_2 inverts its sign and its absolute value reduces by a factor $\lambda \in (0, 1)$ which considers the energy dissipation due to impacts. Therefore, the jump map G can be formulated as follows:

$$G(x) = \begin{bmatrix} x_1 \\ -\lambda x_2 \end{bmatrix} \tag{2.5}$$

2.2.6 Lyapunov-Based Approach for Stability Analysis of Solutions to Hybrid Systems

This section focuses on uniform asymptotic stability of a closed set. To analyze the solutions to a hybrid system, the asymptotic stability of a closed set has more relevance than studying the stability of an equilibrium point. Indeed, asymptotic stability of an equilibrium point is a special case of asymptotic stability of a closed set. Moreover, solutions of a hybrid system often do not settle down to an equilibrium point. For example, in a sampled-data control system the states of plant and controller are expected to reach a constant value, while the timer variable does not converge to a point but rather to an interval.

The rigorous definition of asymptotic stability uses class-$\mathcal{K}$ functions and the distance of a vector $x \in \Re^n$ to a closed set $\mathcal{A} \subset \Re^n$.

Definition 2.2.1 (Class-$\mathcal{K}$ functions [37]). *A function $\alpha \colon \Re_{\geq 0} \to \Re_{\geq 0}$ is said to be of class $\mathcal{K}$ if it is continuous, α is zero at zero, strictly increasing, and unbounded.*

Definition 2.2.2 (Distance to a closed set [37]). *Given a vector $x \in \Re^n$ and a closed set $\mathcal{A}$, the distance of x to $\mathcal{A}$ is defined as $|x|_{\mathcal{A}} = inf_{y \in \mathcal{A}} |x - y|$.*

Definition 2.2.3 (Uniform global pre-asymptotic stability (UGpAS) [37]). *Consider a hybrid system $\mathcal{H}$ on $\Re^n$. Let $\mathcal{A} \subset \Re^n$ be closed. The set $\mathcal{A}$ is said to be*

- *uniformly globally stable for $\mathcal{H}$ if there exists a class-$\mathcal{K}$ function α such that any solution ϕ to $\mathcal{H}$ satisfies $|\phi(t,j)|_{\mathcal{A}} \leq \alpha(|\phi(0,0)|_{\mathcal{A}})$ for all $(t,j) \in \operatorname{dom} \phi$;*
- *uniformly globally pre-attractive for $\mathcal{H}$ if for each $\epsilon > 0$ and $r > 0$ there exists $T > 0$ such that, for any solution ϕ to $\mathcal{H}$ with $|\phi(0,0)|_{\mathcal{A}} \leq r$, $(t,j) \in \operatorname{dom} \phi$ and $t + j \geq T$ imply $|\phi(t,j)|_{\mathcal{A}} \leq \epsilon$;*
- *uniformly globally pre-asymptotically stable for $\mathcal{H}$ if it is both uniformly globally stable and uniformly globally pre-attractive.*

The following theorem provides sufficient conditions on a Lyapunov function that guarantee uniform global pre-asymptotic stability.

Definition 2.2.4 (Lyapunov function candidate [37]). *A function* $V\colon \operatorname{dom} V \mapsto \Re$ *is said to be a Lyapunov function candidate for the hybrid system* $\mathcal{H} = (C, f, D, G)$ *if the following conditions hold:*

- $\bar{C} \cup D \cup G(D) \subset \operatorname{dom} V$*;*
- V *is continuously differentiable on an open set containing* $\bar{C}$*;*

where $\bar{C}$ *denotes the closure of* C*.*

Theorem 2.2.1 (Sufficient Lyapunov conditions [37]). *Let* $\mathcal{H} = (C, f, D, G)$ *be a hybrid system and let* $\mathcal{A} \subset \Re^n$ *be closed. If* V *is a Lyapunov function candidate for* $\mathcal{H}$ *and there exist* $\alpha_1, \alpha_2 \in \mathcal{K}$*, and a continuous positive definite function* ρ *such that*

$$\alpha_1(|x|_{\mathcal{A}}) \leq V(x) \leq \alpha_2(|x|_{\mathcal{A}}) \quad \forall x \in C \cup D \cup G(D) \tag{2.6a}$$

$$\langle \nabla V(x), f(x) \rangle \leq -\rho(|x|_{\mathcal{A}}) \quad \forall x \in C \tag{2.6b}$$

$$V(g) - V(x) \leq -\rho(|x|_{\mathcal{A}}) \quad \forall x,\, g \in G(x) \tag{2.6c}$$

then $\mathcal{A}$ *is uniformly globally pre-asymptotically stable for* $\mathcal{H}$*.*

2.3 Definitions Employed in the Thesis

In the following, we introduce the definitions that will be employed in the remainder of this dissertation to analyze stability property related to the generic hybrid system (2.1).

Definition 2.3.1 (Exponential input-to-state stability). *Consider the hybrid system*

$$\mathcal{H} \begin{cases} \dot{x} &= f(x, \omega) & x \in C,\ \omega \in \Re^{n_\omega} \\ x^+ &\in G(x) & x \in D \end{cases} \tag{2.7}$$

where $\omega \in \Re^{n_\omega}$ *is the input. Let* $\mathcal{A} \subset \Re^{n_x}$ *be closed. The hybrid system* $\mathcal{H}$ *is* exponentially input-to-state-stable *(eISS) with respect to* $\mathcal{A}$ *if there exist* $\kappa, \lambda > 0$*, and* $p \in \mathcal{K}$ *such that* *each maximal solution pair*[2] (ϕ, ω) *to* $\mathcal{H}$ *is complete, and, if* $\|\omega\|_\infty$ *is finite, it satisfies*

$$|\phi(t,j)|_{\mathcal{A}} \leq \max\{\kappa e^{-\lambda(t+j)}|\phi(0,0)|_{\mathcal{A}}, p(\|\omega\|_\infty)\} \tag{2.8}$$

for each $(t,j) \in \operatorname{dom}\phi$, *where* $\|\omega\|_\infty$ *denotes the* $\mathcal{L}_\infty$ *norm of the hybrid signal* ω *as defined in [80].*

Definition 2.3.2 ($\mathcal{L}_2$ norm of a hybrid signal)**.** *The* $\mathcal{L}_2$*-norm of a hybrid signal* ϕ *is defined on a hybrid time domain* $dom\,\phi = \bigcup_{j=0}^{J-1}[t_j, t_{j+1}] \times \{j\}$ *with* J *possibly* ∞ *and/or* $t_J = \infty$ *by*

$$\|\phi\|_{\mathcal{L}_2} = \sqrt{\sum_{j=0}^{J-1} \int_{t_j}^{t_j+1} |\phi(t,j)|^2 dt}$$

When $\|\phi\|_{\mathcal{L}_2}$ *is finite, we say that* $\phi \in \mathcal{L}_2$.

Definition 2.3.3 ($\mathcal{L}_2$-stability)**.** *Consider the hybrid system*

$$\mathcal{H}\begin{cases} \dot{x} &= f(x,\omega) \qquad x \in C, \omega \in \Re^{n_\omega} \\ x^+ &\in G(x) \qquad x \in D \\ y_o &= h(x) \end{cases} \tag{2.9}$$

where $\omega \in \Re^{n_\omega}$ *and* $y_o \in \Re^{n_{y_o}}$ *are, respectively, the input and the output of the system, and* $h : \Re^n \mapsto \Re^{n_{y_o}}$. *The hybrid system* $\mathcal{H}$ *is said to be* $\mathcal{L}_2$*-stable from the input* ω *to the output* y_o *with an* $\mathcal{L}_2$*-gain less than or equal to* γ, *if there exist a* $\mathcal{K}_\infty$*-function* β *such that for any exogenous input* $\omega \in \mathcal{L}_2$, *and any initial condition* $x(0,0) \in \Re^{n_x}$, *each corresponding maximal solution to* $\mathcal{H}$ *is complete and satisfies:*

$$\|y_o\|_{\mathcal{L}_2} \leq \beta(x(0,0)) + \gamma^2\|\omega\|_{\mathcal{L}_2} \tag{2.10}$$

[2]A pair (ϕ, ω) is a solution pair to $\mathcal{H}$ if it satisfies its dynamics; see [15] for more details.

Part I

Analysis and Design of Resilient Networked Control Systems

This page is intentionally left blank.

Introduction

General Overview

In Networked Control Systems (NCSs), controller, sensors, and actuators can be partially or entirely spatially distributed and connected through a digital communication network that can be either wired or wireless. The interest in this kind of control systems is motivated by the benefits obtainable in maintenance, installation, flexibility, and low cost. Despite the benefits, network imperfections can degrade the performance and, in some cases, compromise the stability of control systems. Such a problem is widely studied in the community, as it has been shown in many publications and overview papers [44, 112, 117, 120].

The presence of packet losses and network delays are, in general, unavoidable. Indeed, limited bandwidth, network traffic, and transmission protocols cause packet losses and network-induced delays [108].

Packet losses can be modeled with stochastic or deterministic dropout models. Stochastical models of packet losses are obtained by using Bernoulli distributed white sequences [76, 100, 109] or Markov models [47, 63, 122]. The latter is usually a more complex and sophisticated way to model the packet dropping, but it captures most of the characteristics of this network phenomena. Packet losses are also modeled in deterministic ways. In these cases, packet dropouts are considered as variable sampling intervals. For example, consider a constant sampling interval of T seconds. One can treat n consecutive packet losses as a sampling time that increased to nT seconds [35, 73, 116]. Furthermore, packet losses are also treated together with network delays and modeled as time-varying network delays both in continuous-time and in discrete-time domain [18, 49, 64].

There are two kinds of network delays: sensor to controller and controller to actuator delays. The first type of delay represents the time interval that the sampled measurement needs to reach the controller after traveling on the communication channel. Similarly, the controller to actuator delay represents the time interval that the required control action needs to reach the actuator after being sent through the communication network. Since delays depend on network conditions, they are time-varying, unknown, and random but upper-bounded [120]. Therefore, network delays are modeled as Markov models [98, 118, 119] or as time-varying delays [26, 43, 115].

The effects that variable transmission intervals, packet losses, and network communication delays have on the stability of NCSs are often respectively captured by the *maximum allowable transmission interval* (MATI), the *maximum allowable number of successive packet drops* (MANSD), and the *maximum allowable delay* (MAD). MATI is the maximum time interval between transfers of data through the network between the plant and the controller, such that the control system maintains stability. MATI, which is introduced in [107], is a similar notation to *maximum allowable sampling period* (MASP) or *maximum sampling interval* (MSI) used in sampled-data literature. The term MATI is adopted in this dissertation. MANSD is the upper bound of consecutive packet dropouts such that the networked control system maintains its stability. MAD refers to as the maximum network delay that a transfer of data through the network between the plant and the controller such that the stability of the control system is not compromised.

Literature Review

The effects of variable sampling intervals and variable delays have been extensively investigated, and several publications can be found in the literature. To study the stability of the closed-loop NCS, the emulation approach is commonly employed. More specifically, the emulation approach assumes that a feedback controller has been already designed to guarantee the stability of the "networked-free" closed-loop system. Then, the impact of the networked implementation of the NCS is analyzed. The methodologies commonly used are the time delay, impulsive systems, and discrete-time approaches (see, e.g., [46]). Most of the available literature considers state feedback or static output-feedback controllers and focuses only on either variable transmission intervals or variable network delays. Yet, both aspects are considered in [16, 43, 45, 74, 78, 106]. In particular, [45] deals with including in a single model non-uniform sampling periods and varying network delays of LTI continuous-time systems in digital control loops. Naghshtabrizi et al. [74] study the stability of MIMO sampled-data systems with variable sampling intervals and delay, which are modeled by linear infinite-dimensional impulsive systems. Van de Wouw et al. [106] propose a discrete-time and impulsive differential equation approaches to analyze the input-to-state stability. Building upon [16, 78] by introducing network delays, Heemels et al. [43] model NCSs as a hybrid system and estimate trade-off curves between MATI and MAD in case of networks with schedulers such as Round Robin (RR) or Try-Once-Discard (TOD).

NCSs subject to variable sampling intervals are often named as sampled-data systems. They have been extensively investigated, and several publications can be found in the literature; see, e.g., the comprehensive survey [46]. Three are the main approaches developed to guarantee stability of sampled-data control systems: the input-delay approach [32, 33], the lifting approach [70, 71], and the impulsive system approach [16, 75]. The input-delay approach models the NCS as a continuous-time system subject to a time-varying input delay. In the lifting approach, the sampled-data control problem is converted into an equivalent finite-dimensional discrete control problem. The third approach consists in modeling sampled-data systems as impulsive systems.

Controller design for aperiodic sampled-data systems is typically addressed with two architectures: observer-based controllers and dynamic output feedback controllers. An observer-based controller relies on a dynamic state estimator and a static state-feedback control law computed from the estimated state. Bauer et al. [8] employ switched observer and controller architectures, and address the design problem via LMIs conditions. Ferrante et al. [29] propose an impulsive observer-based controller designed via LMIs obtained through a separation principle. More recently, an approach based on vector Lyapunov functions has been proposed in [91] to design observer-based controllers for sampled-data systems. Another possible design approach consists of considering the controller as a more general dynamical system interconnected to the plant. An LMI-based design of a discrete-time linear time-invariant dynamic output feedback controller is proposed in [19]. Donkers et al. [25], instead, propose an LMI-based synthesis that results in a switched controller. Fridman et al. [34] present the controller design via a time-delay approach. Necessary and sufficient conditions in the form of LMIs are provided in [7] to solve an infinite horizon quadratic optimal control problem for NCS. Lawrence in [53] addresses an output feedback stabilization problem for a class of linear impulsive systems by providing a Youla-type parameterization of all stabilizing compensators. Medina et al. [65] solve an output feedback stabilization problem by proposing a purely discrete-time compensator followed by a memoryless generalized hold device that achieves closed-loop exponential stability.

Most of the above design approaches consider zero-order hold (ZOH) devices to convert impulsive signals, such as measurements and control actions, to continuous-time signals. Many other holding devices can however be employed [14]. For example, first-order hold functions or, more generally, generalized holding devices that can take any form useful to guarantee stability of the control system [50]. The benefits of considering more general holding functions are improved robustness as well as enlarged maximal admissible transmission intervals [92].

Contributions

The contributions of this part of the dissertation aims at proposing new tools for the analysis and design of resilient NCSs.

Regarding the stability analysis, we propose sufficient conditions in the form of matrix inequalities to explicitly estimate upper bounds MATI and MAD for the stability of one-channel output feedback NCSs [44]. Our approach considers NCSs equipped with a linear continuous-time time-invariant dynamic output feedback controller and an impulsive linear time-invariant holding device. The approach we pursue relies on the Lyapunov theory for hybrid systems in the framework [37]. Sufficient conditions for global internal exponential stability and $\mathcal{L}_2$ external stability are given. One of the unique features of our approach is that the parameters of interest, i.e., MATI and MAD, appear explicitly in the resulting conditions. This enables the derivation of a computationally affordable algorithm for the approximation of the trade-off curve between MATI and MAD based on semidefinite programming tools.

The other contribution is related to the design of resilient NCS. Such a design is pursued throughout an LMI-based design procedure for the co-design of the parameters of the dynamic controller and holding device. Our approach relies on the Lyapunov theory for hybrid systems and addresses the stability analysis in a way that is reminiscent of an "input-to-state stability small gain" philosophy. More in detail, we propose a hybrid control scheme constituted by the cascade of a holding device and a dynamic controller. The holding device is a linear time-invariant system whose state is reset to the plant measurement whenever a new transmission occurs. This holding device generates a continuous-time signal that feeds a linear time-invariant dynamic controller. Our approach leads to a computationally efficient co-design of the parameters of the controller and holding device via LMIs. One of the main novelties of our methodology is that we consider the closed-loop NCS as a feedback interconnection of two dynamical systems: the "networked-free" closed-loop continuous-time system and the network-induced error impulsive system. Seeing the NCS closed-loop from this perspective allows us to address the stability analysis via an approach that is reminiscent of an "input-to-state stability small gain" philosophy [48]. A similar approach is employed in [16] for the analysis of the stability of NCS. Differently from [16], stability conditions obtained in this dissertation enable the controller design via the solution to some matrix inequalities. In particular, following the general approach in [95] and [30], we come up with a design algorithm for the controller design based on the solutions to some LMIs coupled with a line search of a few parameters.

Part I of the dissertation is organized as follows:

- Chapter 3 introduces the modeling framework for one-channel output feedback NCSs considered in this dissertation.
- Chapter 4 deals with the problem of estimating maximum allowable transmission interval (MATI) and maximum allowable delay (MAD). Some of the results presented in this chapter can be found in [68].
- Chapter 5 proposes the tools for designing NCSs resilient to variable transmission intervals.

Chapter 3

Modeling of Networked Control Systems

3.1 Introduction

This chapter introduces the architecture of NCSs considered across the whole dissertation. We consider NCSs as in Fig. 3.1, where the sensing path of the closed-loop system is subject to network communication, whereas the control input is a continuous-time signal generated by the controller. Notice that such a control systems architecture is known as *one-channel feedback NCS* [44] and constitutes a relevant case study since it can capture several configurations of NCSs as shown in [44, Section III.A]. More in detail, we consider a network subject to aperiodic transmission intervals and variable network delays. Moreover, we introduce a hybrid control scheme constituted by the cascade of a holding device and a dynamic controller. The holding device is a linear time-invariant system whose state is reset to the plant measurement whenever a new transmission occurs. This holding device generates a continuous-time signal that feeds a linear time-invariant dynamic controller. After describing the system architecture, we introduce the modeling of NCS with the hybrid dynamical system framework in [37].

3.2 System Description

We consider NCSs, depicted in Fig. 3.1, where a plant $\mathcal{P}$ is stabilized by a dynamic controller $\mathcal{K}$ that relies on measurements collected through a packet-based network subject to variable network delays. The presence of the network results in an intermittent stream of information from the plant to the controller, which does not have access to the plant output in a continuous-time fashion. To overcome this problem, we assume that the controller is equipped with a linear time-invariant holding device whose state is reset to the plant measurement whenever a new measurement data are available.

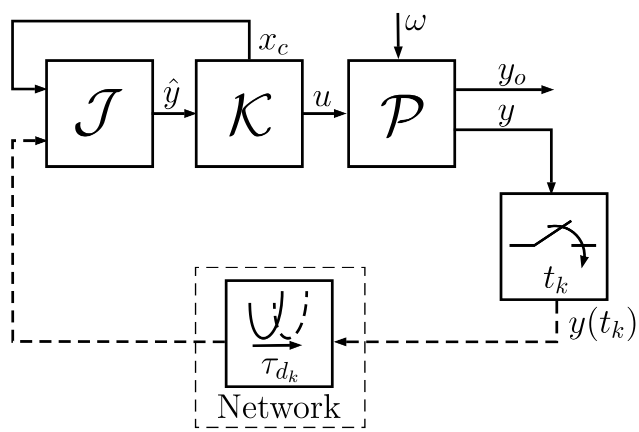

Figure 3.1: Schematic representation of the considered NCSs.

3.2.1 Plant Description

We assume the plant is a linear time-invariant continuous-time system of the form:

$$\mathcal{P}\begin{cases}\dot{x}_p = A_p x_p + B_p u + W\omega \\ y = C_p x_p \\ y_o = C_o x_p\end{cases} \tag{3.1}$$

where $x_p \in \Re^{n_{x_p}}$ represents the state of the plant, $u \in \Re^{n_u}$ represents the control input, $\omega \in \Re^{n_\omega}$ is an exogenous disturbance, $y \in \Re^{n_y}$ is the measured output of the plant, and y_o is the performance output. The constant matrices A_p, B_p, W, and C_p are given and of appropriate dimensions.

3.2.2 Network Description

We consider a setup in which the measurement y is sampled and sent at time $t_k, k \in \mathfrak{N}$ not known in advance and that y is received by the controller after a bounded, possibly time varying, network delay τ_{d_k}. Specifically, we suppose that the sequence $\{t_k\}_{k=1}^{\infty}$ is strictly increasing and unbounded, that the sampling and the transmissions happen at the same time, and that there exists $T_1 > 0$ such that the transmission intervals $t_{k+1} - t_k$ satisfy $T_1 \leq t_{k+1} - t_k < T_2$ for all $k \in \mathfrak{N}$. The quantity T_2 represents the *maximum allowable transmission interval* (MATI). Concerning network delays, we consider that the network delay τ_{d_k} is bounded by T_{mad}, i.e., $0 \leq \tau_{d_k} \leq T_{mad}, k \in \mathfrak{N}$, where $0 \leq T_{mad} \leq T_2$ is the *maximum allowable delay* (MAD). The latter condition employed for network delays implies that the transmitted output measurement must be received by the controller before the next measurement is sampled and sent. This condition is also known as *small delay assumption*. It could seem too strong in practice, but it is widespread in the literature of networked control systems; see, e.g., [27, 43, 44, 97]; to mention a few. The main advantage of employing the so-called small delay assumption is that this rules out the possibility of running into packet disorder phenomena. Indeed, when delays are larger than the sampling time, more recent measurements can become available before older data are received and processed by the controller [55]. As shown in [56], packet disorders render the design of feedback stabilization laws harder. To overcome this problem, when network delays are larger than the sampling time, the implementation of any control algorithm should be accompanied by a *message rejection* mechanism. This scenario is considered, e.g., in [17], where out-of-order packages are discarded. On the other hand, observe that a simpler (although less optimal) message rejection strategy consists of dropping packages received with an incurred delay larger than the sampling time. This mechanism is employed, e.g., in UDP-like networks; see, [55, Section VI]. When this strategy is adopted, packages delivered after a delay larger than the sampling time are assumed to be lost. In other words, in this setting, the effect of large transmission delays is captured by package dropouts. As such, we believe the small delay assumption we consider in our work is not overly restrictive and does not limit the application of our results in realistic scenarios. Nonetheless, we acknowledge that using a less pessimistic message rejection scheme as in [17] could lead to less conservative results, yet the price to pay consists of dealing with more complex models. In this work, following the lines of [43], we preferred not to take this path to provide a simple and unified complex approach to study the effect of intermittent sampling and network delays jointly.

3.2.3 Controller Description

We consider a control scheme, depicted in Fig. 3.1, constituted by a dynamic controller $\mathcal{K}$ and a holding device $\mathcal{J}$. In particular, plant $\mathcal{P}$ is stabilized by a dynamic controller $\mathcal{K}$ that relies on the continuous-time signal $\hat{y}$ generated by the holding device $\mathcal{J}$.

The continuous-time dynamic controller $\mathcal{K}$ is given by:

$$\mathcal{K}\begin{cases}\dot{x}_c = A_c x_c + B_c \hat{y}\\ u = C_c x_c + D_c \hat{y}\end{cases} \tag{3.2}$$

where $x_c \in \mathfrak{R}^{n_{x_c}}$ is the controller state, and A_c, B_c, C_c, and D_c are given constant matrices of appropriate dimensions. By making use of the last received measurement of the plant output and of the controller state (whose value is available at all time), the holding device $\mathcal{J}$ generates an intersample signal that is use to feed controller $\mathcal{K}$. In particular, $\mathcal{J}$ is described by the following dynamics for all $k \in \mathfrak{N}_0$:

$$\mathcal{J}\begin{cases}\dot{\hat{y}}(t) = H\hat{y}(t) + Ex_c(t) & \forall t \neq t_k + \tau_{d_k}\\ \hat{y}(t^+) = y(t_k) & \forall t = t_k + \tau_{d_k}\end{cases} \tag{3.3}$$

where H and E are given matrices of appropriate dimensions. The operating principle of the holding device $\mathcal{J}$ is as follows. The arrival of new measurements instantaneously updates

$\hat{y}$ to y. In between updates, $\hat{y}$ evolves according to the continuous-time dynamics in (3.3) and its value is continuously used by controller $\mathcal{K}$. Matrices A_c, B_c, C_c, D_c, H and E are controller parameters that need to be designed.

Remark 3.2.1. *A general approach consists in using holding device as zero-order hold (ZOH), which converts the impulsive signal of plant measurements to continuous-time signals, by holding a constant value of the last received measurement in between received network packets. This dynamic behavior can be described as follows:*

$$ZOH \begin{cases} \dot{\hat{y}}(t) = 0 & \forall t \neq t_k + \tau_{d_k} \\ \hat{y}(t^+) = y(t_k) & \forall t = t_k + \tau_{d_k} \end{cases} \tag{3.4}$$

As shown in [14] and references therein, many other holding functions can be employed. The benefits of considering more general holding functions are improved robustness as well as enlarged maximal admissible transmission intervals.

3.3 Hybrid Modeling

The closed-loop system in Fig. 3.1 can be modeled as a linear system with jumps in $\hat{y}$. In particular, for all $k \in \mathfrak{N}_0$ one obtains

$$\begin{cases} \begin{cases} \dot{x}_p(t) = A_p x_p(t) + B_p C_c x_c(t) + B_p D_c \hat{y}(t) + W\omega(t) \\ \dot{x}_c(t) = A_c x_c(t) + B_c \hat{y}(t) & \forall t \neq t_k + \tau_{d_k} \\ \dot{\hat{y}}(t) = H\hat{y}(t) + E x_c(t) \end{cases} \\ \begin{cases} x_p(t^+) = x_p(t) \\ x_c(t^+) = x_c(t) & \forall t = t_k + \tau_{d_k} \\ \hat{y}(t^+) = C_p x_p(t_k) \end{cases} \end{cases} \tag{3.5}$$

The closed-loop system evolves with differential equations and experiences jumps. For such a reason, we model it into the hybrid system framework in [37], for which preliminary information is in Chapter 2. To this end, we introduce the auxiliary variables $\tau \in \Re_{\geq 0}$, $s_y \in \Re^{n_y}$, and $l \in \{0, 1\}$. Variable τ is a timer that keeps track of the duration of sampling intervals and network delays, and triggers a jump whenever a new measure that will be successfully received by the controller is sampled (sampling events) or received (update events). Variable s_y represents a memory state that stores the value of the sampled measurement $y(t_k)$. In particular, $y(t_k)$ is stored in s_y at sampling events of successful transmissions, and s_y is assigned to $\hat{y}$ at update events after network delays τ_{d_k}. Similarly as in [23], variable l allows one to model both sampling events (when $l = 0$) and updating events (when $l = 1$). Figure 3.2 depicts timing and working concept of the auxiliary variables s_y and l. Notice that in Fig. 3.2 we considered $\dot{\hat{y}} = 0$ to achieve a clearer representation. We consider the

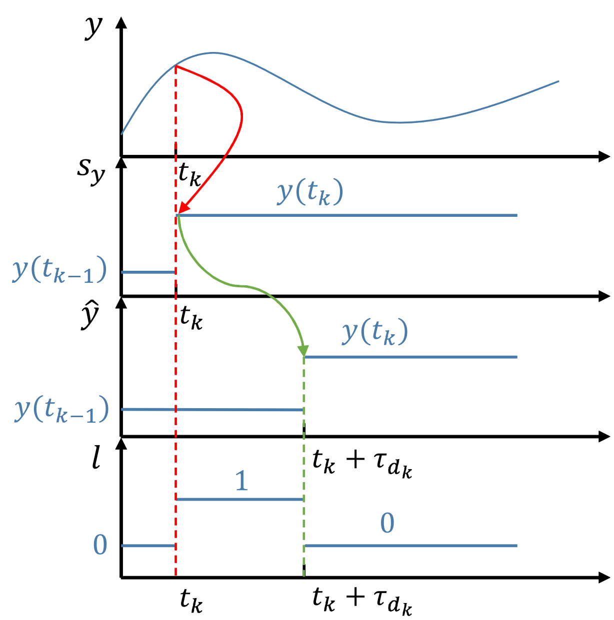

Figure 3.2: Timing and working concept of the auxiliary variables of the hybrid system model.

following hybrid model of the closed-loop system

$$\mathcal{H}_y \begin{cases} \dot{\xi} = f_\xi(\xi, \omega) & \xi \in C_\xi, \omega \in \Re^{n_\omega} \\ \xi^+ = g_\xi(\xi) & \xi \in D_\xi \\ y_o = \bar{C}_o\left(x_p, x_c\right) \end{cases} \tag{3.6}$$

where $\xi := (x_p, x_c, \hat{y}, s_y, \tau, l) \in \mathfrak{R}^{n_\xi}$ with $n_\xi := n_{x_p} + n_{x_c} + 2n_y + 2$ is the state of the hybrid system, $\bar{C}_o := [C_o \quad 0]$,

$$f_\xi(\xi, \omega) := \begin{bmatrix} A_p x_p + B_p C_c x_c + B_p D_c \hat{y} + W\omega \\ A_c x_c + B_c \hat{y} \\ H\hat{y} + E x_c \\ 0 \\ 1 \\ 0 \end{bmatrix} \tag{3.7}$$

and

$$g_\xi(\xi) := \begin{bmatrix} x_p \\ x_c \\ (1-l)\hat{y} + l s_y \\ (1-l)C_p x_p + l s_y \\ l\tau \\ 1-l \end{bmatrix} \tag{3.8}$$

The flow set C_ξ and the jump set D_ξ are respectively defined by

$$C_\xi := \{\xi \in \mathfrak{R}^{n_\xi} | (l = 0 \wedge \tau \in [0, T_2]) \vee (l = 1 \wedge \tau \in [0, T_{mad}])\} \tag{3.9}$$

and

$$D_\xi := \{\xi \in \mathfrak{R}^{n_\xi} | (l = 0 \wedge \tau \in [T_1, T_2]) \vee (l = 1 \wedge \tau \in [0, T_{mad}])\} \tag{3.10}$$

Notice that the model in (3.6) admits aperiodic sampling. In particular, sampling events are triggered for $\tau \in [T_1, T_2]$. This feature is modeled by the condition $(l = 0 \wedge \tau \in [T_1, T_2])$ in the definition of D_ξ. Notice that, by definition, C_ξ and D_ξ overlap each other, and, when the state ξ belongs to $C_\xi \cap D_\xi$, both flowing and jumping are allowed. As such, solutions to (3.6) are not unique. This enables one to capture all possible network behaviors in a unified manner.

Remark 3.3.1. *Notice that a state feedback controllers can be easily characterized by a similar hybrid model. Indeed, in case of state feedback controllers, we assume that the whole state is measurable ($y = x_p$) and that it is sent through the network to a static controller given as:*

$$u(t) = K_c \hat{x}_p(t) \tag{3.11}$$

where $\hat{x}_p$ is the state of the holding device, which, similarly to $\hat{y}$, is described by:

$$\begin{cases} \dot{\hat{x}}_p(t) = H\hat{x}_p(t) & \forall t \neq t_k + \tau_{d_k} \\ \hat{x}_p(t^+) = x_p(t_k) & \forall t = t_k + \tau_{d_k} \end{cases} \tag{3.12}$$

By following the same approach described in above, the impulsive system (3.12) *can be formulated with a hybrid system that has the same structure of that one in* (3.6)*.*

3.3.1 Analysis of Zeno Solutions

In the following we show that the hybrid systems (3.6) does not experience Zeno solutions. Let ϕ be a solution to a hybrid system, and $\operatorname{dom}\phi$ its domain. According to [37, Definition 2.5] a solution ϕ is called Zeno if it is complete and

$$\sup_t \operatorname{dom}\phi := \sup\{t \in \Re_{\geq 0} \colon \exists j \in \mathfrak{N} \,\text{such that}\, (t,j) \in \operatorname{dom}\,\phi\} < \infty \tag{3.13}$$

See [37] for further details. Maximal solutions of the hybrid system $\mathcal{H}_y$ in (3.6) are complete for [37, Proposition 6.10]. In the following, we show that solutions to the hybrid system under analysis are not Zeno.

As described in the previous section, jumps in our model are triggered by the variables τ and l only. More precisely, the jump and the flow sets of $\mathcal{H}_y$ are defined by conditions involving only the auxiliary states τ and l; see the flow and the jump sets in (3.9) and (3.10). Therefore, in the following analysis, we consider only variables τ and l.

Notice that by the definition of the dynamics of $\mathcal{H}_y$, any maximal solution experiences an infinite number of jumps. In particular, the domain of every maximal solution ϕ

to $\mathcal{H}_y$ can be written as follows:

$$\operatorname{dom}\phi = \bigcup_{j \in \mathfrak{N}} (I_j \times \{j\}) \tag{3.14}$$

where $I_j := [t_j, t_{j+1}]$, for all $j \in \mathfrak{N}$, are the flowing intervals of ϕ. Let ϕ_τ and ϕ_l be, respectively, the τ and l components of the solution ϕ. We first analyze the case in which $\phi_\tau(0,0) = \phi_l(0,0) = 0$. It is worth mentioning that this initial condition simplifies the analysis, but it does not compromise the following reasoning; this will be further clarified later in this letter. Figure 3.3 depicts the hybrid domain of ϕ and the evolution of ϕ_l projected onto the ordinary time for this selection of initial conditions.

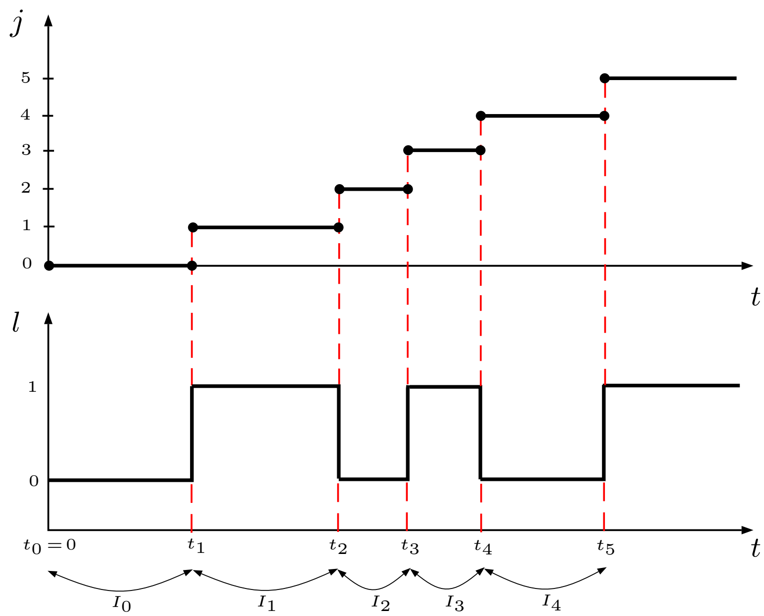

Figure 3.3: Hybrid domain of ϕ (top) and evolution of ϕ_l projected onto the ordinary time (bottom).

For any interval $I \subset \mathfrak{R}$, let $|I|$ denote the length of I. Next, we determine the length of the flowing intervals I_j by inspection of the system dynamics (3.6). To this end, assume $\phi_\tau(0,0) = \phi_l(0,0) = 0$. Pick any $j \in \mathfrak{N}$. Then, since the variable l toggles its value at jumps, for all $t \in I_j$, one has

$$\begin{aligned} \phi_l(t,j) &= 0 \quad \text{if } j \text{ is even} \\ \phi_l(t,j) &= 1 \quad \text{if } j \text{ is odd} \end{aligned} \tag{3.15}$$

Now, by making use of the definition of the dynamics of (3.6), we show that the following relations hold:

(*i*) $|I_0| = L_0$ for some $L_0 \in [T_1, T_2]$

(*ii*) $|I_1| = T_1$, $0 \leq L_1 \leq T_{mad} \leq T_2$

(*iii*) $|I_2| = \bar{L}_2 - L_1 =: L_2$, for some $\bar{L}_2 \in [T_1, T_2]$

Where non-uniqueness of the solutions to (3.6) is captured by the arbitrariness of the scalars L_1 and $\bar{L}_2$.

Now, we describe how to obtain the length of above intervals.

Case (*i*): Consider the length of the flowing interval I_0. Since $\phi_l(0,0) = \phi_\tau(0,0) = 0$, one has that $\phi(0,0) \in C \setminus D$. Hence, $\mathcal{H}_y$ flows until $\phi_\tau(t,0) \in [T_1, T_2]$. This shows that (*i*) holds.

Case (*ii*): Let $|I_1| = L_1$. To determine the value of L_1, observe that by construction $\phi_l(t_1, 1) = 1$ and $\phi_\tau(t_1, 1) = 0$. Hence, $\phi(t_1, 1) \in C \cap D$. This gives rise to two possible solutions: one that jumps right away and another that flows. In the first case, we have that $L_1 = 0$. Instead, in the second case, we have that $L_1 \in (0, T_{mad}]$. This establishes (*ii*).

Case (*iii*): To determine the length of I_2, observe that $\phi_l(t_2, 2) = 0$ and from Case (*ii*) $\phi_\tau(t_2, 2) = L_1$. Depending on the value of L_1, this leads to two possible cases. If $L_1 < T_1$, then $\phi(t_2, 2) \in C \setminus D$. Hence, $\mathcal{H}_y$ flows until $\phi_\tau(t, 2) \in [T_1, T_2]$. Instead, if $L_1 = T_1$, then $\phi(t_2, 2) \in C \cap D$. Hence, $\mathcal{H}_y$ can either jumps right away or flow until $\phi_\tau(t, 2) \in (T_1, T_2]$. This establishes (*iii*).

At this stage, notice that the lengths of the intervals follow a particular pattern that depends on the index j. In particular, one can divide the intervals between those with even indexes and those with odd indexes. Therefore, one can characterize the sequence $\{I_j\}$, $j \in \mathfrak{N}$, as follows:

$$\begin{aligned} &|I_j| = \bar{L}_j - L_{j-1} \coloneqq L_j, \text{ for some } \bar{L}_j \in [T_1, T_2] && \forall j \in \mathfrak{N}\,\text{even},\ j \neq 0 \\ &|I_j| = L_j,\ 0 \leq L_j \leq L_{mad} \leq T_1, && \forall j \in \mathfrak{N}\,\text{odd} \end{aligned} \tag{3.16}$$

Similar pattern can be found when $\phi_l(0,0) = 1$, but even indexes would correspond to $\phi_l(t,j) = 1$. In such a case, one can achieve wholly analogous conclusions.

Now, we consider the relationships in (3.16), and we analyze the worst-case scenarios where the solution ϕ experiences consecutive jumps without flowing:

- Pick j odd. If $|I_j| = 0$ then ϕ experiences two consecutive jumps without flowing. Notice that in this case, from (3.6), $|I_{j+1}| \geq T_1$. Therefore, after two consecutive jumps the solution must flow at least for T_1 units of time. Figure 3.4 depicts an example of this case.

- Pick j odd. If $|I_j| = T_{mad} = T_2$ and $|I_{j+1}| = 0$ then:

  - if $|I_{j+2}| = L_{j+2} > 0$, then ϕ experiences two consecutive jumps without flowing. Therefore, after two consecutive jumps the solution must flow at least for L_{j+2} units of time. Figure 3.5 depicts an example of this case.

  - if $|I_{j+2}| = 0$, then ϕ experience three consecutive jumps without flowing. Notice that in this case $|I_{j+3}| \geq T_1$. Therefore, after three consecutive jumps the solution must flow at least T_1. Figure 3.6 depicts an example of this case.

The above analysis allows one to conclude that any maximal solution ϕ to $\mathcal{H}_y$ can experience at most three consecutive jumps without flowing in an interval of length smaller than T_1. This can be seen as an upper bound on j. In particular, for every solution ϕ

$$j \leq \frac{t}{T_1} + 3, \qquad \forall (t,j) \in \operatorname{dom} \phi \tag{3.17}$$

Indeed, because j is integer, for j to be strictly larger than 3, it has to be $t \geq T_1$. This latter

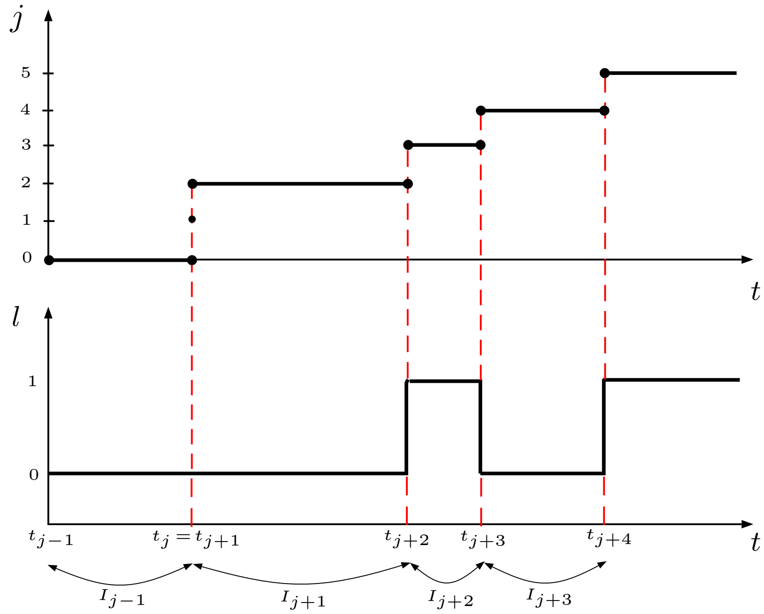

Figure 3.4: Hybrid domain of ϕ (top) and evolution of ϕ_l projected onto the ordinary time (bottom) in case $|I_j| = 0$, j odd.

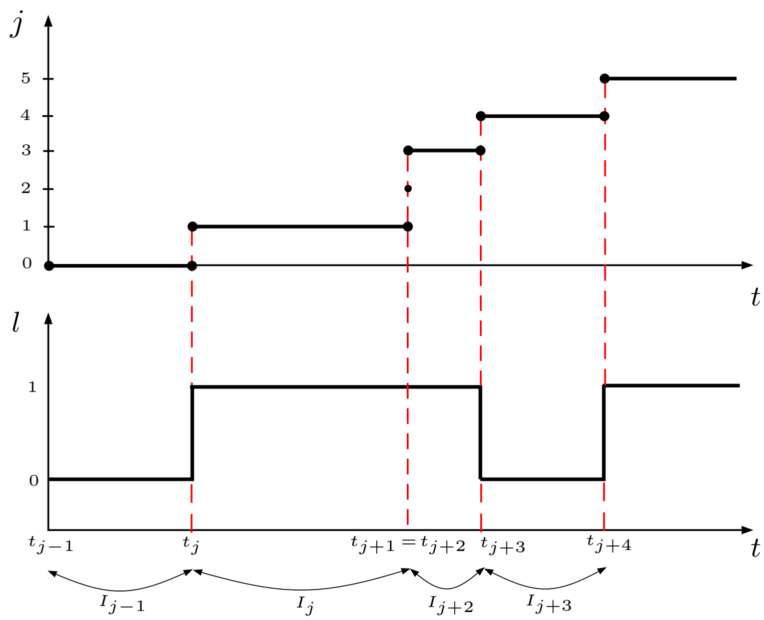

Figure 3.5: Hybrid domain of ϕ (top) and evolution of ϕ_l projected onto the ordinary time (bottom) in case $|I_j| = T_{mad} = T_2$ and $|I_{j+1}| = 0$ and $|I_{j+2}| > 0$, j odd.

property is commonly denoted as average dwell time [37, Example 2.15], and rules out the existence of Zeno solutions. In fact, for j to grow unbounded, t needs to grow unbounded

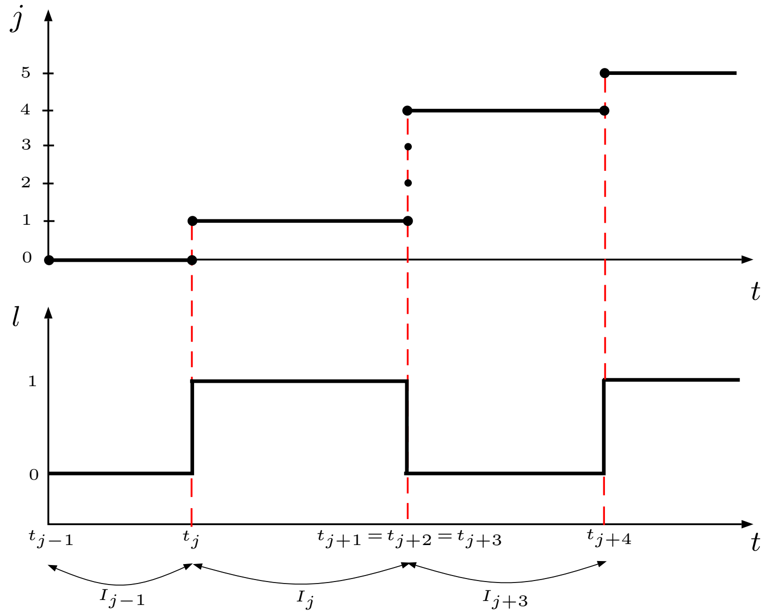

Figure 3.6: Hybrid domain of ϕ (top) and evolution of ϕ_l projected onto the ordinary time (bottom) in case $|I_j| = T_{mad} = T_2$ and $|I_{j+1}| = 0$ and $|I_{j+2}| = 0$, j odd.

as well. This, of course, prevents ϕ from being Zeno.

3.4 Conclusion

In this chapter, we introduce the architecture of NCSs considered in this dissertation. In particular, we take into consideration NCSs where only the sensing path is subject to a communication network that leads to aperiodic transmission intervals and variable network delays. From a control architecture point of view, we consider a hybrid control scheme constituted by the cascade of a holding device and a dynamic controller, and we model the closed-loop system in the hybrid system framework in [37]. Finally, we show that considered NCSs cannot experience Zeno solutions.

This page is intentionally left blank.

Chapter 4

Stability Analysis of Networked Control Systems

4.1 Introduction

This chapter deals with the problem of estimating maximum allowable transmission interval (MATI) and maximum allowable delay (MAD) of output feedback linear networked control systems (NCSs). Given the plant, the controller, and the holding device, this chapter describes two methodologies for the estimation of the trade-off curves that provide a resiliency metric for the NCS with respect to variable transmission intervals and variable network delays. In particular, following the lines of [16, 43, 79], in this chapter, we pursue an emulation approach to study the stability of the closed-loop NCS. More specifically, we assume that a dynamic output feedback controller and holding device have been already designed to guarantee the stability of the closed-loop system, and we analyze the stability in its networked implementation. In particular, we determine explicit bounds on the transmission interval and the network delay for which closed-loop stability is preserved. Internal exponential stability and $\mathcal{L}_2$ external stability are studied with two approaches that rely on solutions of LMIs. The first approach, already introduced in [23, 43], is applicable only to NCS, where ZOH is chosen as the holding device. By following this approach, the trade-off curves are obtained indirectly after solving some LMIs. The second approach, which extends our previous work [68] to variable transmission intervals, considers NCS with a generic holding device as in (3.3). In this case, the trade-off curves are obtained directly from solutions of LMIs. Indeed, MATI and MAD appear explicitly in the resulting conditions. After formalizing the problem we solve, the two approaches are discussed and compared with numerical examples.

4.2 Problem Statement

We consider NCSs introduced in Chapter 3 and depicted in Fig. 3.1. In such NCSs, output measurements of plant $\mathcal{P}$ are shared in a packet-based network characterized by aperiodic transmission intervals and variable network delays. The *maximum allowable transmission interval* (MATI) and the *maximum allowable delay* (MAD) are respectively denoted as T_2 and T_{mad}. Furthermore, we assume the NCS is stabilized by a linear time-invariant dynamic controller $\mathcal{K}$ that relies on the holding device $\mathcal{J}$, which is a linear time-invariant system whose state is reset to the plant measurement whenever a new measurement is received. This holding device generates a continuous-time signal that feeds a linear time-invariant dynamic controller. The plant $\mathcal{P}$, controller $\mathcal{K}$, and holding device $\mathcal{J}$ are, respectively, in (3.1), (3.2), and (3.3). Refer to Chapter 3 for further details on the NCSs under analysis.

The problem we solve is as follows:

Problem 4.2.1. *Given plant $\mathcal{P}$, the controller $\mathcal{K}$ and the holding device $\mathcal{J}$, determine the largest achievable values of T_{mad} and T_2 such that the closed-loop NCS is $\mathcal{L}_2$ stable from the disturbance ω to the performance output y_o with $\mathcal{L}_2$-gain less than or equal to γ.*

Expected outcomes of the solution to Problem 4.2.1 are estimated trade-off curves between T_{mad} and T_2. These trade-off curves represent metrics to evaluate resiliency to variable transmission intervals and network delays of NCS. In particular, we aim at estimating a relation between T_{mad} and T_2 such that the NCS satisfies $\mathcal{L}_2$ stability properties.

4.3 Trade-off Curves Estimation for NCS: An Indirect Approach

In this section, we describe the first approach for the estimation of the trade-off curve. This approach assumes only ZOH holding devices, which limits the analysis of NCS taken into consideration in this dissertation. The stability results of these approaches are comprehensively described in [43] and reference therein. This material is added to this dissertation to provide some degree of self-containment since these results are employed in the controller design introduced in the second part of the thesis.

4.3.1 Modeling

To properly address the stability analysis from an indirect approach point of view, we need to suitably manipulate the hybrid system $\mathcal{H}_y$ in (3.6) where the holding device is a ZOH; see Remark 3.2.1 for further details. In particular, we perform the following change of coordinates:

$$\begin{aligned} \eta &\coloneqq \hat{y} - y \\ s &\coloneqq s_y - \hat{y} \end{aligned} \tag{4.1}$$

By straightforward calculation, one can obtain the closed-loop hybrid system in the new coordinates which reads as follows:

$$\mathcal{H}_{cl_I} \begin{cases} \dot{x}_I = f_I(x_I, \omega) & x_I \in C_I, \omega \in \mathfrak{R}^{n_\omega} \\ x_I^+ = g_I(x_I) & x_I \in D_I \\ y_o = \bar{C}_o x_{cl} \end{cases} \tag{4.2}$$

where $x_I \coloneqq (x_{cl}, \eta, s, \tau, l) \in \mathfrak{R}^{n_x}$ is the state with $n_x \coloneqq n_{x_p} + n_{x_c} + 2n_y + 2$, and $x_{cl} \coloneqq (x_p, x_c)$. The flow map is given, $\forall x_I \in C, \omega \in \mathfrak{R}^{n_\omega}$, by

$$f_I(x_I, \omega) \coloneqq \begin{bmatrix} A_{11}x_{cl} + A_{12}\eta + A_{13}\omega & A_{21}x_{cl} + A_{22}\eta + A_{23}\omega & 0 & 1 & 0 \end{bmatrix}^\top \tag{4.3}$$

where

$$A_{11} := \left[\begin{array}{c|c} A_p + B_p D_c C_p & B_p C_c \\ \hline B_c C_p & A_c \end{array}\right],\ A_{12} := \left[\begin{array}{c} B_p D_c \\ \hline B_c \end{array}\right],\ A_{13} := \left[\begin{array}{c} W \\ \hline \mathbf{0} \end{array}\right], \tag{4.4}$$

$$A_{21} := \left[\begin{array}{c|c} -C_p A_p - C_p B_p D_c C_p & -C_p B_p C_c \end{array}\right],\ A_{22} := -C_p B_p D_c,\ A_{23} := -C_p W$$

derive from (3.1), (3.2) and (4.16). The jump map is defined for all $x \in D_I$ by

$$g_I(x_I) := \begin{bmatrix} x_{cl} \\ \eta + ls \\ -(1-l)\eta \\ l\tau \\ 1-l \end{bmatrix} \tag{4.5}$$

The flow set C_I and the jump set D_I are respectively defined as

$$C_I := \{x_I \in \mathfrak{R}^{n_x} | (l = 0 \wedge \tau \in [0, T_2]) \vee (l = 1 \wedge \tau \in [0, T_{mad}])\} \tag{4.6}$$

and

$$D_I := \{x_I \in \mathfrak{R}^{n_x} | (l = 0 \wedge \tau \in [T_1, T_2]) \vee (l = 1 \wedge \tau \in [0, T_{mad}])\} \tag{4.7}$$

4.3.2 Stability Results

To address the stability of $\mathcal{H}_{cl_I}$ we employ the definitions 2.3.2 and 2.3.3 introduced in Chapter 2. Consider the following two assumptions:

Assumption 4.3.1. *There exist a continuously differentiable function $V : \mathfrak{R}^{n_p+n_c} \mapsto \mathfrak{R}_{\geq 0}$ and constants θ, γ, $\mu \in \mathfrak{R}_{>0}$ such that*

$$\langle \nabla V(x_{cl}), A_{11}x_{cl} + A_{12}\eta + A_{13}\omega \rangle \leq \mu(\gamma^2|\omega|^2 - |y_o|^2) + \theta^2|\eta|^2 - |A_{21}x_{cl} + A_{22}\eta + A_{23}\omega|^2 \tag{4.8}$$

where A_{11}, A_{12}, and A_{13}, A_{21}, A_{22}, and A_{23} are as in (4.4).

Assumption 4.3.2. *There exists a pair of values* (T_2, T_{mad}) *such that*

$$\gamma_1\phi_1(\tau) \geq \gamma_0\phi_0(\tau), \quad \forall\tau \in [0, T_{mad}] \tag{4.9a}$$

$$\gamma_0\phi_0(\tau) \geq \lambda^2\gamma_1\phi_1(0), \quad \forall\tau \in [0, T_2] \tag{4.9b}$$

with $T_2 \geq T_{mad} \geq 0$, $\lambda \in (0,1)$, *constants*

$$\gamma_0 := \theta, \qquad \gamma_1 := \frac{\theta}{\lambda}, \tag{4.10}$$

and where, for $l \in \{0,1\}$, ϕ_l *is solution to*

$$\dot{\phi}_l = -\gamma_l(\phi_l^2 + 1) \tag{4.11}$$

with initial conditions $\gamma_1\phi_1(0) \geq \gamma_0\phi_0(0) \geq \lambda^2\gamma_1\phi_1(0)$.

Relying on Assumptions 4.3.1 and 4.3.2 it is possible to state the following result for the $\mathcal{L}_2$-stability of $\mathcal{H}_{cl_I}$.

Theorem 4.3.1. *Let the Assumption 4.3.1 and Assumption 4.3.2 hold, then the hybrid system* $\mathcal{H}_{cl_I}$ *is* $\mathcal{L}_2$*-stable from the input* ω *to the output* y_o *with an* $\mathcal{L}_2$*-gain less than or equal to* γ.

The proof is given in Appendix B.

4.3.3 (T_{mad}, T_2) Trade-off Curves Estimation

In the following, we describe how to employ the stability results in the previous subsection to estimate the (T_{mad}, T_2) trade-off curves for the $\mathcal{L}_2$-stability of the hybrid system $\mathcal{H}_{cl_I}$ with $\mathcal{L}_2$-gain less than or equal to γ. To this end, we make the following choice for function $V\colon \mathfrak{R}^{n_p+n_c} \mapsto \mathfrak{R}$:

$$V(x_{cl}) := x_{cl}^\top P x_{cl} \tag{4.12}$$

where $P \in \mathcal{S}_+^{n_{x_{cl}}}$. At this stage, it is trivial to show that Assumption 4.3.1 holds if there exist $P \in \mathcal{S}_+^{n_{x_{cl}}}$, and constants θ, γ, $\mu \in \Re_{>0}$ such that

$$\mathcal{F}_0 \coloneqq \begin{bmatrix} \mathrm{He}(PA_{11}) + A_{21}^\top A_{21} + \mu \bar{C}_o^\top \bar{C}_o & PA_{12} + A_{21}^\top A_{22} & A_{21}^\top A_{24} + PA_{13} \\ \bullet & A_{22}^\top A_{22} - \theta^2 \mathbf{I} & A_{22}^\top A_{24} \\ \bullet & \bullet & A_{24}^\top A_{24} - \mu\gamma^2 \mathbf{I} \end{bmatrix} \preceq 0 \quad (4.13)$$

Remark 4.3.1. *Assumption 4.3.1 represents an $\mathcal{L}_2$-gain condition on the linear system $\dot{x}_{cl} = A_{11}x_{cl} + A_{12}\eta + A_{13}\omega$ where γ is the $\mathcal{L}_2$-gain upper bound between ω and y_o, while θ is the $\mathcal{L}_2$-gain upper bound for the influence of the networked-induced error η on x_{cl}. Therefore, the smaller the value of θ, the less the influence of η on x_{cl}, hence, the largest the values of T_2 and T_{mad} [43].*

To estimate the (T_{mad}, T_2) trade-off curves, one needs to follow the following two steps. As first step, given the values of γ and matrices A_{11}, A_{12}, A_{13}, A_{21}, A_{22}, and A_{23} as in (4.4), one can set up the optimization problem

$$\begin{aligned} \underset{P,\,\mu}{\text{minimize}} \quad & \theta \\ \text{subject to} \quad & P \in \mathcal{S}_+^{n_{x_{cl}}}, \mathcal{F}_0 \preceq 0 \end{aligned} \quad (4.14)$$

which can be efficiently solved via available semidefinite programming tools [12]. Next step is to determine the (T_{mad}, T_2) trade-off curve. A single (T_{mad}, T_2) combination is obtained by using the solutions of (4.11) for a finite set of initial conditions. In particular, for each $\lambda \in (0, 1)$, $l \in \{0, 1\}$, one can solve the differential equation (4.11) with initial conditions

$$\phi_0(0) = \frac{1}{\lambda},\ \phi_1(0) \in \left(\frac{\phi_0\gamma_0}{\gamma_1}, \frac{\phi_0\gamma_0}{\gamma_1\lambda}\right) \quad (4.15)$$

For each given solution of ϕ_l, for $l \in \{0, 1\}$, the value of T_{mad} is computed as the intersection between the functions $\gamma_0\phi_0$ and $\gamma_1\phi_1$, while T_2 is obtained as intersection between $\gamma_0\phi_0$ and $\lambda^2\gamma_1\phi_1(0)$, see also [43] for further details. Then, the above procedure needs to be repeated for various values of λ and $\phi_1(0)$ in order to compute other (T_{mad}, T_2)-combinations which lead to establish the (T_{mad}, T_2)-trade-off curve.

4.4 Trade-off Curves Estimation for NCS: A Direct Approach

In this section, we provide Lyapunov-like conditions to ensure: 0-input global exponential stability of a closed set containing the origin of the interconnection of the plant and the controller, and $\mathcal{L}_2$ external stability from an exogenous disturbance to a given performance output. From stability conditions, we obtain a set of linear matrix inequalities that are employed in a computationally affordable algorithm to estimate the trade-off curves is proposed. Trade-off curves are estimated by solving LMIs explicitly, including the values of MATI and MAD.

4.4.1 Modeling

To properly address the stability analysis from a direct approach point of view, we need to suitably manipulate the hybrid system $\mathcal{H}_y$ in (3.6). In particular, we perform the following change of coordinates:

$$\eta := \hat{y} - y, \, \sigma := s_y - y \tag{4.16}$$

By straightforward calculations, one can obtain the closed-loop hybrid system in the new coordinates which reads as follows:

$$\mathcal{H}_{cl_D} \begin{cases} \dot{x}_D = f_D(x_D, \omega) & x_D \in C_D, \omega \in \Re^{n_\omega} \\ x_D^+ = g_D(x_D) & x_D \in D_D \\ y_o = \bar{C}_o x_{cl} \end{cases} \tag{4.17}$$

where $x_D := (x_{cl}, \eta, \sigma, \tau, l) \in \mathfrak{R}^{n_x}$ is the state. The flow map is given, $\forall x_D \in C_D, \omega \in \mathfrak{R}^{n_\omega}$, by

$$f_D(x_D, \omega) := \begin{bmatrix} A_{xx}x_{cl} + A_{x\eta}\eta + A_{x\omega}\omega \\ A_{\eta x}x_{cl} + A_{\eta\eta}\eta + A_{\eta\omega}\omega \\ A_{\sigma x}x_{cl} + A_{\sigma\eta}\eta + A_{\sigma\omega}\omega \\ 1 \\ 0 \end{bmatrix} \tag{4.18}$$

where

$$\begin{gathered} A_{xx} := \left[\begin{array}{c|c} A_p + B_pD_cC_p & B_pC_c \\ \hline B_cC_p & A_c \end{array}\right], \; A_{x\eta} := \left[\begin{array}{c} B_pD_c \\ \hline B_c \end{array}\right], \; A_{x\omega} := \left[\begin{array}{c} W \\ \hline \mathbf{0} \end{array}\right], \\ A_{\sigma x} := -\left[\begin{array}{c|c} C_pA_p + C_pB_pD_cC_p & C_pB_pC_c \end{array}\right], \; A_{\sigma\eta} := -C_pB_pD_c, \; A_{\sigma\omega} := -C_pW, \\ A_{\eta x} := \left[\begin{array}{c|c} HC_p & E \end{array}\right] + A_{\sigma x}, \; A_{\eta\eta} := H + A_{\sigma\eta}, \; A_{\eta\omega} := A_{\sigma\omega} \end{gathered} \tag{4.19}$$

derive from (3.1), (3.2) and (4.16). The jump map is defined for all $x \in D_D$ by

$$g_D(x) := \begin{bmatrix} x_{cl} \\ l\sigma + (1-l)\eta \\ l\sigma \\ l\tau \\ 1-l \end{bmatrix} \tag{4.20}$$

The flow set C_D and the jump set D_D are respectively defined as

$$C_D := \{x_D \in \mathfrak{R}^{n_x} | (l = 0 \wedge \tau \in [0, T_2]) \vee (l = 1 \wedge \tau \in [0, T_{mad}])\} \tag{4.21}$$

and

$$D_D := \{x_D \in \mathfrak{R}^{n_x} | (l = 0 \wedge \tau \in [T_1, T_2]) \vee (l = 1 \wedge \tau \in [0, T_{mad}])\} \tag{4.22}$$

4.4.2 Stability Results

To solve Problem 4.2.1, the direct approach consists of deriving sufficient conditions in the form of matrix inequalities ensuring that the following set

$$\mathcal{A} := \{0\} \times \{0\} \times \{0\} \times [0, T_2] \times \{0, 1\} \tag{4.23}$$

is exponentially stable whenever $\omega \equiv 0$ and, in case of nonzero disturbance ω, the hybrid system $\mathcal{H}_{cl_D}$ in (3.6) is input-to-state stable with respect to $\mathcal{A}$.

Definition 2.3.1 introduced in Chapter 2 will be employed in the following to obtain sufficient conditions for the stability of $\mathcal{H}_{cl_D}$ with respect to $\mathcal{A}$. At this stage, consider the following assumption.

Assumption 4.4.1. *Let γ be a given positive real number. There exist three continuously differentiable functions $V_1 : \mathfrak{R}^{n_{x_{cl}}} \to \mathfrak{R}$, $V_2 : \mathfrak{R}^{n_y+2} \to \mathfrak{R}$, $V_3 : \mathfrak{R}^{n_y+2} \to \mathfrak{R}$ and positive real numbers α_1, α_2, β_1, β_2, θ_1, θ_2, and λ_t, such that*

(A1) $\alpha_1 |x_{cl}|^2 \leq V_1(x_{cl}) \leq \alpha_2 |x_{cl}|^2, \quad \forall x \in C$

(A2) $\beta_1 |\eta|^2 \leq V_2(\eta, \tau, l) \leq \beta_2 |\eta|^2, \quad \forall x \in C$

(A3) $\theta_1 |\sigma|^2 \leq V_3(\sigma, \tau, l) \leq \theta_2 |\sigma|^2, \quad \forall x \in C$

(A4) $V_2(\eta, 0, 1) + V_3(0, 0, 1) \leq V_2(\eta, \tau, 0) + V_3(\sigma, \tau, 0)$, $\forall \eta \in \mathfrak{R}^{n_y}$, $\sigma \in \mathfrak{R}^{n_y}$, $\tau \in [T_1, T_2]$

(A5) $V_2(\sigma, \tau, 0) + V_3(\sigma, \tau, 0) \leq V_2(\eta, \tau, 1) + V_3(\sigma, \tau, 1)$, $\forall \eta \in \mathfrak{R}^{n_y}$, $\sigma \in \mathfrak{R}^{n_y}$, $\tau \in [0, T_{mad}]$

(A6) the function $x \mapsto V(x) := V_1(x_{cl}) + V_2(\eta, \tau, l) + V_3(\sigma, \tau, l)$ satisfies $\langle \nabla V(x), f(x, \omega) \rangle \leq -2\lambda_t V(x) - x_{cl}^\top \bar{C}_o^\top \bar{C}_o x_{cl} + \gamma^2 \omega^\top \omega$ for each $x \in C, \omega \in \mathfrak{R}^{n_\omega}$

The result given next provides sufficient conditions for the solution to Problem 4.2.1.

Theorem 4.4.1. *Let Assumption 4.4.1 hold. Then:*

(i) The hybrid system $\mathcal{H}_{cl_D}$ is eISS with respect to $\mathcal{A}$;

(ii) There exists $\alpha > 0$ such that any solution pair (ϕ, ω) to $\mathcal{H}_{cl_D}$ satisfies

$$\sqrt{\int_{\mathcal{I}} |y_o(r, j(r))|^2 dr} \leq \alpha |\phi(0,0)|_{\mathcal{A}} + \gamma \sqrt{\int_{\mathcal{I}} |\omega(r, j(r))|^2 dr} \tag{4.24}$$

where $\mathcal{I} := [0, \sup_t \operatorname{dom} \phi] \cap \operatorname{dom}_t \phi$.

The proof is given in Appendix B.

4.4.3 Construction of the Lyapunov Function

To determine the values of T_2 and T_{mad}, one needs to explicitely identify functions V_1, V_2 and V_3 in Assumption 4.4.1. Let $P_1 \in \mathcal{S}_+^{n_{x_{cl}}}$,

$$P_{2,l} := (1-l)P_{2,0} + lP_{2,1},\ P_{3,l} := (1-l)P_{3,0} + lP_{3,1} \tag{4.25}$$

with $P_{2,0}$, $P_{2,1}$, $P_{3,0}$, $P_{3,1} \in \mathcal{S}_+^{n_y}$, $l \in \{0,1\}$, and δ be positive real number. Inspired by [28] we operate the following selection:

$$V_1(x_{cl}) = x_{cl}^\top P_1 x_{cl}, \quad V_2(\eta, \tau, l) = e^{-\delta\tau}\eta^\top P_{2,l}\eta, \quad V_3(\sigma, \tau, l) = e^{-\delta\tau}\sigma^\top P_{3,l}\sigma \tag{4.26}$$

By exploiting the (quasi)-quadratic nature of the Lyapunov function candidate $x \mapsto V_1(x_{cl}) + V_2(\eta, \tau, l) + V_3(\sigma, \tau, l)$, such a choice for V_1, V_2, and V_3 allows us to cast the solution to Problem 4.2.1 as a solution to some matrix inequalities.

Theorem 4.4.2. *If there exist $P_1 \in \mathcal{S}_+^{n_{x_{cl}}}$, $P_{2,0}$, $P_{2,1}$, $P_{3,0}$, and $P_{3,1} \in \mathcal{S}_+^{n_y}$ with*

$$P_{2,1} - e^{-\delta T_2} P_{2,0} \preceq 0 \tag{4.27a}$$

$$P_{2,0} + P_{3,0} - P_{3,1} \preceq 0 \tag{4.27b}$$

such that

$$\begin{aligned} \mathcal{M}(0,1) \prec 0 \qquad \mathcal{M}(T_{mad}, 1) \prec 0 \\ \mathcal{M}(T_{mad}, 0) \prec 0 \qquad \mathcal{M}(T_2, 0) \prec 0 \end{aligned} \tag{4.28}$$

where for each $\tau \in [0, T_2]$ *and* $l \in \{0, 1\}$

$$\mathcal{M}(\tau, l) = \begin{bmatrix} He(P_1 A_{xx}) + \bar{C}_o^\top \bar{C}_o & P_1 A_{x\eta} + e^{-\delta\tau} A_{\eta x}^\top P_{2,l} & e^{-\delta\tau} A_{\sigma x}^\top P_{3,l} & P_1 A_{x\omega} \\ \bullet & e^{-\delta\tau} (\mathrm{He}(P_{2,l} A_{\eta\eta}) - \delta P_{2,l}) & e^{-\delta\tau} A_{\sigma\eta}^\top P_{3,l} & e^{-\delta\tau} P_{2,l} A_{\eta\omega} \\ \bullet & \bullet & -\delta e^{-\delta\tau} P_{3,l} & e^{-\delta\tau} P_{3,l} A_{\sigma\omega} \\ \bullet & \bullet & \bullet & -\gamma^2 \boldsymbol{I} \end{bmatrix} \tag{4.29}$$

then the Assumption 4.4.1 holds.

The proof is given in Appendix B.

Remark 4.4.1. *Conditions* (4.27) *and* (4.28) *with* $\mathcal{M}(\tau, l)$ *without the forth row and the forth column, and* $C_o = \boldsymbol{0}$ *are sufficient conditions to solve Problem 4.2.1 when only the internal exponential stability* ($\omega \equiv 0$) *is considered.*

4.4.4 LMI-Based Algorithm for (T_{mad}, T_2) Trade-off Curves Estimation

In the previous subsection, we provided sufficient conditions for the solution to Problem 4.2.1 in the form of matrix inequalities. The objective of the current subsection is to make use of the proposed sufficient conditions to include some optimization aspects in the solution to Problem 4.2.1. In particular, as our goal is to provide estimates of the largest allowable transmission interval and communication delay, next we illustrate an algorithm for the approximation of the trade-off curve between this two objectives. Specifically, to accomplish this goal, we make use of conditions (4.27) and (4.28) to formulate the following optimization problem:

$$\begin{array}{ll} \underset{P_1, P_{2,0}, P_{2,1}, P_{3,0}, P_{3,1}, \delta}{\text{maximize}} & (T_2, T_{mad}) \\ \text{subject to} & (4.27), (4.28), T_{mad} \in [0, T_2] \end{array} \tag{4.30}$$

where the above maximization is intended in a Pareto sense [13]. In particular, we provide a systematic approach to build an approximation of the trade-off curve of the above multi-objective optimization problem. Notice that we assume the value of γ is given and strictly positive. To obtain a numerically efficient solution to (4.30), we make use of semidefinite programming tools. Specifically, observe that when δ, T_2, and T_{mad} are fixed, conditions (4.27) and (4.28) turn into LMIs, which can be efficiently solved via available semidefinite programming solvers [12]. Therefore, checking the feasibility of (4.27) and (4.28) can be used in a numerical scheme by performing line search for the scalars δ, T_2, and T_{mad}.

Algorithm 1 describes our approach to solve the optimization problem (4.30). The algorithm gives as output the vectors $\vec{T_2}$ and $\vec{T}_{mad}$ that provide an estimation of the trade-off curve between T_2 and T_{mad}. Indeed, the trade-off curve identifies the maximum allowable delay for each given value of the transmission interval. In particular, given the value of T_2, one can identify the maximum allowable delay that can affect the last received packet without compromising the stability of the NCS.

Algorithm 1 Trade-off curve approximation

1: Define a grid $\vec{T_2} \subset \Re_{>0}$ containing a finite number of values for T_2.
2: **for** i=1 to size of $\vec{T_2}$ **do**
3: $\quad T_M \leftarrow \vec{T_2}[i]$
4: $\quad$ maximize T_m on $[0, T_M]$ subject to (4.27)-(4.28) by performing line search on δ for given value of T_M.
5: $\quad \vec{T}_{mad}[i] \leftarrow T_m$
6: **end for**
7: **return** $\vec{T}_{mad}$, $\vec{T_2}$

Algorithm 1 gives as outputs the vectors $\vec{T_2}$ and $\vec{T}_{mad}$ that, if plotted, provides an estimation of the trade-off curves between T_2 and T_{mad}. Indeed, the trade-off curve identifies the maximum allowable delay for each given value of T_2 and identifies the greatest maximum allowable transmission interval in correspondence to $T_{mad} = 0$.

4.5 Numerical Examples

In this section, we showcase Algorithm 1. All the following numerical results are obtained through the solver *SEDUMI* [102] and coded in Matlab® via *YALMIP* [61].

Two examples are considered. In the first example, we consider the well-known batch reactor controlled by a dynamic output feedback controller, presented, e.g., in [43] and many others. The second example pertains to state feedback control. In these examples, we consider $\mathcal{J}$ being a ZOH device; see Remark 3.2.1. The two approaches introduced in this chapter are considered. In particular, trade-off curves computed with the approaches in Section 4.3 and Section 4.4 are computed and compared.

Example 4.5.1. *We consider the well known batch reactor controlled by a dynamic output feedback controller presented, e.g., in [43, 78] and many others. Numerical values of the plant and controller can be found in [78] as follows*

$$\begin{gathered} A_p = \begin{bmatrix} 1.38 & -0.207 & 6.715 & -5.676 \\ -0.5814 & -4.29 & 0 & 0.675 \\ 1.067 & 4.273 & -6.654 & 5.893 \\ 0.048 & 4.273 & 1.343 & -2.104 \end{bmatrix}, \\ B_p = \begin{bmatrix} 0 & 0 \\ 5.679 & 0 \\ 1.136 & -3.146 \\ 1.136 & 0 \end{bmatrix}, C_p = \begin{bmatrix} 1 & 0 & 1 & -1 \\ 0 & 1 & 0 & 0 \end{bmatrix} \end{gathered} \tag{4.31}$$

while

$$C_o = C_p \tag{4.32}$$

and

$$W = \begin{bmatrix} 10 & 0 & 10 & 0 \\ 0 & 5 & 0 & 5 \end{bmatrix}^\top \tag{4.33}$$

can be found in [43]. The controller

$$A_c = \begin{bmatrix} 0 & 0 \\ 0 & 0 \end{bmatrix}, B_c = \begin{bmatrix} 0 & 1 \\ 1 & 0 \end{bmatrix}, C_c = -\begin{bmatrix} 2 & 0 \\ 0 & -8 \end{bmatrix}, D_c = -\begin{bmatrix} 0 & 2 \\ -5 & 0 \end{bmatrix} \tag{4.34}$$

is the same introduced in [78].

The input-output stability is studied for different values of $\mathcal{L}_2$ gains: $\gamma \leq 2.5$ and $\gamma \leq 5$. In Fig. 4.1 are depicted the trade-off curves obtained by using the two approaches described in this chapter.

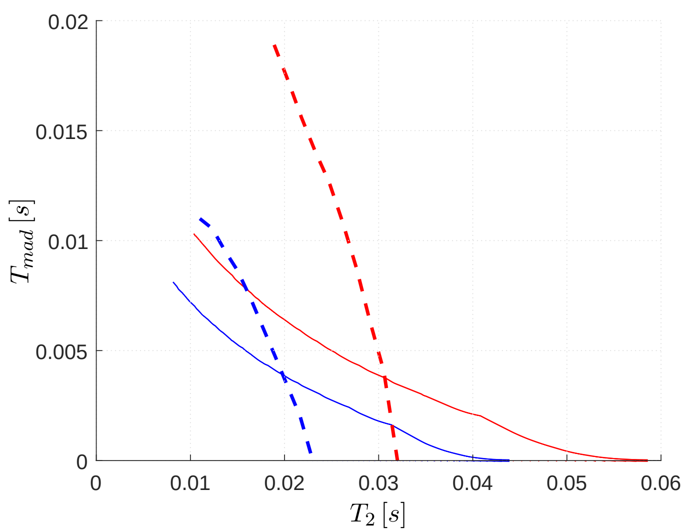

Figure 4.1: Trade-off curves between T_2 and T_{mad} computed for the NCS in Example 4.5.1 for different values of $\mathcal{L}_2$ gains: 2.5 (in blue) and 5 (in red). Dashed lines represent the trade-off curves computed by following Algorithm 1 in Section 4.4, whereas continuous lines represent the trade-off curves obtained by following the approach in Section 4.3. Note that the trade-off curves end where $T_2 = T_{mad}$.

Example 4.5.2. *We consider an unstable plant stabilized by a state feedback controller through the network. Numerical values of plant and controller are given as follows [54]:*

$$A_p = \begin{bmatrix} 0 & 1 \\ 1 & 0 \end{bmatrix}, B_p = \begin{bmatrix} 0 \\ -1 \end{bmatrix}, K_c = \begin{bmatrix} 2 & 2 \end{bmatrix}$$

In Fig. 4.2 the trade-off curves are depicted. Note that in this example, Remarks 3.3.1 and

4.4.1 are employed.

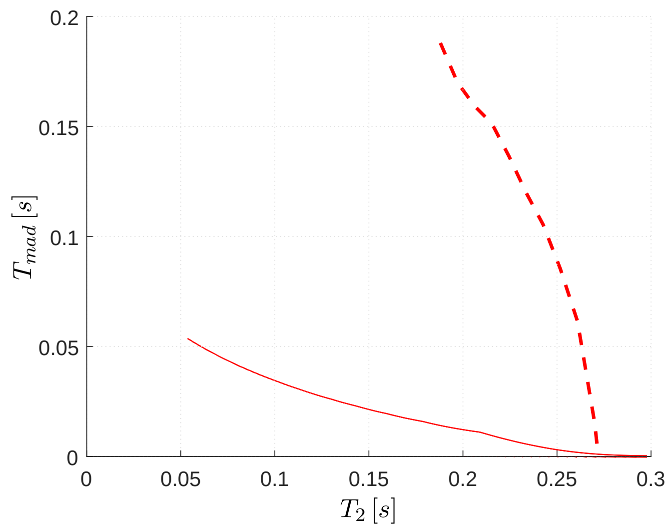

Figure 4.2: Trade-off curves between T_2 and T_{mad} computed for the NCS in Example 4.5.2. Dashed lines represent the trade-off curves computed by following Algorithm 1 in Section 4.4, whereas continuous lines represent the trade-off curves obtained by following the approach in Section 4.3. Note that the trade-off curves end where $T_2 = T_{mad}$.

Observe that in Fig. 4.1 and Fig. 4.2 the trade-off curves end where $T_2 = T_{mad}$ even though for those points the trade-off curves exist. In fact, a straight line from the origin to the left top point of each curve could be drawn, but it would have complicated the readability of the figures. This limitation on T_2 and T_{mad} is due to the fact that the model does not include delays larger than the transmission intervals; see Section 3.2.2.

From the examples, it emerges that the two approaches provide different trade-off curves. In particular, for the considered examples, the indirect approach (Section 4.3) provides a less conservative estimation of the trade-off curves regarding the value of T_2; the direct approach (Section 4.4), instead, provides a less conservative estimation of T_{mad}. In more detail, the indirect approach allows estimating trade-off curves that have larger maximum transmission intervals, whereas the direct approach provides an estimation of trade-off curves that have larger maximum allowable delays.

It is worthwhile remarking that the direct approach in Section 4.4 enables the estimation of trade-off curves for NCS with a holding device as in (3.3), while the indirect approach can take into account only ZOH.

4.6 Conclusion

In this chapter, we present two methodologies for studying the stability of NCSs affected by variable transmission intervals and variable transmission delays. The main goal of these two approaches is to estimate the trade-off curves between the maximum allowable transmission intervals and the maximum allowable network delays. The first approach assumes NCS with ZOH as the holding device and provides a tool to indirectly estimate the trade-off curves after solving some LMIs. The second approach takes into account holding device as in (3.3), and provides a tool to estimate trade-off curves directly from the solutions of some LMI. Indeed, in the latter case, MATI and MAD explicitly appear in the resulting conditions. The two approaches are compared through numerical results. It emerges that the indirect approach allows estimating trade-off curves that have larger maximum transmission intervals, whereas the direct approach provides an estimation of trade-off curves that have larger maximum allowable delays.

Chapter 5

$\mathcal{H}_\infty$ Control Design of Network-Resilient Control Systems

5.1 Introduction

This chapter considers the problem of stabilizing a linear time-invariant system in the presence of plant measurements that are available in an intermittent fashion. In particular, we consider NCSs as introduced in Chapter 3, and we propose a methodology for the co-design of output feedback dynamic controller and holding device. In this chapter, we propose a dynamic output feedback controller equipped with a holding device that is a linear time-invariant system whose state is reset when a new measure is available. We provide an LMI-based design procedure for the co-design of the parameters of the dynamic controller and holding device. Our approach relies on the Lyapunov theory for hybrid systems and addresses stability analysis in a way that is reminiscent of an “input-to-state stability small gain” philosophy. The effectiveness of the proposed LMI-based design is showcased in a numerical example.

5.2 Problem Statement and Solution Outline

5.2.1 System Description

We consider NCSs introduced in Chapter 3 and depicted in Fig. 3.1. In particular, we assume the plant $\mathcal{P}$ is stabilized by a linear time-invariant dynamic controller $\mathcal{K}$ that relies on a holding device $\mathcal{J}$, which is a linear time-invariant system whose state is reset to the plant measurement whenever a new measurement is received. This holding device generates a continuous-time signal that feeds a linear time-invariant dynamic controller; see Chapter 3 for further details. In this chapter, we aim the design of the controller and holding device. To this end, in the following, we consider NCSs, as in Fig. 5.1, where the network is characterized only by variable transmission intervals. This differs from previous Chapters 3 and 4, where variable transmission intervals and network delays are considered together. However, simplifying the network makes the control problem more tractable and allows us to devise a design procedure. More in details, we assume output measurements of plant $\mathcal{P}$ are measurable only at some time instances t_k, $k \in \mathfrak{N}_{>0}$, not known in advance. In particular, we assume that the sequence $\{t_k\}_{k=1}^{\infty}$ is strictly increasing and unbounded, and that there exist two positive real scalars $T_1 \leq T_2$ such that

$$0 \leq t_1 \leq T_2, \quad T_1 \leq t_{k+1} - t_k \leq T_2 \quad \forall k \in \mathfrak{N}_{>0} \tag{5.1}$$

The lower bound T_1 in condition (5.1) introduces a strictly positive minimum time in between consecutive measurements. As such, this avoids the existence of Zeno behaviors, which are unwanted in practice [37]. Moreover, T_2 defines the Maximum Allowable Transmission Interval (MATI).

Given plant $\mathcal{P}$ and the measurement setup above, the problem we solve in this chapter is to design an output feedback dynamic controller such that the closed-loop NCS is input-output exponentially stable with some required performance satisfied with the largest achievable value of T_2; a formal problem statement will be provided next in the chapter. To

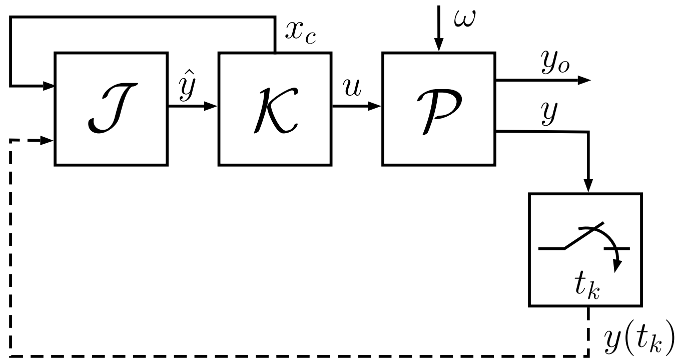

Figure 5.1: Schematic representation of the NCS considered for the design of holding device and controller. Solid lines represent the continuous-time signals, whereas the dashed line depicts the sporadic measurements.

this end, we consider the plant $\mathcal{P}$ as in (3.1), and we design the controller $\mathcal{K}$ and holding device $\mathcal{J}$. The proposed controller is an output-feedback dynamic controller as in (3.2). The proposed holding device $\mathcal{J}$ is selected as follows:

$$\mathcal{J}\begin{cases} \dot{\hat{y}}(t) = \widehat{H}\hat{y}(t) + \widehat{E}x_c(t) + C_pB_pu(t) & \forall t \neq t_k \\ \hat{y}(t^+) = y(t) & \forall t = t_k \end{cases} \tag{5.2}$$

which reads as (3.3) with

$$\begin{aligned} H &= \widehat{H} + C_pB_pD_c \\ E &= \widehat{E} + C_pB_pC_c \end{aligned} \tag{5.3}$$

This choice of $\mathcal{J}$ simplifies the dynamics of the closed-loop NCS enabling the design of holding device and controller as shown next in this chapter.

5.2.2 Hybrid Modeling

The closed-loop system in Fig. 5.1 can be modeled as a linear system with jumps in $\hat{y}$. In particular, for all $k \in \mathfrak{N}_0$ one obtains

$$\left.\begin{aligned} \dot{x}_p(t) &= A_p x_p(t) + B_p C_c x_c(t) + B_p D_c \hat{y}(t) + W\omega(t) \\ \dot{x}_c(t) &= A_c x_c(t) + B_c \hat{y}(t) \\ \dot{\hat{y}}(t) &= (\widehat{H} + C_p B_p D_c)\hat{y}(t) + (\widehat{E} + C_p B_p C_c) x_c(t) \end{aligned}\right\} \quad \forall t \neq t_k$$
$$\left.\begin{aligned} x_p(t^+) &= x_p(t) \\ x_c(t^+) &= x_c(t) \\ \hat{y}(t^+) &= C_p x_p(t) \end{aligned}\right\} \quad \forall t = t_k \tag{5.4}$$

To devise a design algorithm for $\mathcal{K}$ and $\mathcal{J}$, we model the impulsive system in (5.4) into the hybrid system framework in [37]; see for a brief introduction Chapter 2. To this end, we augment the state of the closed-loop system with the auxiliary variable $\tau \in \mathfrak{R}_{\geq 0}$, which is a timer that keeps track of the duration of intervals in between transmissions. As in [30], to enforce (5.1), we make τ decrease as ordinary time t increases and, whenever $\tau = 0$, reset it to any point in $[T_1, T_2]$. The whole closed-loop system composed by the states x_p, x_c, $\hat{y}$, and τ can be represented by the following hybrid system:

$$\begin{cases} \dot{\xi} = f_\xi(\xi, \omega) & \xi \in \mathcal{C},\ \omega \in \mathfrak{R}^{n_\omega} \\ \xi^+ \in G_\xi(\xi) & \xi \in \mathcal{D} \\ y_o = \bar{C}_o(x_p, x_c) \end{cases} \tag{5.5}$$

where $\xi := (x_p, x_c, \hat{y}, \tau) \in \mathfrak{R}^{n_\xi}$ with $n_\xi := n_{x_p} + n_{x_c} + n_y + 1$ is the state of the hybrid system,

$$f_\xi(\xi, \omega) := \begin{bmatrix} A_p x_p + B_p C_c x_c + B_p D_c \hat{y} + W\omega \\ A_c x_c + B_c \hat{y} \\ (\widehat{H} + C_p B_p D_c)\hat{y} + (\widehat{E} + C_p B_p C_c) x_c \\ -1 \end{bmatrix} \tag{5.6}$$

is the flow map,

$$G_\xi(\xi) := \begin{bmatrix} x_p \\ x_c \\ C_p x_p \\ [T_1, T_2] \end{bmatrix} \tag{5.7}$$

is the jump map, and the the flow set $\mathcal{C}$ and the jump set $\mathcal{D}$ are defined as follows

$$\mathcal{C} := \Re^{n_p+n_c+n_y} \times [0, T_2], \quad \mathcal{D} := \Re^{n_p+n_c+n_y} \times \{0\} \tag{5.8}$$

The set-valued jump map allows to capture all possible transmission intervals of length within T_1 and T_2. Specifically, the hybrid model in (5.5) is able to characterize any sequence satisfying (5.1).

At this stage, to simplify the analysis, we introduce the change of coordinates

$$\eta := y - \hat{y} \tag{5.9}$$

which leads, by straightforward calculations, to the closed-loop hybrid system in the new coordinates:

$$\mathcal{H}_{cl} \begin{cases} \dot{x} = f(x, \omega) & x \in \mathcal{C},\ \omega \in \Re^{n_\omega} \\ x^+ \in G(x) & x \in \mathcal{D} \\ y_o = \bar{C}_o x_{cl} \end{cases} \tag{5.10}$$

where $x := (x_{cl}, \eta, \tau) \in \mathcal{X} := \Re^{n_p+n_c+n_y+1}$ is the state, and $x_{cl} := (x_p, x_c)$. The flow map is given by

$$f(x) := (\mathbb{A}x_{cl} + \mathbb{B}\eta + \mathbb{V}\omega, \mathbb{J}x_{cl} + \widehat{H}\eta + \mathbb{W}\omega, -1) \quad \forall x \in \mathcal{C},\ \omega \in \Re^{n_\omega} \tag{5.11}$$

where

$$\mathbb{A} := \left[\begin{array}{c|c} A_p + B_p D_c C_p & B_p C_c \\ \hline B_c C_p & A_c \end{array}\right], \quad \mathbb{B} := -\left[\begin{array}{c} B_p D_c \\ \hline B_c \end{array}\right], \quad \mathbb{V} := \left[\begin{array}{c} W \\ \hline \mathbf{0} \end{array}\right], \tag{5.12}$$

$$\mathbb{J} := \left[\begin{array}{c|c} C_p A_p - \widehat{H} C_p & -\widehat{E} \end{array}\right], \quad \mathbb{W} := C_p W$$

derive from (3.1), (3.2), (5.2), and (5.9). The jump map is defined for all $x \in \mathcal{D}$ by

$$G(x) := \begin{bmatrix} x_{cl} \\ 0 \\ [T_1, T_2] \end{bmatrix} \tag{5.13}$$

Observe that, as shown in Fig. 5.2, $\mathcal{H}_{cl}$ can be interpreted as the feedback interconnection of two different dynamical systems $\Sigma_{x_{cl}}$ and Σ_η. In particular, $\Sigma_{x_{cl}}$ is a continuous-time system described by:

$$\Sigma_{x_{cl}} \begin{cases} \dot{x}_{cl} = \mathbb{A} x_{cl} + \mathbb{B}\eta + \mathbb{V}\omega \\ y_o = \bar{C}_o x_{cl} \end{cases} \tag{5.14}$$

whereas Σ_η is a hybrid dynamical system given as follows:

$$\Sigma_\eta \begin{cases} \begin{bmatrix} \dot{\eta} \\ \dot{\tau} \end{bmatrix} = \begin{bmatrix} \widehat{H}\eta + \mathbb{J} x_{cl} + \mathbb{W}\omega \\ -1 \end{bmatrix} & \eta \in \mathfrak{R}^{n_y},\ x_{cl} \in \mathfrak{R}^{n_p + n_c},\ \omega \in \mathfrak{R}^{n_\omega},\ \tau \in [0, T_2] \\ \begin{bmatrix} \eta^+ \\ \tau^+ \end{bmatrix} \in \begin{bmatrix} 0 \\ [T_1, T_2] \end{bmatrix} & \eta \in \mathfrak{R}^{n_y}, \tau = 0 \end{cases} \tag{5.15}$$

It is worth mentioning that considering $\mathcal{H}_{cl}$ as the interconnection of $\Sigma_{x_{cl}}$ and Σ_η allows us to address stability analysis of the closed-loop system by employing an approach that is reminiscent of an "input-to-state stability small gain" philosophy [48]. A conceptually similar approach can be found in [16].

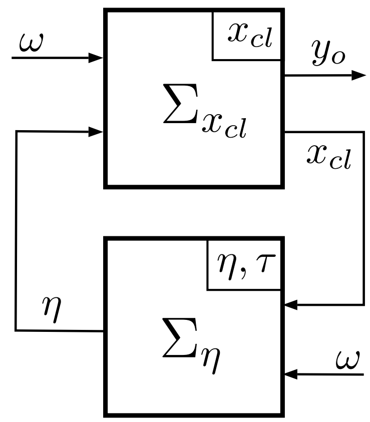

Figure 5.2: Representation of $\mathcal{H}_{cl}$ as the interconnection of the dynamical systems $\Sigma_{x_{cl}}$ and Σ_η.

5.2.3 Problem Statement

To formalize our control problem, we rely on the notions of exponential input-to-state stability of closed sets for a generic hybrid system $\mathcal{H}$ with state in $\mathfrak{R}^n$; see Definition 2.3.1 introduced in Chapter 2 for further details.

The proposed approach aims at designing the holding device $\mathcal{J}$ and the controller $\mathcal{K}$ such that without disturbance, i.e., $\omega \equiv 0$, the following set[1]

$$\mathcal{A} := \{0\} \times \{0\} \times [0, T_2] \tag{5.16}$$

is exponentially stable, and, when the disturbances are nonzero, the hybrid system $\mathcal{H}_{cl}$ is input-to-state stable with respect to $\mathcal{A}$. In particular, the problem we solve is as follows:

Problem 5.2.1. *Given the plant $\mathcal{P}$ in* (3.1)*, design*

$$\Delta_{\mathcal{K}} := \left[\begin{array}{c|c} A_c & B_c \\ \hline C_c & D_c \end{array}\right], \quad \Delta_{\mathcal{J}} = \left[\begin{array}{c|c} \widehat{H} & \widehat{E} \end{array}\right] \tag{5.17}$$

such that the closed-loop system satisfies the following properties with the largest achievable value of T_2:

[1]Notice that, by definition of the system $\mathcal{H}_{cl}$ and of the set $\mathcal{A}$, for all $x \in \mathcal{C}$, one has $|x|_{\mathcal{A}} = |(x_{cl}, \eta)|$.

(P1) the set $\mathcal{A}$ is global exponentially stable when the input ω is identically zero;

(P2) when the disturbance ω is nonzero, the hybrid system $\mathcal{H}_{cl}$ in (5.10) *is input-to-state stable with respect to $\mathcal{A}$;*

(P3) $\mathcal{L}_2$ stability from the disturbance ω to the performance output y_o is ensured with a desired $\mathcal{L}_2$-gain γ.

5.3 Lyapunov-based Stability Analysis

In a naive way, sufficient conditions to enforce the stability properties required in Problem 5.2.1 could be derived by following results in [68]. However, those results would lead to matrix inequalities having the controller's and holding device's parameters appearing in a nonlinear fashion. Therefore, this approach turns into conditions that are not computationally tractable to provide a viable solution to Problem 5.2.1. With the purpose of obtaining more tractable conditions, in this chapter, we consider the closed-loop hybrid system $\mathcal{H}_{cl}$ as the interconnection of two dynamical systems $\Sigma_{x_{cl}}$ and Σ_η as depicted in Fig. 5.2. Moreover, we exploit such a structural characteristic of $\mathcal{H}_{cl}$ to introduce conditions on the single systems $\Sigma_{x_{cl}}$ and Σ_η, and their interconnection such that requirements in Problem 5.2.1 are satisfied. In particular, consider the following property:

Property 5.3.1. *There exist continuously differentiable functions $V_1\colon \mathfrak{R}^{n_p+n_c} \to \mathfrak{R}$ and $V_2\colon \mathfrak{R}^{n_y+1} \to \mathfrak{R}$, positive definite functions $\rho_1\colon \mathfrak{R}^{n_p+n_c} \to \mathfrak{R}$ and $\sigma_1\colon \mathfrak{R}^{n_y} \to \mathfrak{R}$, functions $\rho_2\colon \mathfrak{R}^{n_y} \to \mathfrak{R}$ and $\sigma_2\colon \mathfrak{R}^{n_c+n_p} \to \mathfrak{R}$, and some positive scalars $\overline{c}_{v_1}, \overline{c}_{v_2}, \underline{c}_{v_1}, \underline{c}_{v_2}, k_{v_1}$, and k_{v_2} such that*

$$\underline{c}_{v_1}|x_{cl}|^2 \leq V_1(x_{cl}) \leq \overline{c}_{v_1}|x_{cl}|^2, \quad \forall x_{cl} \in \mathfrak{R}^{n_p+n_c} \tag{5.18a}$$

$$\underline{c}_{v_2}|\eta|^2 \leq V_2(\eta,\tau) \leq \overline{c}_{v_2}|\eta|^2, \quad \forall (\eta,\tau) \in \mathfrak{R}^{n_y+1} \tag{5.18b}$$

$$\langle \nabla V_1(x_{cl}), \mathbb{A}x_{cl} + \mathbb{B}q_1 + \mathbb{V}\omega \rangle \leq -\rho_1(x_{cl}) + \rho_2(q_1) + \rho_3(x_{cl}, \omega), \forall (x_{cl}, q_1) \in \mathfrak{R}^{n_p+n_c+n_y}, \omega \in \mathfrak{R}^{n_\omega} \tag{5.18c}$$

$$\begin{aligned} &\langle \nabla V_2(\eta, \tau), H\eta + \mathbb{J}q_2 + \mathbb{W}\omega \rangle \leq \\ &\qquad - \sigma_1(\eta) + \sigma_2(q_2) + \sigma_3(\omega), \forall (\eta, \tau, q_2) \in \mathfrak{R}^{n_y} \times [0, T_2] \times \mathfrak{R}^{n_p+n_c}, \omega \in \mathfrak{R}^{n_\omega} \end{aligned} \tag{5.18d}$$

$$-\rho_1(x_{cl}) + \sigma_2(x_{cl}) \leq -k_{v_1}|x_{cl}|^2, \quad \forall x_{cl} \in \mathfrak{R}^{n_p+n_c} \tag{5.18e}$$

$$-\sigma_1(\eta) + \rho_2(\eta) \leq -k_{v_2}|\eta|^2, \quad \forall \eta \in \mathfrak{R}^{n_y} \tag{5.18f}$$

$$\rho_3(x_{cl}, \omega) + \sigma_3(\omega) \leq -x_{cl}^\top \bar{C}_o^\top \bar{C}_o x_{cl} + \gamma^2 \omega^\top \omega, \forall x_{cl} \in \mathfrak{R}^{n_p+n_c}, \omega \in \mathfrak{R}^{n_\omega} \tag{5.18g}$$

Remark 5.3.1. *It is worth mentioning that conditions in Property 5.3.1 resemble Lyapunov inequalities for input-output stability. In particular, conditions* (5.18c) *and* (5.18d) *refer to input-output stability conditions for, respectively,* $\Sigma_{x_{cl}}$ *and* Σ_η*. Conditions* (5.18e), (5.18f) *and* (5.18g)*, instead, provide relations for the input-output stability of the system* $\mathcal{H}_{cl}$ *obtained by the interconnection of* $\Sigma_{x_{cl}}$ *and* Σ_η*.*

The following theorem employs Definition 2.3.1, and provides sufficient conditions for the solution to Problem 5.2.1.

Theorem 5.3.1. *Let Property 5.3.1 hold. Then:*

(i) The hybrid system $\mathcal{H}_{cl}$ *is eISS with respect to* $\mathcal{A}$*;*

(ii) There exists $\alpha > 0$ *such that any solution pair* (ϕ, ω) *to* $\mathcal{H}_{cl}$ *satisfies*

$$\sqrt{\int_{\mathcal{I}} |y_o(r, j(r))|^2 dr} \leq \alpha |\phi(0,0)|_{\mathcal{A}} + \gamma \sqrt{\int_{\mathcal{I}} |\omega(r, j(r))|^2 dr} \tag{5.19}$$

where $\mathcal{I} := [0, \sup_t \operatorname{dom} \phi] \cap \operatorname{dom}_t \phi$*.*

The proof is given in Appendix B.

With the purpose of deriving constructive design algorithms for the controller and the holding device, we perform a particular choice for the functions V_1 and V_2 in Property 5.3.1. In particular, let $P_1 \in \mathcal{S}_+^{n_p+n_c}$, $P_2 \in \mathcal{S}_+^{n_y}$, and δ a positive real number. Inspired by [30], we operate the following selection:

$$V_1(x_{cl}) \coloneqq x_{cl}^\top P_1 x_{cl}, \quad V_2(\eta, \tau) \coloneqq e^{\delta\tau} \eta^\top P_2 \eta \tag{5.20}$$

The structure of the selected functions V_1 and V_2 allows to provide sufficient conditions for stability properties required in Problem 5.2.1 in the form of matrix inequalities. To this end, consider the following proposition:

Proposition 5.3.1. *If there exist $P_1, S, R \in \mathcal{S}_+^{n_p+n_c}$, $P_2, Q, T \in \mathcal{S}_+^{n_y}$, positive real numbers $\delta, \gamma_1, \gamma_2$, and matrices $A_c \in \mathfrak{R}^{n_c \times n_c}$, $B_c \in \mathfrak{R}^{n_c \times n_y}$, $C_c \in \mathfrak{R}^{n_u \times n_c}$, $D_c \in \mathfrak{R}^{n_u \times n_y}$, $\widehat{H} \in \mathfrak{R}^{n_y \times n_y}$, and $\widehat{E} \in \mathfrak{R}^{n_y \times n_c}$, such that*

$$Q - T \prec 0 \tag{5.21a}$$

$$R - S \prec 0 \tag{5.21b}$$

$$\mathcal{M}_1 \coloneqq \begin{bmatrix} \mathrm{He}(P_1\mathbb{A}) + S + \bar{C}_o^\top \bar{C}_o & P_1\mathbb{B} & P_1\mathbb{V} \\ \bullet & -Q & 0 \\ \bullet & \bullet & -\gamma_1 \boldsymbol{I} \end{bmatrix} \preceq 0 \tag{5.21c}$$

$$\mathcal{M}_2(0) \preceq 0, \quad \mathcal{M}_2(T_2) \preceq 0 \tag{5.21d}$$

$$\gamma_1 + \gamma_2 \leq \gamma^2 \tag{5.21e}$$

where

$$[0, T_2] \in \tau \mapsto \mathcal{M}_2(\tau) := \begin{bmatrix} (\mathrm{He}(P_2\widehat{H}) - \delta P_2)e^{\delta\tau} + T & P_2\mathbb{J}e^{\delta\tau} & P_2\mathbb{W}e^{\delta\tau} \\ \bullet & -R & 0 \\ \bullet & \bullet & -\gamma_2\boldsymbol{I} \end{bmatrix} \tag{5.22}$$

then Property 5.3.1 holds.

The proof is given in Appendix B.

5.4 LMI-based Controller Design

In the previous section, sufficient conditions were provided to guarantee the stability properties required from Problem 5.2.1. In particular, through Proposition 5.3.1, these conditions turn into the feasibility problem of some matrix inequalities, which are not suitable to be a tool for the solution of Problem 5.2.1 because nonlinear in variables P_1, P_2, A_c, B_c, C_c, D_c, $\widehat{H}$, $\widehat{E}$, δ. Therefore, further manipulations are needed to derive a computationally efficient design procedure for the controller. While the nonlinearity in δ can be easily overcome through a line search, other nonlinearities must be properly treated. To this end, in the following, we provide sufficient conditions to turn the solution to Problem 5.2.1 into the feasibility problem of some LMIs.

Lemma 5.4.1. *Let $F \in \mathcal{S}_+^n$. Then, for any $\alpha \in \mathfrak{R}$ the following relation holds:*

$$F^{-1} - 2\alpha\mathbf{I} + \alpha^2 F \succeq 0 \tag{5.23}$$

The proof is given in Appendix B.

Theorem 5.4.1. *Given the plant $\mathcal{P}$ in (3.1), and scalars $\delta, \gamma_1, \gamma_2, T_2 \in \mathfrak{R}_{>0}$ and $\alpha \in \mathfrak{R}$. Assume there exist $P_2, T, Q \in \mathcal{S}_+^{n_y}$, $R, F \in \mathcal{S}_+^{2n_p}$, $X, Y \in \mathcal{S}_+^{n_p}$, $K \in \mathfrak{R}^{n_p \times n_p}$, $L \in \mathfrak{R}^{n_p \times n_y}$, $M \in \mathfrak{R}^{n_u \times n_p}$, $N \in \mathfrak{R}^{n_u \times n_y}$, $J \in \mathfrak{R}^{n_y \times n_y}$, $Z \in \mathfrak{R}^{n_y \times n_p}$, and a nonsingular matrix $V \in$*

$\mathfrak{R}^{n_p \times n_p}$, *such that*

$$\Theta := \begin{bmatrix} Y & \mathbf{I} \\ \mathbf{I} & X \end{bmatrix} \succ 0 \tag{5.24a}$$

$$Q - T \prec 0 \tag{5.24b}$$

$$R - 2\alpha I + \alpha^2 F \prec 0 \tag{5.24c}$$

$$\widehat{\mathcal{M}_1} := \begin{bmatrix} \mathrm{He}(\Lambda) & \Pi & \Xi & \Phi^\top & \Phi^\top \bar{C}_o^\top \\ \bullet & -Q & 0 & 0 & 0 \\ \bullet & \bullet & -\gamma_1 \mathbf{I} & 0 & 0 \\ \bullet & \bullet & \bullet & -F & 0 \\ \bullet & \bullet & \bullet & \bullet & -\mathbf{I} \end{bmatrix} \preceq 0 \tag{5.24d}$$

$$\widehat{\mathcal{M}_2}(0) \preceq 0, \quad \widehat{\mathcal{M}_2}(T_2) \preceq 0 \tag{5.24e}$$

$$\gamma_1 + \gamma_2 \leq \gamma^2 \tag{5.24f}$$

where

$$[0, T_2] \in \tau \mapsto \widehat{\mathcal{M}_2}(\tau) := \left[\begin{array}{c|c|c} e^{\delta\tau}(\mathrm{He}(J) - \delta P_2) + T & e^{\delta\tau} \left[\begin{array}{c|c} P_2 C_p A_p - J C_p & -Z \end{array}\right] & e^{\delta\tau} P_2 \mathbb{W} \\ \hline \bullet & -R & 0 \\ \hline \bullet & \bullet & -\gamma_2 \mathbf{I} \end{array}\right] \tag{5.25}$$

$$\Phi := \begin{bmatrix} Y & I \\ V^\top & 0 \end{bmatrix} \tag{5.26}$$

$$\Lambda := \begin{bmatrix} A_pY + B_pM & A_p + B_pNC_p \\ K & XA_p + LC_p \end{bmatrix}, \quad \Pi := -\begin{bmatrix} B_pN \\ L \end{bmatrix}, \quad \Xi := \begin{bmatrix} W \\ XW \end{bmatrix} \tag{5.27}$$

Then, matrix $\mathbf{I} - XY$ *is nonsingular. Let* $U \in \Re^{n_p \times n_p}$ *be any nonsingular matrix such that*

$$XY + UV^\top = \mathbf{I} \tag{5.28}$$

Then, conditions in Proposition 5.3.1 are satisfied; hence, Property 5.3.1 holds. Furthermore, selecting

$$\begin{aligned} \Delta_{\mathcal{K}} &= \begin{bmatrix} U^{-1} & -U^{-1}XB_p \\ 0 & \mathbf{I} \end{bmatrix} \left[\begin{array}{c|c} K - XA_pY & L \\ \hline M & N \end{array}\right] \begin{bmatrix} V^{-\top} & 0 \\ -C_pYV^{-\top} & \mathbf{I} \end{bmatrix} \\ \Delta_{\mathcal{J}} &= \left[\begin{array}{c|c} P_2^{-1}J & P_2^{-1}Z \end{array}\right] \end{aligned} \tag{5.29}$$

solve Problem 5.2.1.

The proof is given in Appendix B.

Remark 5.4.1. *Theorem 5.4.1 requires matrix V to be nonsingular. Although this constraint is hard to formulate in an LMI setting, nonsingularity of V can be easily enforced, e.g., by considering the following constraint $V + V^\mathsf{T} \succ 0$.*

Notice that when δ, α, and T_2 are fixed, conditions in Theorem 5.4.1 become LMIs. As such, Theorem 5.4.1 can be employed to design the controller gains by performing a line search on parameters δ, α, and T_2 with the purpose of solving the following optimization problem:

$$\begin{aligned} \underset{\delta,\gamma_1,\gamma_2,\alpha,P_2,T,Q,R,F,X,Y,K,L,M,N,J,Z,V}{\text{maximize}} \quad & T_2 \\ \text{subject to} \quad & (5.24) \end{aligned} \tag{5.30}$$

Remark 5.4.2. *It is worth mentioning that it can be easily shown that conditions* (5.24) *can be simplified to achieve sufficient conditions to solve Problem 5.2.1 when only the internal* *exponential stability ($\omega \equiv 0$) is considered. In particular, those conditions are obtained by the set of conditions* (5.24) *with the following modifications:*

1. *Condition* (5.24f) *is not included;*

2. *Matrix $\widehat{\mathcal{M}_1}$ is as follows:*

$$\widehat{\mathcal{M}_1} := \begin{bmatrix} \mathrm{He}(\Lambda) & \Pi & \Phi^\top \\ \bullet & -Q & 0 \\ \bullet & \bullet & -F \end{bmatrix} \preceq 0 \tag{5.31}$$

3. *Matrix $\widehat{\mathcal{M}_2}(\tau)$ is as follows:*

$$[0, T_2] \in \tau \mapsto \widehat{\mathcal{M}_2}(\tau) := \left[\begin{array}{c|c} e^{\delta\tau}(\mathrm{He}(J) - \delta P_2) + T & e^{\delta\tau} \left[\begin{array}{c|c} P_2 C_p A_p - J C_p & -Z \end{array}\right] \\ \hline \bullet & -R \end{array}\right] \tag{5.32}$$

5.5 Numerical Example

In this section, we showcase the proposed design approach for a double integrator plant, i.e.

$$\left[\begin{array}{c|c|c|c|c} A_p & B_p & W & C_p^\top & C_o^\top \end{array}\right] = \left[\begin{array}{cc|c|c|c|c} 0 & 1 & 0 & 1 & 1 & 1 \\ 0 & 0 & 1 & 1 & 0 & 0 \end{array}\right] \tag{5.33}$$

Numerical solutions to LMIs are obtained through the solver *SDPT3* [104] and coded in Matlab® via *YALMIP* [61]. Simulations of hybrid systems are performed in Matlab® via the *Hybrid Equations (HyEQ) Toolbox* [93].

The purpose of this section is to show the result of the controller design by using the approach described earlier in this chapter when input-output stability with $\mathcal{L}_2$-gain $\gamma \leq 5$

is required. To this end, we consider the following additional constraints:

$$2\alpha_2\Theta \preceq \mathrm{He}(\Lambda) \preceq 2\alpha_1\Theta \tag{5.34a}$$

$$\begin{bmatrix} \sin(\theta)(\Lambda+\Lambda^\top) & -\cos(\theta)(\Lambda-\Lambda^\top) \\ \cos(\theta)(\Lambda-\Lambda^\top) & \sin(\theta)(\Lambda+\Lambda^\top) \end{bmatrix} \tag{5.34b}$$

where Θ and Λ are respectively defined in (5.24a) and (5.27), $\alpha_1 = -0.5$, $\alpha_2 = -25$, and $\theta = \frac{\pi}{4}$. In particular, the constraints in (5.34) ensures that the spec($\mathbb{A}$), which characterizes the closed-loop continuous-time dynamics, is contained in the gray area of the complex plain in Fig. 5.3. These further constraints have the objective of avoiding ill conditioned controller parameters; see [95].

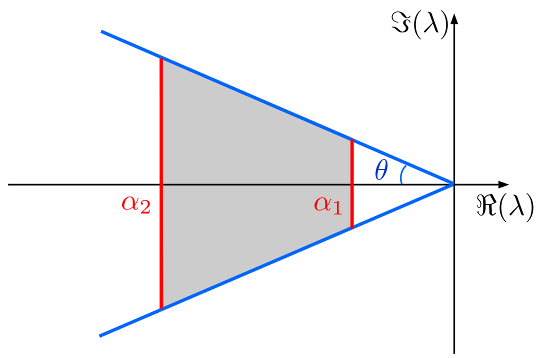

Figure 5.3: Representation of the complex plane where the eigenvalues of the closed-loop NCS are contained (gray area). Constrain in (5.34a) are represented in red, while constrain in (5.34b) are represented in blue.

By pursing the design approach introduce in this chapter, our design methodology leads to $T_2 = 0.39, \delta = 4, \alpha = 1.58$, and the following values of the controller parameters:

$$\Delta_{\mathcal{K}} = \left[\begin{array}{cc|c} -48.01 & 3.96 & 3.4 \\ -180.32 & 0.17 & 12.15 \\ \hline 417.26 & -80.26 & -31.83 \end{array}\right], \quad \Delta_{\mathcal{J}} = \left[\begin{array}{c|cc} -0.53 & -0.014 & 0.009 \end{array}\right] \tag{5.35}$$

To visualize the behavior of the closed-loop system with the controller in (5.35), in

Fig. 5.4 we report the evolution of the plant state x_p, the state of the holding device $\hat{y}$, the control signal u, the timer variable τ, and the input disturbance ω. In this simulation, $x_p(0,0) = (0.85, 0.52)$, $x_c(0,0) = 0$, $\hat{y}(0,0) = 0$, $T_1 = 0.01$,

$$\omega(t) = \begin{cases} 1 & t \in [0,7) \\ -1 & t \in [7,15) \\ 0 & t \geq 15 \end{cases} \tag{5.36}$$

where $t \in [0, 20]$ is the simulation time. Transmission intervals are selected between T_1 and T_2 accordingly to a sinusoidal law with frequency 10.5.

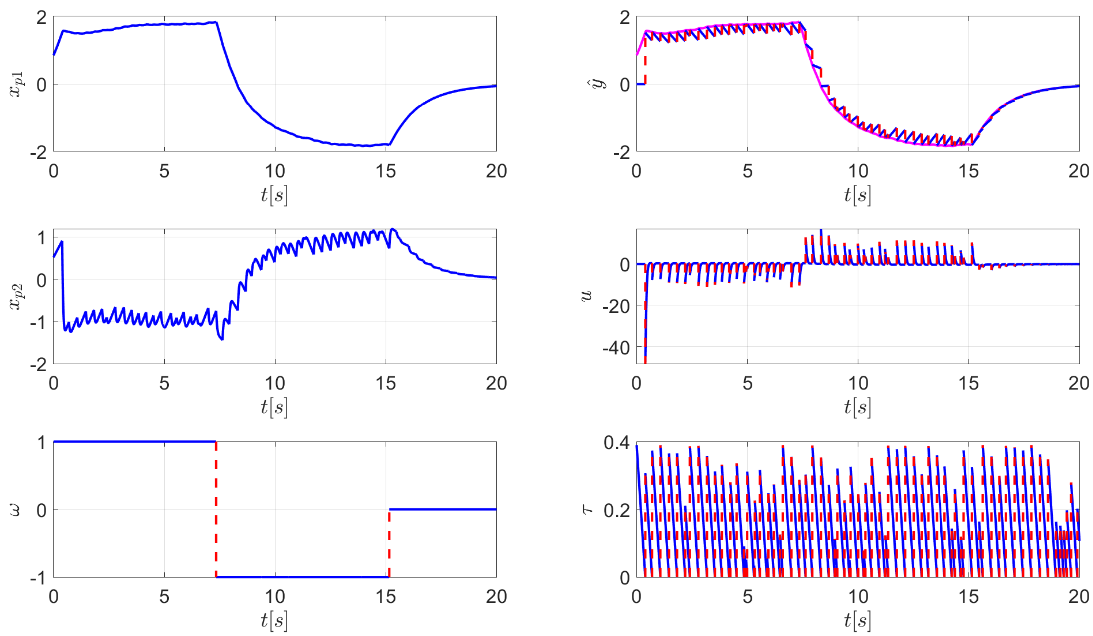

Figure 5.4: Response of the closed-loop system in presence of the unknown disturbance input ω. First column, from the top to the bottom: first and second component of plant state x_p, and ω. Second column, from the top to the bottom: state of the holding device $\hat{y}$ (blue) and plant output y (magenta), control signal u, and timer variable τ.

In the following, we show the beneficial effect of taking into consideration the bound of the $\mathcal{L}_2$-gain in the design procedure. In particular, by employing conditions in Remark 5.4.2, we design a controller that solves the problem of internal exponential stability for $T_2 = 0.39$, which is the same value of T_2 obtained for the controller in (5.35). Then, we graphically compare the attenuation of both controllers of the disturbance ω on the performance output y_o.

By following Remark 5.4.2, the controller designed for internal exponential stability for $T_2 = 0.39$ leads to $\delta = 2, \alpha = 0.53$, and the following values of the controller parameters:

$$\Delta_{\mathcal{K}} = \left[\begin{array}{cc|c} -45.01 & 3.24 & 2.25 \\ -178.15 & -1.45 & 8.65 \\ \hline 521.71 & -87.32 & -27.41 \end{array}\right], \quad \Delta_{\mathcal{J}} = \left[\begin{array}{c|cc} -0.72 & -0.003 & 0.002 \end{array}\right] \tag{5.37}$$

By employing the same simulation scenario of Fig. 5.4, we compare in Fig. 5.5 the responses of the performance output y_o for both controllers. As expected, the effect of the disturbance ω on the performance output y_o is less when the controller is designed to minimize γ.

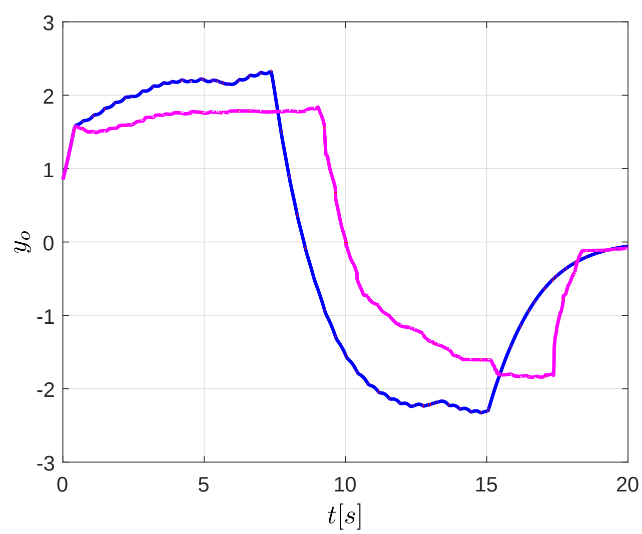

Figure 5.5: Response of the performance output for controller and holding device designed for internal exponential stability for $T_2 = 0.39$ as in (5.37), in blue. Response of the performance output for controller and holding device designed for input-output stability for $T_2 = 0.39$ and $\mathcal{L}_2$-gain less than or equal to 5 as in (5.35), in red.

5.6 Conclusion

In this chapter, we discuss the problem of designing output feedback controllers for linear time-invariant systems where measurements are available in an intermittent aperiodic fashion. In particular, our design methodology aims at obtaining a controller such that the closed-loop NCS is global exponentially stable with the largest achievable interval without measurements. These results are accomplished by relying on Lyapunov theory for hybrid dynamical systems. Moreover, by employing an approach that is reminiscent of an "input-to-state stability small gain" philosophy, we obtain sufficient conditions that are suitably converted into LMIs. The effectiveness of the proposed approach is showcased throughout a numerical example.

Conclusion of Part I

In the first part of the dissertation, we introduce tools for stability analysis and design for resilient NCSs.

At first, in Chapter 3, we introduce the architecture of NCSs adopted in this dissertation. In particular, we take into consideration NCSs, where only the sensing path is subject to a communication network that leads to aperiodic transmission intervals and variable network delays. We consider a hybrid control scheme constituted by the cascade of a holding device and a dynamic controller, and we model the closed-loop system in the hybrid system framework in [37].

In Chapter 4, we present two methodologies for estimating the trade-off curves between the maximum allowable transmission intervals and the maximum allowable network delays. The first approach assumes NCS with ZOH as holding device and provides a tool to indirectly estimate the trade-off curves after solving some LMIs. The second approach takes into account a class of linear holding devices and provides a tool to estimate trade-off curves directly from the solutions of some LMI. Indeed, the second methodology allows the estimation of MATI and MAD explicitly throughout the resulting stability conditions. The two approaches are compared through numerical results. It emerges that the indirect approach allows estimating trade-off curves that have larger maximum transmission intervals, whereas the direct approach provides an estimation of trade-off curves that have larger maximum allowable delays.

To conclude, in Chapter 5, we discuss the problem of designing output feedback controllers for linear time-invariant systems where measurements are available in an intermittent aperiodic fashion. Our design methodology aims at obtaining a controller such that the closed-loop NCS is global exponentially stable with the largest achievable interval without measurements. These results are accomplished by relying on Lyapunov theory for hybrid dynamical systems. Moreover, by employing an approach that is reminiscent of an “input-to-state stability small gain” philosophy, we obtained sufficient conditions that are suitably converted into LMIs.

The effectiveness of the proposed approaches is showcased throughout numerical examples throughout this part of the dissertation.

Part II

Resilient Control for Vehicle Platooning

This page is intentionally left blank.

Introduction

General Overview

While the demand for mobility is growing over the years, Intelligent Transportation Systems (ITS) is a promising advanced solution capable of improving the efficiency and safety of the whole mobility infrastructure. Such ITS' benefits are expected to be achieved by Connected and Autonomous Vehicles (CAVs). This new technology employs the concept of Vehicle to Vehicle (V2V) communication [62, 105] by employing, e.g., Dedicated Short Range Communication (DSRC) [58].

Probably the most famous application involving connectivity between vehicles is the Cooperative Adaptive Cruise Control (CACC). CACC is an application of connected automated vehicles that extends the functionality of Adaptive Cruise Control (ACC) by employing V2V networks, such as Dedicated Short Range Communication (DSRC). This allows shared information between cars in the same inter-vehicle communication network (IVC). In particular, by employing IVC and on-board sensors, e.g., radar and lidar, CACC improves features of the ACC by reducing the distance between vehicles and by providing enhanced stability properties. Indeed, CACC can guarantee inter-vehicle time gaps smaller than 1 second, whereas ACC can not [77, 88].

Common metrics for CACC are *individual vehicle stability* and *string stability*. The former refers to the reduced distance between vehicles and leads to higher traffic throughput and higher fuel economy [99, 105]. The latter refers to the attenuation of disturbances and shock waves throughout the string of vehicles and improves traffic flow by avoiding the so-called phantom traffic jam [88, 105] due to an amplification of disturbance, i.e., a speed variation of the first vehicle that propagates throughout the string of vehicles leads to excessive breaking [88].

Besides the benefits introduces by IVC, this wireless network exposes vehicle control systems to network induced imperfections, i.e., packet dropping and network delays [43], and network vulnerabilities, i.e., cyber attacks [20]. Such an unreliable and compromised network can affect vehicle platoons by leading to loss of performance and safety-related issues such as collisions, which could lead to loss of human lives [3, 20, 82].

The packet-based nature of communication networks introduces imperfections such as limits on the transmission rates and variable delays on the communication channel. As shown in [82], these network-induced imperfections can compromise the performance of vehicle platoons when transmission rates are too slow, or network induced delays are too large. However, having high transmission rates can degrade the performance of the DSRC network, as shown in [90].

From a security perspective, in this dissertation, we focus on Denial-of-Service (DoS) attacks. To this end, it is worth mentioning that DoS is the easiest attack to accomplish and aims at making the network unavailable for the longest time possible by generating consecutive packet dropouts [24, 114]. Notice that DoS attacks generate a totally different pattern compared to communication losses naturally present in the IVC [5]. Natural packet dropouts are generally unpredictable and follow a random pattern according to the packet rate associated with the network protocol [69, 90]. For such a reason, DoS-resilient design approaches differ from traditional ones. In particular, DoS-resilient approaches must maximize the number of consecutive packet dropouts while maintaining the stability and performance of the vehicle platooning.

Literature Review

In the literature, several results can be found about modeling and design of vehicle platoons with the CACC controller, as it emerges from [57, 77, 82, 85, 87] and references therein, to cite a few. Ploeg et al. [85] introduce a continuous-time based decentralized string stable CACC design where the maximum allowable network delay is computed after designing the controller. The same authors propose in [87] a $\mathcal{H}_\infty$ controller design for one and two-vehicle look-ahead string stable platooning. In this case, the design procedure focuses on string stability, with only general considerations about the vehicle's performance. Both the above-mentioned contributions model the signal exchanged through the network as a continuous-time signal affected by a delay. Indeed, such designs are based on continuous-time control techniques that do not consider the discrete packet-based nature of the IVC. To this end, the research community has analyzed and enhanced the CACC in [85] by considering an unreliable packet-based network. In [83], hybrid modeling is used to analyze the stability of vehicle platoons controlled by CACC, where IVC is employed by adopting scheduling protocols. In [38] a sampled-data design approach is proposed, whereas [23, 59] discuss event-triggered control strategies. The event-driven communication strategies aim at using the communication channel only when the transmissions of new data are needed. To cope with communication losses, [86] introduces a graceful degradation algorithm, Harfouch et al. [41] propose a switching strategy between CACC and ACC, and Wu et al. [111] enhance CACC with an adaptive Kalman filter.

While the design of stable vehicle platoons with cars connected via an unreliable network has been widely investigated, the design of control systems for connected vehicles in the presence of cyber-attacks is still an active research area despite being significantly critical. Indeed, compromised networks lead to severe consequences with the involvement of human lives and safety; see, i.e., Dadras et al. [20]. DoS jamming attack is investigated in [4], where string stability is analyzed under packet dropping generated by jamming actions. Biron et al. [10, 11] detect and estimate the entity of a DoS attacks in a vehicle platoon by modeling it as an unknown constant delay and propose a control architecture able to mitigate the effect of the attack. In [10], DoS attacks are modeled as an unknown constant delay. Attacks detection is performed by adopting a set of Luenberger's observer and a delay estimator, while attack compensation is achieved by modifying the CACC control architecture. Savaia et al. [94] build upon [10] and propose a DoS-resilient receding horizon switching control approach. In [81], a decision support system (DSS) based on a fuzzy detector is developed to predict the speed of the leader vehicle using state estimator and adjusts the safe distance. Dolk et al. [24] employ the CACC as a case study for evaluating a design procedure for DoS-resilient event-triggered mechanisms. Another event trigger design approach is presented in [103]. The proposed approach is capable of mitigating DoS attacks when their frequency of occurrences satisfies specific regularity criteria.

Contributions

The contributions of this part of the dissertation aims at proposing new tools for the design of network-resilient and DoS-resilient vehicle platooning controlled by CACC.

To the best of our knowledge, none of the existing works propose a tuning strategy for the CACC with the purpose of increasing the resilience to consecutive communication losses or network delays. Such a tuning could increase the resilience of the CACC to DoS attacks and unreliable networks. Furthermore, few control strategies deal with the vehicle's performance in regulating the distance gap between cars, along with improving resiliency. In this part of the dissertation, we focus on addressing these research gaps by proposing two design approaches for CACC that aims at maximizing the resiliency to unreliable network and to DoS attacks while guaranteeing required performance and string stability.

We propose a decentralized hybrid controller that modifies the continuous-time proportional derivative regulator in [85] by adding a Zero Order Hold (ZOH) device that allows taking into account the packet-based nature of the IVC.

Regarding the design of network-resilient CACC, we consider the problem of designing a decentralized CACC controller with quantifiable robustness margin to transmission intervals and network delays in the presence of performance requirements. The conditions for the solution of the control design problem leads to dealing with an optimization problem over non-linear matrix inequality constraints, whose solution is difficult from a numerical standpoint [12]. Therefore, we propose an algorithm that is tailored to the CACC application, which allows overcoming this numerical complexity. Our approach allows finding a suboptimal solution to the non-linear optimization problem by using a one-parameter line search over a compact interval where lower and upper bounds can be computed.

Related to DoS-resilient CACC, the main contributions of this part of the dissertation are as follows. We devise a numerically efficient tuning algorithm based on linear matrix inequalities (LMI), which aims at finding optimal gains for the controller, with the aim of maximizing the resiliency to DoS while guaranteeing performance requirements and string stability of the vehicle platooning. The proposed algorithm estimates the value of the *maximum allowable number of successive packet dropouts* (MANSD) that identifies the worst DoS attack that the control system can overcome without compromising string stability.

It is worth mentioning that the design approaches proposed in this part of the dissertation are not meant to be concurrent with those presented in the literature review introduced in the previous section. Indeed, these design strategies could be used with those to enhance the resilience of the vehicle platoons. In fact, they allow having a higher resilience that leads to postponing or improving fallback to safer strategies, e.g., ACC.

Part II of the dissertation is organized as follows:

- Chapter 6 introduces the design of network-resilient CACC. Some of the results presented in this chapter can be found in [67].
- Chapter 7 describes the design approach for DoS-resilient CACC. Some of the results presented in this chapter are published in [66].

This page is intentionally left blank.

Chapter 6

Tuning Algorithm for Network-Resilient Control of Vehicle Platooning

6.1 Introduction

In this chapter, we model the CACC strategy in [85] as a hybrid controller by considering the packet-based nature of the inter-vehicle communication (IVC) network. We consider the problem of designing a decentralized CACC controller with quantifiable robustness margin to transmission intervals and network delays in the presence of performance requirements. The conditions for the solution of the control design problem leads to dealing with an optimization problem over non-linear matrix inequality constraints, whose solution is difficult from a numerical standpoint. In this chapter, we propose an algorithm that is tailored to the CACC application, which allows overcoming this numerical complexity. Our approach allows finding a suboptimal solution to the non-linear optimization problem by using a one-parameter line search over a compact interval where lower and upper bounds can be computed.

6.2 Modeling

6.2.1 Platooning Dynamics

We consider a homogeneous vehicle platooning formed by m identical cars. The vehicle that leads the platoon is denoted by $\mathcal{V}_0$, whereas $\mathcal{V}_i$, $i \in P_m := \{1, 2, \ldots, m\}$, identifies the following vehicles. As a target of the vehicle platooning, $\mathcal{V}_i$ must maintain the reference distance d_{r_i} from its preceding vehicle $\mathcal{V}_{i-1}$ by employing a constant time gap policy reference. In particular, $d_{r_i} = r_i + h\, v_i$, $i \in P_m$, where r_i and v_i are, respectively, the standstill reference distance and the speed of $\mathcal{V}_i$, and $h \in \Re_{>0}$ is the constant time gap between vehicles. The spacing error e_i is given by

$$e_i := (q_{i-1} - q_i - L) - (r_i + h\, v_i) = d_i - d_{r_i} \tag{6.1}$$

where q_i, L, and $d_i := q_{i-1} - q_i - L$ denote, respectively, the position, the length of vehicles in the platoon, and the distance between vehicles $\mathcal{V}_i$ and $\mathcal{V}_{i-1}$.

The longitudinal vehicle dynamics of $\mathcal{V}_i$ can be described by a nonlinear model [39]. However, by applying a control law that achieves feedback linearization, one can assume that each vehicle in the platooning can be modeled as a continuous-time linear time-invariant dynamical system; see [101] for further details. In particular, we consider

$$\mathcal{V}_0 : \begin{bmatrix} \dot{v}_0 \\ \dot{a}_0 \end{bmatrix} = \begin{bmatrix} a_0 \\ -\frac{1}{\tau_d} a_0 + \frac{1}{\tau_d} u_0 \end{bmatrix} \tag{6.2}$$

$$\mathcal{V}_i : \begin{bmatrix} \dot{e}_i \\ \dot{v}_i \\ \dot{a}_i \end{bmatrix} = \begin{bmatrix} v_{i-1} - v_i - h a_i \\ a_i \\ -\frac{1}{\tau_d} a_i + \frac{1}{\tau_d} u_i \end{bmatrix}, \quad i \in P_m \tag{6.3}$$

where v_i (v_0), a_i (a_0), and u_i (u_0) are, respectively, the speed, the acceleration, and the control input of $\mathcal{V}_i$ ($\mathcal{V}_0$), and τ_d represents the time constant of the powertrain dynamics of the vehicles in the platooning. Since we consider a homogeneous vehicle platooning, h and

τ_d are identical for each vehicle.

We modify the decentralized CACC controller in [85] by considering a more realistic network behavior that takes into consideration aperiodic transmission intervals and variable network delays. Such a controller is given by the following dynamics

$$\dot{u}_i = \mathcal{K}_h(u_i, \chi_i) \tag{6.4a}$$

$$\chi_i = \mathcal{K}_{PD}(e_i) + u_{i-1} \tag{6.4b}$$

where u_{i-1} is the control signal of $\mathcal{V}_{i-1}$, $\mathcal{K}_h(u_i, \chi_i) \coloneqq -\frac{1}{h}u_i + \frac{1}{h}\chi_i$, and $\mathcal{K}_{PD}(e_i) \coloneqq k_p e_i + k_d \dot{e}_i$, and k_p and k_d are the controller gains. Observe that each vehicle is controlled by a dynamic controller as in (6.4), where gains k_p and k_d are independent from the vehicle's index. Controller (6.4) is designed to rely on on-board sensors (e.g., radars, lidars and accelerometers) for measurements of e_i and $\dot{e}_i$, and IVC for the signal u_{i-1} of the preceding vehicle $\mathcal{V}_{i-1}$. However, in [85], the remote signal u_{i-1} is treated as a continuous-time signal even though it is shared through a network. We modify the structure of the controller (6.4) by proposing a hybrid controller able to deal with the discrete behavior of the packet-based network communication used to share the value of u_{i-1}. Notice that in real scenarios, also measurements of e_i and $\dot{e}_i$ are gathered via a packet-based network, e.g., Controller Area Network (CAN bus). However, we realistically assume that measurements from on-board sensors have a much higher sampling rate. Therefore, we assume those as available continuously over time. A similar assumption is used in [83].

6.2.2 Communication Network

We assume that the measurement of u_{i-1} is sampled and sent over a data network from vehicle $\mathcal{V}_{i-1}$ at time $t_{k_{i-1}}, k_{i-1} \in \mathfrak{N}$, not known in advance, and that u_{i-1} is received by the controller of vehicle $\mathcal{V}_i$ after a bounded, possibly time varying, network delay $\tau_{d_{k_{i-1}}}$. Specifically, we suppose that the sequence $\{t_{k_{i-1}}\}_{k_{i-1}=1}^{\infty}$ is strictly increasing and unbounded, that the sampling and transmissions occur at the same time, and that there exists $T_1 > 0$

such that $T_1 \leq t_{k_{i-1}+1} - t_{k_{i-1}} < T_2$ for all $k_{i-1} \in \mathfrak{N}$, where T_2 represents the *maximum allowable transmission interval* (MATI). Furthermore, the delay $\tau_{d_{k_{i-1}}}$ is bounded by T_{mad}, i.e., $0 \leq \tau_{d_{k_{i-1}}} \leq T_{mad}, k_{i-1} \in \mathfrak{N}$, where $0 \leq T_{mad} \leq T_2$ is the *maximum allowable delay* (MAD). This assumption, which has been already considered in Chapter 3 , ensures that the transmitted output measurement must be received by the controller before the next measurement is sampled and sent.

6.3 Controller Outline and Problem Formulation

6.3.1 Proposed Networked Controller

We propose a modified version of the controller in (6.4) that takes into account the discrete nature of the data available through the network. The control scheme is depicted in Fig. 6.1, where H represents the spacing policy filter, which is given by $H(s) = hs + 1$ [23].

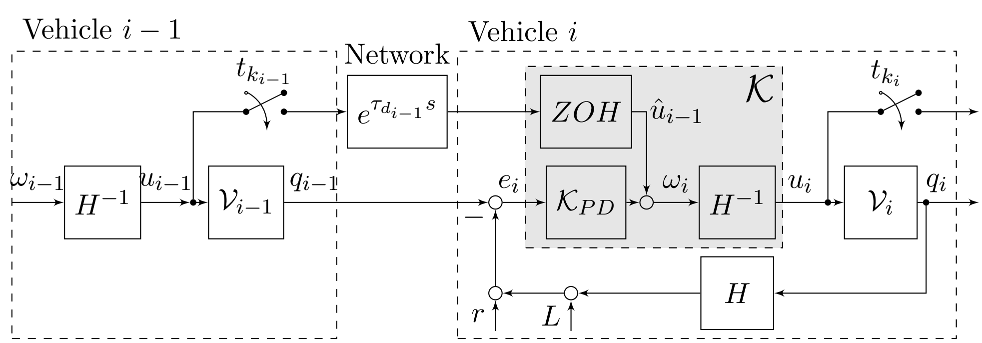

Figure 6.1: Schematic of the dynamics of vehicles $i-1$ and i, along with the proposed hybrid controller $\mathcal{K}$ (in the gray area) and the network delays.

For each i, the proposed hybrid controller handles discrete measurements of u_{i-1}, which are available through network packets only at time $t_{k_{i-1}}$, $k_{i-1} \in \mathfrak{N}$. Specifically, the controller in (6.4) is augmented with a memory state $\hat{u}_{i-1} \in \mathfrak{R}$, which stores the last received value of u_{i-1}. The arrival of a new packet with the information of $u_{i-1}(t_{k_{i-1}})$ triggers an instantaneous jump in $\hat{u}_{i-1}$, which is updated to the last received value of u_{i-1}. Then, in between received packets, $\hat{u}_{i-1}$ is kept constant in a ZOH fashion. More precisely, dynamics of $\hat{u}_{i-1}$ can be modeled as a system with jumps in its state. In particular, its dynamics are as follows for all $k_{i-1} \in \mathfrak{N}$:

$$\begin{cases} \dot{\hat{u}}_{i-1}(t) = 0 & \forall t \neq t_{k_{i-1}} + \tau_{d_{k_{i-1}}} \\ \hat{u}_{i-1}(t^{+}) = u_{i-1}(t_{k_{i-1}}) & \forall t = t_{k_{i-1}} + \tau_{d_{k_{i-1}}} \end{cases} \tag{6.5}$$

Differently from (6.4), the controller is fed with $\hat{u}_{i-1}$, and its continuous-time dynamics are given by:

$$\dot{u}_i = \mathcal{K}_h(u_i, \omega_i), \quad \omega_i := \mathcal{K}_{PD}(e_i) + \hat{u}_{i-1} \tag{6.6}$$

The interconnection between the ZOH device in (6.5) and the controller in (6.6) is denoted by $\mathcal{K}$ and represents the proposed hybrid controller.

6.3.2 Hybrid Modeling

The stability of the vehicle platooning is studied by analyzing the dynamics of the closed-loop system obtained by the interconnection of (6.3), (6.5), and (6.6). To this end, let $e_{1,i} := e_i$, $e_{2,i} := \dot{e}_i$ and $e_{3,i} := \ddot{e}_i$. By straightforward calculations one obtains that for all $k_{i-1} \in \mathfrak{N}$ the continuous-time dynamics of the closed-loop system are defined as

$$\begin{cases} \dot{e}_{1,i} = e_{2,i} \\ \dot{e}_{2,i} = e_{3,i} \\ \dot{e}_{3,i} = -\dfrac{k_p}{\tau_d}e_{1,i} - \dfrac{k_d}{\tau_d}e_{2,i} - \dfrac{1}{\tau_d}e_{3,i} + \dfrac{1}{\tau_d}u_{i-1} - \dfrac{1}{\tau_d}\hat{u}_{i-1} \qquad \forall t \neq t_{k_{i-1}} + \tau_{d_{k_{i-1}}} \\ \dot{u}_{i-1} = -\dfrac{1}{h}u_{i-1} + \dfrac{1}{h}\omega_{i-1} \\ \dot{\hat{u}}_{i-1} = 0 \end{cases} \tag{6.7}$$

whereas the state instantaneous updates due to communication events are defined as

$$\begin{cases} e_{1,i}(t^+) = e_{1,i}(t) \\ e_{2,i}(t^+) = e_{2,i}(t) \\ e_{3,i}(t^+) = e_{3,i}(t) & \forall t = t_{k_{i-1}} + \tau_{d_{k_{i-1}}} \\ u_{i-1}(t^+) = u_{i-1}(t) \\ \hat{u}_{i-1}(t^+) = u_{i-1}(t) \end{cases} \tag{6.8}$$

For the sake of notation, notice that the dependence on time in continuous-time dynamics is omitted. Due to the hybrid controller and the network behavior, such error dynamics are characterized by the interplay of differential equations and instantaneous jumps. Therefore, we model such a system into the hybrid systems framework in [37], for which preliminary information is in Chapter 2. To reformulate the model as a hybrid dynamical system, we introduce the auxiliary variables $s_{u_{i-1}} \in \mathfrak{R}$, $\tau_{i-1} \in \mathfrak{R}_{\geq 0}$, and $l_{i-1} \in \{0, 1\}$. Variable $s_{u_{i-1}}$ represents a storage variable of the measurement u_{i-1} when u_{i-1} is sampled and sent at time $t_{k_{i-1}}$. τ_{i-1} is a timer that keeps track of the duration of the sampling intervals and the network delays, and triggers jumps whenever conditions on τ_{i-1} are verified. Variable l_{i-1} keeps track of the fact that the next event is either a sampling event (when $l_{i-1} = 0$) or an updating event (when $l_{i-1} = 1$). At this stage, consider the change of coordinates $s_{i-1} := s_{u_{i-1}} - \hat{u}_{i-1}$ and $\eta_{i-1} := \hat{u}_{i-1} - u_{i-1}$, where s_{i-1} defines the error between the sampled and transmitted value of u_{i-1} and its stored value in the ZOH, whereas the variable η_{i-1} defines the network-induced error. Similar approach is employed in Section 4.3.

From (6.7) and (6.8), one can define the hybrid system $\mathcal{H}_i$ as follows:

$$\begin{cases} \dot{x}_i = f(x_i, \omega_{i-1}) & x_i \in C_i, \omega_{i-1} \in \mathbb{R} \\ x_i^+ = g(x_i) & x_i \in D_i \end{cases} \tag{6.9}$$

where $x_i := (\tilde{x}_i, \eta_{i-1}, s_{i-1}, \tau_{i-1}, l_{i-1}) \in \mathfrak{R}^8$ is the state, $\tilde{x}_i := (e_{1,i}, e_{2,i}, e_{3,i}, u_{i-1})$ and ω_{i-1} is the input. For every $x_i \in C_i, \omega_{i-1} \in \mathfrak{R}$, the flow map is given by

$$f(x_i, \omega_{i-1}) := (f_{\tilde{x}}(\tilde{x}_i, \eta_{i-1}, \omega_{i-1}), f_\eta(\tilde{x}_i, \omega_{i-1}), 0, 1, 0) \tag{6.10}$$

where

$$\begin{aligned} f_{\tilde{x}}(\tilde{x}_i, \eta_{i-1}, \omega_{i-1}) &:= A_{11}\tilde{x}_i + A_{12}\eta_{i-1} + A_{13}\omega_{i-1} \\ f_\eta(\tilde{x}_i, \omega_{i-1}) &:= A_{21}\tilde{x}_i + A_{23}\omega_{i-1},\ A_{23} = -\tfrac{1}{h} \end{aligned} \tag{6.11}$$

and

$$\begin{aligned} A_{11} &= \begin{bmatrix} A_e & \mathbf{0} \\ \mathbf{0} & -\frac{1}{h} \end{bmatrix}, A_{12} = \begin{bmatrix} 0 & 0 & -\frac{1}{\tau_d} & 0 \end{bmatrix}^\top \\ A_{13} &= \begin{bmatrix} 0 & 0 & 0 & \frac{1}{h} \end{bmatrix}^\top, A_{21} = \begin{bmatrix} 0 & 0 & 0 & \frac{1}{h} \end{bmatrix} \end{aligned} \tag{6.12}$$

with

$$A_e = \begin{bmatrix} 0 & 1 & 0 \\ 0 & 0 & 1 \\ -\frac{k_p}{\tau_d} & -\frac{k_d}{\tau_d} & -\frac{1}{\tau_d} \end{bmatrix} \tag{6.13}$$

For every $x_i \in D_i$, the jump map is given by

$$g(x_i) := (\tilde{x}_i, \eta_{i-1} + l_{i-1}s_{i-1}, -(1 - l_{i-1})\eta_{i-1}, l_{i-1}\tau_{i-1}, 1 - l_{i-1}) \tag{6.14}$$

The flow set C_i and the jump set D_i are respectively

$$C_i := \{x_i \in \mathbb{R}^8 | (l_{i-1} = 0 \wedge \tau_{i-1} \in [0, T_2]) \vee (l_{i-1} = 1 \wedge \tau_{i-1} \in [0, T_{mad}])\} \tag{6.15}$$

and

$$D_i := \{x_i \in \mathbb{R}^8 | (l_{i-1} = 0 \wedge \tau_{i-1} \in [\delta_T, T_2]) \vee (l_{i-1} = 1 \wedge \tau_{i-1} \in [0, T_{mad}])\} \tag{6.16}$$

To evaluate the string stability an input-output relation is needed. As already done in [23], we select the signal ω_i as performance output of the hybrid system $\mathcal{H}_i$ and we study the input-output stability from input ω_{i-1} to output $\omega_i := C\tilde{x}_i + D\eta_{i-1}$ where $C = \begin{bmatrix} k_p & k_d & 0 & 1 \end{bmatrix}$ and $D = 1$. The hybrid system model $\mathcal{H}_i$ expanded with the output ω_i is denoted by $\mathcal{H}_i^{\omega}$.

Remark 6.3.1. *The hybrid model $\mathcal{H}_i$ in* (6.9) *considers the error dynamics of a single vehicle in the platooning. Therefore, values of T_2 and T_{mad} that characterize the network imperfections can assume different values for each vehicle i, for $i \in P_m$.*

Remark 6.3.2. *Vehicle platooning can be characterized by different network topology, such as, e.g., two vehicles ahead or one vehicle ahead and leader; see, e.g., [22, 87, 121]. In those cases, the hybrid model $\mathcal{H}_i$ in* (6.9) *could be appropriately modified by introducing further auxiliary variables that take into account instantaneous jumps related to the communication events that occur between the vehicles. Notice that less auxiliary variables would be necessary if the vehicles are assumed to send information in a synchronized fashion.*

6.3.3 Problem Formulation

A platoon of vehicles controlled by CACC needs to accomplish two main goals [23]: 1) regulate the spacing error in (6.1), and 2) attenuate disturbance and shock waves along the vehicle platooning, due, e.g., to speed variations of the leader vehicle.

The first property we want to guarantee is usually referred to as individual vehicle stability. When satisfied, if $\mathcal{V}_0$ travels at some constant speed, the CACC ensures that $\lim_{t\to\infty} e_i(t) = 0$ for the rest of the vehicles in the platoon. Therefore, the individual vehicle stability is strictly connected with the eigenvalues of A_e, which depend on the gains k_p and k_d. Moreover, the error dynamics reflect the dynamic response of the vehicle platooning and can influence the passenger's comfort. To this end, performance requirements need to be taken into account along with the satisfaction of the individual vehicle stability. In this chapter, we characterize performance requirements by introducing the set

$$\mathbb{P}(\lambda_M, \zeta_m) := \{A \in \mathfrak{R}^{n\times n} | \Lambda_{\max}(A) = \lambda_M,\, \zeta_{\min}(A) \geq \zeta_m\} \tag{6.17}$$

where $\lambda_M < 0$ and $\zeta_m \in (0, 1]$ are design parameters. The set $\mathbb{P}(\lambda_M, \zeta_m)$ defines constraints on the location of the eigenvalues of A_e in the complex plane. In particular, the eigenvalues of A_e associated with the slowest mode of the error dynamics must have real part equal to λ_M, and, if complex, also have damping ratio greater than ζ_m (i.e., lying on the dashed segment in Fig. 6.2), whereas the other eigenvalues must have real part smaller than λ_M and, if complex, damping ratio greater than ζ_m (i.e., being within the gray area in Fig. 6.2). To meet the required performance, we design controller gains such that $A_e \in \mathbb{P}(\lambda_M, \zeta_m)$.

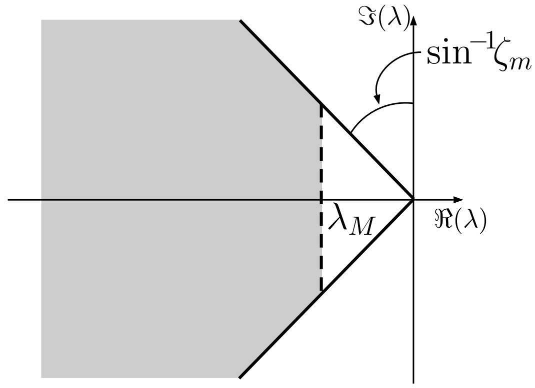

Figure 6.2: Representation of the set $\mathbb{P}(\lambda_M, \zeta_m)$ in the complex plane. To satisfy performance requirements, the proposed design procedure aims at placing the eigenvalues of A_e within the gray area represented in the picture.

The second property we want to guarantee is also referred to as the string stability of the vehicle platooning. It is related to the notion of input-output stability. String stability is widely investigated and analyzed via $\mathcal{L}_p$ stability [88]. In particular, $\mathcal{L}_2$ stability, e.g, in [23, 83, 87], and $\mathcal{L}_\infty$ stability, e.g., in [85, 88], are commonly used. Generally, string stability analyzed via $\mathcal{L}_2$ stability finds physical motivation in the energy dissipation across the platoon. In contrast, the usage of $\mathcal{L}_\infty$ stability is motivated by enforcing traffic safety due to the fact that $\mathcal{L}_\infty$ norm correlates to maximum overshoot [88]. In this chapter, we adopt the following notion of $\mathcal{L}_2$-stability, introduced in Definition 2.3.3, to study string stability of the vehicle platooning.

Definition 6.3.1 (String stability)**.** *The vehicle platooning given by* (6.2), (6.3), (6.5)*, and* (6.6) *is said to be string stable if the hybrid systems $\mathcal{H}_i^\omega$, $i \in P_m$, are $\mathcal{L}_2$-stable from the* *input $\omega_{i-1} \in \mathcal{L}_2$ to the output $\omega_i \in \mathcal{L}_2$ with an $\mathcal{L}_2$-gain less than or equal to one.*

Remark 6.3.3. *Because of vehicle homogeneity, the analysis of string stability of the whole vehicle platooning, regardless of its length, can be streamlined by focusing on the input-output properties of the single vehicle, i.e., on the $\mathcal{L}_2$-stability of $\mathcal{H}_i^{\omega}$, for $i \in P_m$. A similar approach can be found in [23].*

A critical aspect of the string stability is that it is negatively influenced by the IVC. Indeed, string stability can be degraded or compromised when network imperfections lead to prolonged unavailability of updated measurements; see [51, 60, 82, 83, 96]. Therefore, it is important to estimate the largest values of T_2 and T_{mad}, such that string stability is maintained. Indeed, knowing the trade-off curve between T_2 and T_{mad} allows one to be aware of the maximum values of transmission intervals and network delays such that string stability is guaranteed, which provides an important metric for the evaluation of the network-resiliency of the overall platooning.

Given the structure of the controller in (6.6), the gains k_p and k_d have an important role in satisfying the properties stated above. Therefore, it is crucial to design the parameters of the CACC controller in such a way to guarantee *individual stability* and *string stability* of the vehicle platooning for the largest transmission intervals and the largest delays as possible within acceptable limits in performance and comfort.

The problem we solve in this chapter can now be introduced as follows.

Problem 6.3.1. *Given the values of the constant time gap h, the time constant of the drive-line dynamics τ_d, and the performance requirements $\mathbb{P}$, determine the values of the gains k_p and k_d of the controller* (6.6) *such that:*

(P1) each vehicle is individually asymptotically stable with performance requirements $\mathbb{P}$ satisfied;

(P2) the vehicle platooning is string stable, i.e., $\mathcal{H}_i^{\omega}$ is $\mathcal{L}_2$-stable from the input ω_{i-1} to the output ω_i with an $\mathcal{L}_2$-gain less than or equal to one, and with the largest achievable values of T_2 and T_{mad}.

6.4 Tuning Algorithm

In this section, we illustrate our approach to solve Problem 6.3.1. After describing how to meet the required performance for the individual vehicle stability, we provide sufficient conditions for $\mathcal{L}_2$-stability of $\mathcal{H}_i^\omega$, i.e., string stability of the vehicle platoon. Finally, we describe a procedure to design the controller gains to maximize the trade-off curves between T_2 and T_{mad}, while satisfying the two stability properties described in the previous section.

6.4.1 Individual Vehicle Stability with Performance Requirements

To ensure individual vehicle stability with satisfactorily performance, we design k_p and k_d such that $A_e \in \mathbb{P}(\lambda_M, \zeta_m)$. In particular, we aim at identifying numerical values of k_p and k_d such that for any matrix $A_e \in \mathbb{P}(\lambda_M, \zeta_m)$ one of the following conditions holds:

(C1) the real eigenvalue is equal to λ_M and, the other two eigenvalues have real part less than or equal to λ_M with damping ratio greater than ζ_m;

(C2) the spectrum of A_e is characterized by a single couple of complex eigenvalues with real part equal to λ_M and damping ratio greater than ζ_m, and the other real eigenvalue is less than λ_M.

Remark 6.4.1. *Notice that, due to $A_e \in \mathfrak{R}^{3\times 3}$, $A_e \in \mathbb{P}$ if and only if either C1 or C2 are satisfied. In particular, to satisfy $A_e \in \mathbb{P}$ either C1 or C2 must hold. To this end, notice that conditions C1 and C2 can hold simultaneously for some specific selection of k_p and k_d. When this happens, all the eigenvalues of A_e have the same real part which is equal to λ_M.*

Next, we provide necessary and sufficient conditions on k_p and k_d such that C1 or C2 hold.

Proposition 6.4.1 (N.S.C. for C1)**.** *Let k_p, $k_d \in \mathfrak{R}$, $\lambda_M \in \mathfrak{R}_{<0}$, and $\zeta_m \in \mathfrak{R}_{>0}$. Then, C1* *is satisfied if and only if the following conditions hold:*

$$k_d = f_{C1}(k_p) := -\frac{1}{\lambda_M}k_p - \lambda_M^2\tau_d - \lambda_M \tag{6.18a}$$

$$k_p \leq \frac{|\lambda_M|(\lambda_M\tau_d + 1)^2}{4\tau_d\zeta_m^2} := \bar{k}_{pC1} \tag{6.18b}$$

$$k_p \geq 2\tau_d\lambda_M^3 + \lambda_M^2 := \underline{k}_{pC1} \tag{6.18c}$$

$$\lambda_M > -\frac{1}{3\tau_d} \tag{6.18d}$$

Now we provide necessary and sufficient conditions on the gains k_p and k_d to guarantee C2.

Proposition 6.4.2 (N.S.C. for C2)**.** *Let* k_p, $k_d \in \Re$, $\lambda_M \in \Re_{<0}$, *and* $\zeta_m \in (0,1)$. *Then, C2 holds if and only if the following conditions hold:*

$$k_d = f_{C2}(k_p) := -\frac{8\lambda_M^3\tau_d^2 + 8\lambda_M^2\tau_d + 2\lambda_M - \tau_d k_p}{2\lambda_M\tau_d + 1} \tag{6.19a}$$

$$k_p \leq \frac{\lambda_M^2(2\lambda_M\tau_d + 1)}{\zeta_m^2} := \bar{k}_{pC2} \tag{6.19b}$$

$$k_p > 2\tau_d\lambda_M^3 + \lambda_M^2 := \underline{k}_{pC2} \tag{6.19c}$$

$$\lambda_M > -\frac{1}{3\tau_d} \tag{6.19d}$$

Proofs of Proposition 6.4.1 and Proposition 6.4.2 are given in Appendix C.

Remark 6.4.2. *Conditions* (6.18d) *and* (6.19d) *impose constraints that connect the time constant* τ_d *to the performance parameter* λ_M. *In particular, if the performance* $\mathbb{P}$ *requires* *that the slowest mode of the error dynamics is characterized by time constant smaller than $3\tau_d$, then the proposed design procedure cannot be employed.*

6.4.2 String Stability: $\mathcal{L}_2$-Stability Analysis

In this section, we analyze $\mathcal{L}_2$-stability of $\mathcal{H}_i^\omega$ when the matrices in (6.12) and (6.13) are given. Consider the following two assumptions:

Assumption 6.4.1. *There exist constants $\gamma, \epsilon \in \Re_{\geq 0}$, $\mu \in \Re_{>0}$ and $P = P^\top > 0$ such that*

$$\begin{bmatrix} He(PA_{11}) + A_{21}^\top A_{21} + \mu C^\top C & PA_{12} + \mu C^\top D & A_{21}^\top A_{23} + PA_{13} \\ \bullet & \mu D^\top D - \gamma^2 & 0 \\ \bullet & \bullet & A_{23}^T A_{23} - \mu(1+\epsilon) \end{bmatrix} \prec 0 \tag{6.20}$$

holds with A_{11}, A_{12}, A_{13}, A_{21} and A_{23} as in (6.12)*.*

Assumption 6.4.2. *There exists a pair of values (T_2, T_{mad}) such that*

$$\gamma_1\phi_1(\tau_{i-1}) \geq \gamma_0\phi_0(\tau_{i-1}), \quad \forall\tau_{i-1} \in [0, T_{mad}] \tag{6.21a}$$

$$\gamma_0\phi_0(\tau_{i-1}) \geq \lambda^2\gamma_1\phi_1(0), \quad \forall\tau_{i-1} \in [0, T_2] \tag{6.21b}$$

with $T_2 \geq T_{mad} \geq 0$, $\lambda \in (0,1)$, constants $\gamma_0 := \gamma$ and $\gamma_1 := \frac{\gamma}{\lambda}$, and where $\phi_{l_{i-1}} : \Re_{\geq 0} \mapsto \Re, l_{i-1} \in \{0,1\}$ is solution of

$$\dot{\phi}_{l_{i-1}} = -\gamma_{l_{i-1}}(\phi_{l_{i-1}}^2 + 1) \tag{6.22}$$

with initial conditions $\phi_1(0) \geq \phi_0(0) \geq \lambda^2\phi_1(0)$, $\phi_0(T_2) \geq 0$.

Relying on Assumptions 6.4.1 and 6.4.2 it is possible to state the following result.

Theorem 6.4.1. *Let the Assumption 6.4.1 with $\epsilon = 0$ and Assumption 6.4.2 hold, then the hybrid system $\mathcal{H}_i^\omega$ is $\mathcal{L}_2$-stable from the input ω_{i-1} to the output ω_i with an $\mathcal{L}_2$-gain less than or equal to one.*

Theorem 6.4.1 is a particular case of the results presented in [43], which has been customized for the string stability in [23]. For such a reason, we omit the proof, which follows the same approach as in Theorem 4.3.1.

Remark 6.4.3. *As in [23], we consider a small value of* ϵ *to make* (6.20) *numerically treatable.*

To find the trade-off curve between T_2 and T_{mad} such that the string stability is satisfied, we need to employ the result described in Theorem 6.4.1. As first step, given the matrices in (6.12), the values of γ, μ and P can be computed by solving the optimization problem in which γ is minimized subject to (6.20) with ϵ selected small. Next, one can determine (T_{mad}, T_2) trade-off curves by employing the differential equation in (6.22) and conditions (6.21). Refer to [43] for further details.

6.4.3 Controller Tuning Algorithm

The proposed tuning algorithm relies on the fact that γ represents the influence of the networked-induced error η_{i-1} on $\tilde{x}_i$. Therefore, the higher the value of γ, the higher the influence of η_{i-1} on $\tilde{x}_i$. As such, a smaller value of γ is more likely to induce larger values of the MATI and MAD. On the other hand, as illustrated in Section 6.4.1, we want to enforce suitable performance on the "networked-free" closed-loop dynamics. Building upon these facts, our approach aims at designing the controller gains k_p and k_d, such that the following properties hold:

- the closed-loop matrix $A_e \in \mathbb{P}$;
- $\mathcal{H}_i^\omega$ is $\mathcal{L}_2$-stable with $\mathcal{L}_2$-gain $\gamma \leq 1$.

Observe that finding (k_p, k_d) such that the above conditions are satisfied, constitutes a solution to Problem 6.3.1.

Thanks to Theorem 6.4.1, Problem 6.3.1 can be recast as the following optimization problem:

$$\begin{aligned} &\underset{P,k_p,k_d,\mu}{\text{minimize}} && \gamma \\ &\text{subject to} && A_e \in \mathbb{P}, (6.20) \end{aligned} \tag{6.23}$$

Notice that optimization problem (6.23) is nonlinear in the decision variables. For this reason, the solution to (6.23) is difficult from a numerical standpoint [12]. On the other hand, when the gains k_p and k_d are selected, (6.23) is a semidefinite program and its solution can be efficiently obtained via available solvers. One possible strategy to obtain a suboptimal solution to (6.23) consists of performing a bidimensional line search on the parameters k_p and k_d. However, this approach can be computationally expensive if the values of the gains are not chosen wisely. We propose to solve (6.23) by employing the results introduced in Propositions 6.4.1 and 6.4.2, which essentially provide upper and lower bounds on k_p and allow one to eliminate k_d from the design problem. Following this approach, k_p becomes the only design parameter. This, of course, dramatically reduces the complexity of the design algorithm, which reduces to a one-parameter line search over a compact interval. Therefore, for each couple (k_p, k_d) obtained by using Propositions 6.4.1 and 6.4.2, one can employ Theorem 6.4.1 by following the procedure described in Section 6.4.2. The sub-optimal tuning will be obtained for the couple (k_p, k_d) such that the value of γ is minimum. Next, one can use the minimum value of γ for the computation of the (T_{mad}, T_2) trade-off curves.

6.5 Simulation Results

In this session, we apply the previously described LMI-based approach to tune the controller in (6.6) for a homogeneous platoon of 6 vehicles. All the following numerical results are obtained through the solver *SEDUMI* [102] and coded in Matlab® via *YALMIP* [61].

We aim at showing that by choosing the suitable $\mathbb{P}$ we can tune the hybrid controller in (6.6) such that the platoon of vehicles can achieve performances that are as close as in

[85], while being resilient to higher transmission intervals and delays. Notice that [85] does not consider network behaviors, and it is tuned by following continuous-time control design techniques.

From [85], we select $h = 0.7$ and $\tau_d = 0.1$ for the platooning parameters, and $\lambda_M = -0.367$ and $\zeta_m = 0.7$ for the performance $\mathbb{P}$. Furthermore, in [85] the controller is tuned with $k_p = 0.2$ and $k_d = 0.7$ based on speed of response and passenger comfort.

The values of k_p and k_d such that Conditions C1 and C2 are satisfied are depicted in in Fig. 6.3. The value of γ as function of the controller gain k_p is shown in Fig. 6.4. Notice that the design algorithm leads to obtain the minimum $\gamma^* = 2.17$ with $(k_p, k_d) = (1.15, 3.5)$.

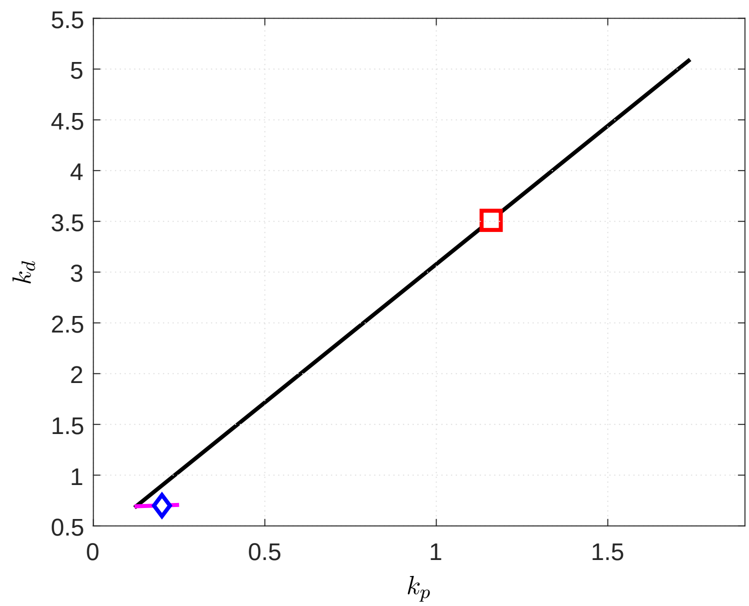

Figure 6.3: Locus of (k_p, k_d) such that Conditions C1 (black) and C2 (magenta) for $\Lambda(A_e)$ are satisfied. The blue diamond and the red square respectively identify $\Lambda(A_e)$ and (k_p, k_d) for the controller tuned as [85] and tuned by following the proposed approach.

Figure 6.5 depicts the (T_{mad}, T_2) trade-off curves for $\gamma = 5.66$, obtained from the gains in [85], and for γ^*. The lines depicted in Fig. 6.5 represent the upper bounds in (T_{mad}, T_2). Beyond those limits, the string stability is no longer guaranteed. Therefore, we can state that the controller tuned with our approach is able to guarantee string stability for larger allowable transmission intervals and larger allowable delays than the controller

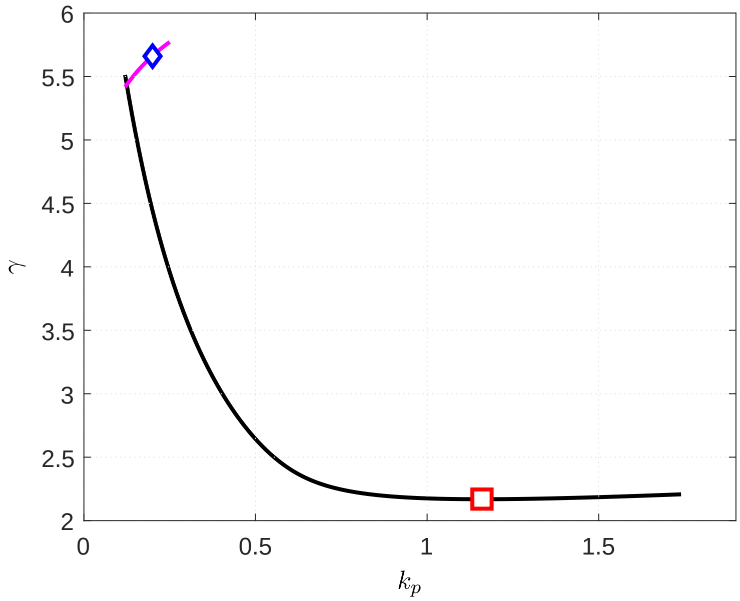

Figure 6.4: Locus of (k_p, γ) such that Conditions C1 (black) and C2 (magenta) for $\Lambda(A_e)$ are satisfied. The blue diamond and the red square respectively identify the final tuning (k_p, γ) for the controller tuned as [85] and tuned by following the proposed approach.

tuned in [85].

To validate our approach we consider a platoon of six vehicles where the leader vehicle performs a step variation in velocity. We select three different network conditions:

1. Transmission intervals and network delays equal to $150.4\,ms$.

2. Transmission intervals of $400\,ms$ and network delays equal to $60\,ms$.

3. Transmission intervals of $700\,ms$ and no network delays.

Simulation results of the considered vehicle platooning with the three network conditions described above are represented respectively in Fig. 6.6, Fig. 6.7, and Fig. 6.8. In particular, these figures depict velocity and distance profiles for vehicle platoons with the controller tuned as in [85] (in subplots (a)-(b)), and tuned with the proposed approach (in subplots (c)-(d)) for different network configurations: Figure 6.6 depicts the case of network delays and transmission intervals equal to $150.4\,ms$; Figure 6.7 shows the case of network characterized by transmission intervals of $400\,ms$ and network delays equal to $60\,ms$; Figure 6.8

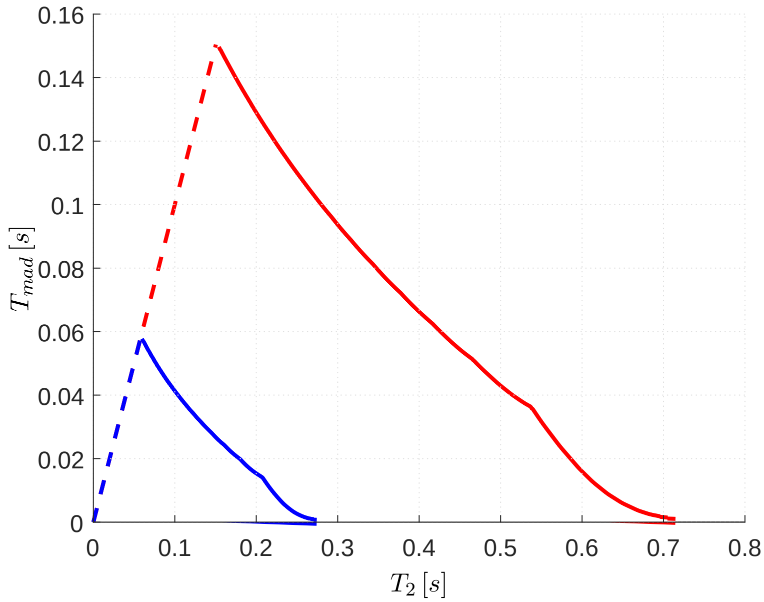

Figure 6.5: (T_{mad}, T_2) trade-off curves. In blue the (T_{mad}, T_2) trade-off curve for the controller as tuned in [85]. In red the (T_{mad}, T_2) trade-off curve computed with the controller tuned by the proposed approach. The dashed lines represent $T_{mad} = T_2$.

depicts the case of transmission intervals of $700\,ms$ and no network delays. Moreover, those figures depict in red the speed of $\mathcal{V}_0$ (in subplots (a)-(c)), and the relative distance between $\mathcal{V}_0$ and $\mathcal{V}_1$ (in subplots (b)-(d)). From light grey to black are respectively depicted speeds of vehicles with indexes from 1 to 5 and relative distances of vehicles with indexes from 2 to 5.

Figures 6.6, 6.7, and 6.8 show that the controller tuned with the proposed approach is less influenced by network imperfections. It is noticeable by the increase in overshoot for increasing vehicle index in case of the vehicle platoon controlled by the tuning in [85].

6.6 Conclusion

In this chapter, we consider the problem of designing a CACC controller with quantifiable robustness margin to variable transmission intervals and variable network delays in the presence of performance requirements.

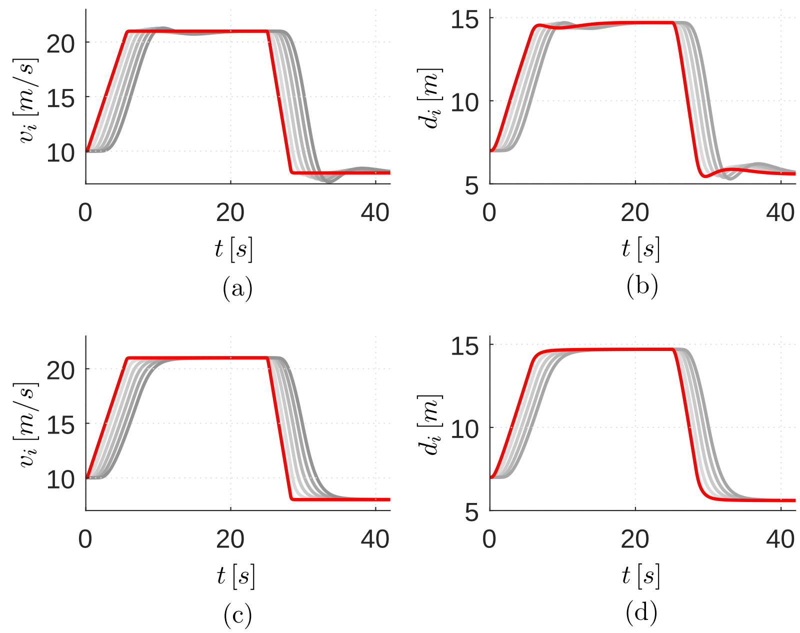

Figure 6.6: Vehicle platoons characterized by network delays and transmission intervals equal to $150.4\,ms$.

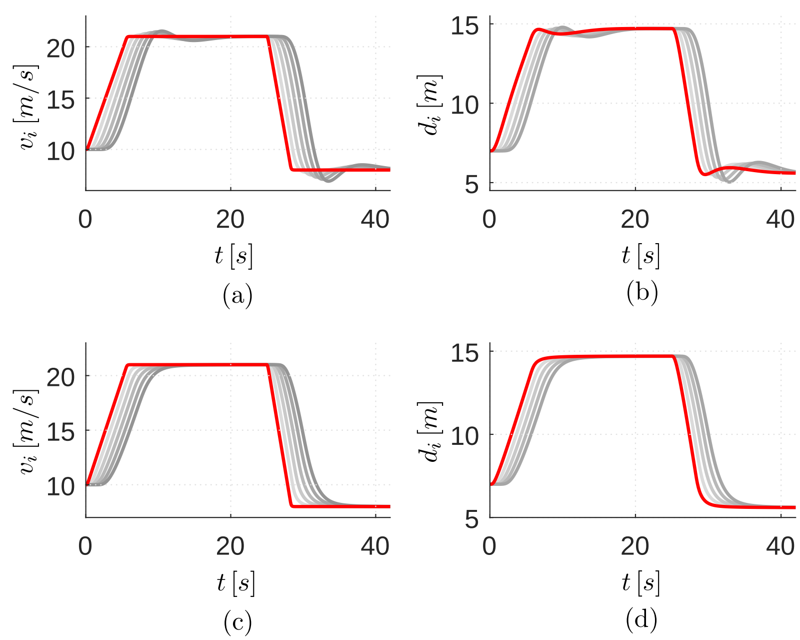

Figure 6.7: Vehicle platoons characterized by transmission intervals of $400\,ms$ and network delays equal to $60\,ms$.

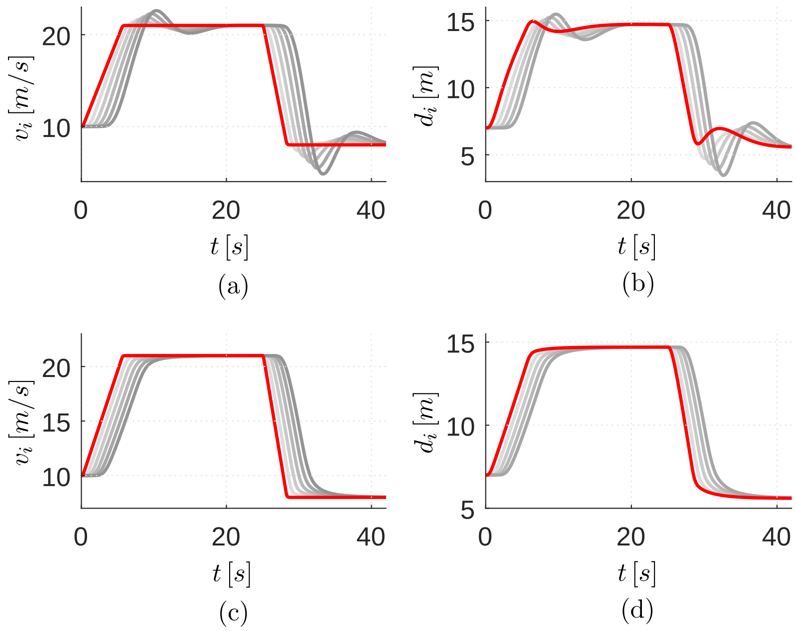

Figure 6.8: Vehicle platoons characterized by transmission intervals of $700\,ms$ and no network delays.

Conditions are provided to design the controller in such a way that the performance requirements and string stability are satisfied. Furthermore, we describe an algorithm tailored to this particular application, which allows solving the control problem in a computationally efficient way by employing a one parameter line search over a compact interval.

Simulation results show the effectiveness of our approach. We show that the hybrid controller designed in this chapter is more resilient to network imperfections compared to [85], which is designed with a continuous-time control approach.

Chapter 7

A Hybrid Controller for DoS-Resilient String-Stable Vehicle Platoons

7.1 Introduction

In this chapter, we introduce a decentralized hybrid controller that modifies the continuous-time proportional-derivative regulator in [85]. Closer to real implementation, our controller takes into account the packet-based nature of the IVC. To overcome the network imperfections due to the intermittent remote measurements exchanged through IVC, we equip our controller with a Zero Order Hold (ZOH) device that stores the last received measurements in between IVC packet updates.

We consider DoS attacks as a sequence of limited time intervals in which the attacker interrupts the communication channel. During each DoS attack, the communication network experiences a limited number of packet dropouts. The maximum number of packet dropouts that the CACC can overcome without compromising the stability of the vehicle platooning is denoted as the *maximum allowable number of successive packet dropouts* (MANSD). In this chapter, MANSD is considered as the evaluation metric of the resiliency of the vehicle platooning to DoS attacks.

The design approach is based on a numerically efficient tuning algorithm based on linear matrix inequalities (LMI), which aims at finding optimal gains for the controller that maximizes the resiliency to DoS while guaranteeing performance requirements and string stability of the vehicle platooning. Furthermore, the proposed algorithm estimates the value of MANSD, which identifies the worst DoS attack that the control system can overcome without compromising string stability.

7.2 Modeling

7.2.1 Platooning Dynamics

In this section, we briefly recall the dynamics of the platooning, which is wholly presented in Section 6.2.1.

We consider a homogeneous vehicle platooning formed by m identical cars. The i-th vehicle in the platoon is identified as $\mathcal{V}_i$. Each vehicle must maintain the reference distance d_{r_i} from its preceding vehicle by employing a constant time gap policy reference. The longitudinal vehicle dynamics of $\mathcal{V}_i$ can be described as follows

$$\mathcal{V}_i : \begin{bmatrix} \dot{e}_i \\ \dot{v}_i \\ \dot{a}_i \end{bmatrix} = \begin{bmatrix} v_{i-1} - v_i - ha_i \\ a_i \\ -\frac{1}{\tau_d} a_i + \frac{1}{\tau_d} u_i \end{bmatrix}, \quad i \in P_m \tag{7.1}$$

where v_i, a_i, and u_i are, respectively, the speed, the acceleration, and the control input of $\mathcal{V}_i$, and τ_d represents the time constant of the powertrain dynamics of the vehicles in the platooning. Since we consider a homogeneous vehicle platooning, h and τ_d are identically for each vehicle.

The continuous-time controller introduced in [85] is given by the following dynamics

$$\dot{u}_i = \mathcal{K}_h(u_i, \chi_i) \tag{7.2a}$$

$$\chi_i = \mathcal{K}_{PD}(e_i) + u_{i-1} \tag{7.2b}$$

where u_{i-1} is the control signal of $\mathcal{V}_{i-1}$, $\mathcal{K}_h(u_i, \chi_i) \coloneqq -\frac{1}{h}u_i + \frac{1}{h}\chi_i$, and $\mathcal{K}_{PD}(e_i) \coloneqq k_p e_i + k_d \dot{e}_i$, and k_p and k_d are the controller gains.

7.2.2 Communication Network and DoS Attacks

We assume that the measurement u_{i-1} is sampled and sent periodically at instants $t_{k_{i-1}}$, $k_{i-1} \in \mathfrak{N}$ with constant transmission interval $T_s \in \mathfrak{R}_{>0}$, i.e., $t_{k_{i-1}+1} - t_{k_{i-1}} = T_s$, $t_0 = 0$. In addition, we consider that the presence of IVC exposes the vehicle platooning to DoS attacks. DoS attacks aim at making the network unavailable, e.g., by injecting excessive traffic [5, 114] or by adopting jamming strategies [89]. Hence, under DoS attacks, the IVC experiences packet dropouts and connected vehicles are unable to cooperate properly [6]. Indeed, during DoS attacks, vehicles in the platooning do not receive any signal from the preceding vehicles, hence, u_{i-1} is unavailable to the controllers.

7.2.3 Adversarial Model of DoS attacks

We consider that the objective of the attacker is to perform a DoS attack by using a radio jamming strategy, which deliberately disrupts communications over a geographic area [6]. The jamming strategy is unknown to the controller. However, it is assumed that it is energy and geography constrained: the attacker can perform DoS attacks that generate packet dropouts only for a finite period in time due to limited amount of resources and because the platoon could move to an attack-free area. Notice that detection and mitigation techniques could be implemented in the vehicle network to reduce the duration of the DoS attacks further [6, 40]. As such, packet losses due to DoS attacks can be assumed to be persistent only for a limited period of time [5], and can be modeled by considering an upper bound to the maximum number of successive packet dropouts.

Inspired by [24, 27], we model a DoS attack as a limited time period where an attacker succeeds in blocking the signal u_{i-1} in such a way that it cannot reach the controller in vehicle $\mathcal{V}_i$. Therefore, several DoS attacks can be seen as a sequence of intervals $\{H_n\}_{n\in\mathbb{N}}$, each one of finite length, where the IVC network is interrupted. Specifically, we assume that the n-th DoS attack produces $\iota_n \in \{0, 1, \ldots, \Delta\}, \forall n \in \mathbb{N}$, consecutive packet dropouts, where $\Delta \in \mathfrak{N}_0$ is the *maximum allowable number of successive packet dropouts* (MANSD), i.e., the maximum number of consecutive packet losses such that the vehicle platooning maintains his stability properties. Furthermore, we assume that at least one successful transmission is expected to occur in between intervals $\{H_n\}_{n\in\mathbb{N}}$. A feasible sequence $\{H_n\}_{n\in\mathbb{N}}$ is shown in Fig. 7.1.

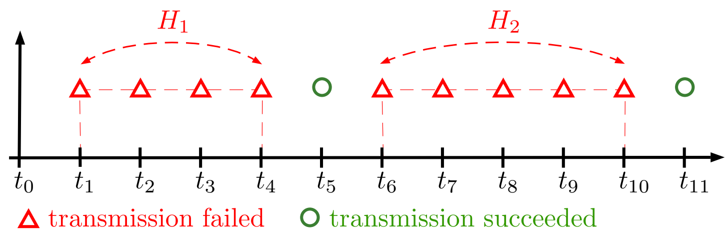

Figure 7.1: Evolution of packet dropouts due to DoS attacks.

It is worth mentioning that, as discussed in [21], there are less conservative models for DoS attacks. However, we employ a characterization of DoS attacks via MANSD to reduce the complexity of the design procedure. Nevertheless, regardless the selected adversarial model, prolonged unavailability of network data can degrade or compromise string stability; see [51, 60, 82, 83, 96]. Therefore, tuning the CACC in such a way to maximize the resilience to DoS attacks is of paramount importance. This is achieved by selecting the controller gains to maximize the value of MANSD. Moreover, notice that the estimation of MANSD is significant as a resiliency metric that allows one to be aware of the limits of the design approach.

7.3 Controller Outline and Problem Formulation

7.3.1 Proposed Networked Controller

In this section, we propose a modified version of the controller in (7.2) that takes into account the discrete nature of the data available through the network. The control scheme is depicted in Fig. 7.2.

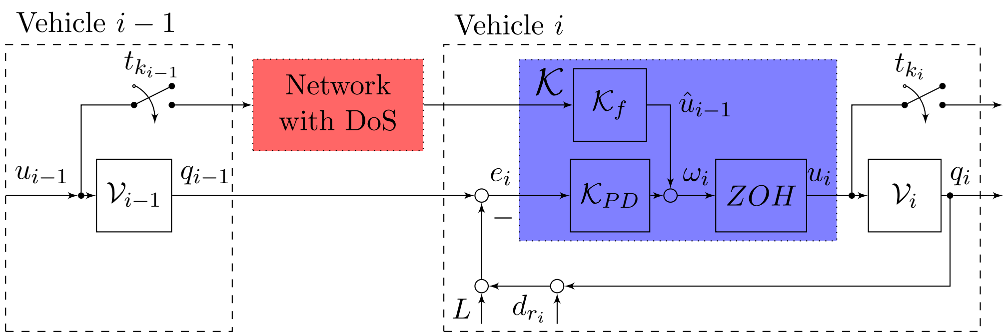

Figure 7.2: Schematic of the control system in $\mathcal{V}_i$. In particular, signal connections between vehicles $\mathcal{V}_{i-1}$ and $\mathcal{V}_i$ along with the proposed hybrid controller $\mathcal{K}$ (in the purple area) are shown.

For each i, the proposed hybrid controller handles discrete measurements of u_{i-1}, which are available through network packets only at time $t_{k_{i-1}}$, $k_{i-1} \in \mathfrak{N}_0$. Specifically, the controller in (7.2) is augmented by the state $\hat{u}_{i-1} \in \mathfrak{R}$, which stores the network signal u_{i-1}. The arrival of a new packet with the information of $u_{i-1}(t_{k_{i-1}})$ triggers an instantaneous jump in $\hat{u}_{i-1}$, which is updated to the last received value of u_{i-1}. Then, in between received packets, $\hat{u}_{i-1}$ is kept constant in a Zero Order Hold (ZOH) fashion. More precisely, dynamics of $\hat{u}_{i-1}$ can be modeled as a system with jumps in its state. In particular, its dynamics can be given as follows for all $k_{i-1} \in \mathfrak{N}_0$:

$$\begin{cases} \dot{\hat{u}}_{i-1}(t) = 0 & \forall t \neq t_{k_{i-1}} \ \vee \ t_{k_{i-1}} \in \bigcup_{n\in\mathfrak{N}} H_n \\ \hat{u}_{i-1}(t^+) = u_{i-1}(t_{k_{i-1}}) & \forall t = t_{k_{i-1}} \ \wedge \ t_{k_{i-1}} \notin \bigcup_{n\in\mathfrak{N}} H_n \end{cases} \tag{7.3}$$

Notice that $\hat{u}_{i-1}$ is set to $u_{i-1}(t_{k_{i-1}})$ only in case of successful transmissions.

Differently from (7.2), the controller is fed with $\hat{u}_{i-1}$, and its continuous-time dynamics are given by:

$$\dot{u}_i = \mathcal{K}_h(u_i, \omega_i), \quad \omega_i := \mathcal{K}_{PD}(e_i) + \hat{u}_{i-1} \tag{7.4}$$

The interconnection between the ZOH device in (7.3) and the controller in (7.4) is denoted by $\mathcal{K}$ and represents the proposed hybrid controller.

7.3.2 Hybrid Modeling

The stability of the vehicle platooning is studied by analyzing the dynamics of the closed-loop system obtained by the interconnection of (7.1), (7.3), and (7.4). To this end, let $e_{1,i} := e_i$, $e_{2,i} := \dot{e}_i$ and $e_{3,i} := \ddot{e}_i$, by straightforward calculations one obtains that for all $k_{i-1} \in \mathfrak{N}_0$

$$\begin{cases} \dot{e}_{1,i} = e_{2,i} \\ \dot{e}_{2,i} = e_{3,i} \\ \dot{e}_{3,i} = -\dfrac{k_p}{\tau_d} e_{1,i} - \dfrac{k_d}{\tau_d} e_{2,i} - \dfrac{1}{\tau_d} e_{3,i} + \dfrac{1}{\tau_d} u_{i-1} - \dfrac{1}{\tau_d} \hat{u}_{i-1} & \begin{array}{l} \forall t \neq t_{k_{i-1}} \vee \\ t_{k_{i-1}} \in \bigcup\limits_{n \in \mathfrak{N}} H_n \end{array} \\ \dot{u}_{i-1} = -\dfrac{1}{h} u_{i-1} + \dfrac{1}{h} \omega_{i-1} \\ \dot{\hat{u}}_{i-1} = 0 \end{cases}$$

$$\begin{cases} e_{1,i}(t^+) = e_{1,i}(t) \\ e_{2,i}(t^+) = e_{2,i}(t) \\ e_{3,i}(t^+) = e_{3,i}(t) & \begin{array}{l} \forall t = t_{k_{i-1}} \wedge \\ t_{k_{i-1}} \notin \bigcup\limits_{n \in \mathfrak{N}} H_n \end{array} \\ u_{i-1}(t^+) = u_{i-1}(t) \\ \hat{u}_{i-1}(t^+) = u_{i-1}(t) \end{cases} \tag{7.5}$$

For the sake of notation, notice that the dependence on time in continuous-time dynamics is omitted. By following the same approach in Section 6.3.2, we model we model the impulsive system (7.5) into the hybrid systems framework in [37], , for which preliminary information is in Chapter 2. To this end, we introduce the auxiliary variable $\tau_{i-1} \in \mathfrak{R}_{\geq 0}$ and the change of coordinates $\eta_{i-1} := \hat{u}_{i-1} - u_{i-1}$. This leads, by straightforward calculation, to the following hybrid system:

$$\mathcal{H}_i^\omega \begin{cases} \dot{x}_i = f(x_i, \omega_{i-1}) & x_i \in C, \omega_{i-1} \in \mathfrak{R} \\ x_i^+ = g(x_i) & x_i \in D \\ \omega_i = C_\omega \tilde{x}_i + \eta_{i-1} \end{cases} \tag{7.6}$$

where $x_i := (\tilde{x}_i, \eta_{i-1}, \tau_{i-1}) \in \mathfrak{R}^6$ is the state, and $\tilde{x}_i := (e_{1,i}, e_{2,i}, e_{3,i}, u_{i-1}) \in \mathfrak{R}^4$, and ω_i, with $C_\omega = \begin{bmatrix} k_p & k_d & 0 & 1 \end{bmatrix}$, is the performance output employed to evaluate string stability. The flow map is given by

$$f(x_i, \omega_{i-1}) := (f_{\tilde{x}}(\tilde{x}_i, \eta_{i-1}, \omega_{i-1}), f_\eta(\tilde{x}_i, \eta_{i-1}, \omega_{i-1}), 1) \tag{7.7}$$

where

$$\begin{aligned} f_{\tilde{x}}(\tilde{x}_i, \eta_{i-1}, \omega_{i-1}) &:= A_{xx}\tilde{x}_i + A_{x\eta}\eta_{i-1} + A_{x\omega}\omega_{i-1} \\ f_\eta(\tilde{x}_i, \eta_{i-1}, \omega_{i-1}) &:= A_{\eta x}\tilde{x}_i - \tfrac{1}{h}\omega_{i-1} \end{aligned} \tag{7.8}$$

with

$$A_{xx} = \begin{bmatrix} A_e & \mathbf{0} \\ \mathbf{0} & -\frac{1}{h} \end{bmatrix}, A_{x\eta} = \begin{bmatrix} 0 & 0 & -\frac{1}{\tau_d} & 0 \end{bmatrix}^\top$$
$$A_{x\omega} = \begin{bmatrix} 0 & 0 & 0 & \frac{1}{h} \end{bmatrix}^\top, A_{\eta x} = \begin{bmatrix} 0 & 0 & 0 & \frac{1}{h} \end{bmatrix}$$

and

$$A_e = \begin{bmatrix} 0 & 1 & 0 \\ 0 & 0 & 1 \\ -\frac{k_p}{\tau_d} & -\frac{k_d}{\tau_d} & -\frac{1}{\tau_d} \end{bmatrix}$$

The jump map is given by

$$g(x_i) := (\tilde{x}, 0, 0) \tag{7.9}$$

whereas the flow set and the jump set are respectively given by

$$C := \mathfrak{R}^5 \times [0, (\Delta + 1)T_s] \tag{7.10}$$

and

$$D := \Re^5 \times T_s\Theta_\Delta \tag{7.11}$$

where $\Theta_\Delta := \{1, 2, \ldots, \Delta + 1\}$.

Remark 7.3.1. *The model in* (7.6) *considers only successful transmissions. In particular, successful transmissions occur for $\tau_{i-1} = T_s$ when no DoS occurs, whereas they occur for $\tau_{i-1} \in \iota T_s$, with $\iota := \{2, \ldots, \Delta + 1\}$, for DoS attacks generating a number of consecutive packet dropouts within* 1 *and Δ. This characteristic is captured by the definition of D_ξ. Furthermore, by definition, C_ξ and D_ξ overlap each other, and, when ξ belongs to $C_\xi \cap D_\xi$, the state of the system can either flow or jump because of a successful transmission. As such, solutions to* (7.6) *are not unique. For this reason, our model captures all possible network behaviors, in presence or not of DoS attacks, in a unified fashion.*

7.3.3 Problem Formulation

As extensively described in Chapter 6, a platoon of vehicles controlled by CACC needs to accomplish two main goals [23]: 1) regulate the spacing error in (6.1) (also known as individual vehicle stability), and 2) attenuate disturbance and shock waves along the vehicle platooning (also known as string stability). In the following, we briefly introduce those two properties; refer to Section 6.3.3 for further details.

The first property we want to guarantee is usually referred to as individual vehicle stability. When satisfied, if $\mathcal{V}_0$ travels at some constant speed, the CACC ensures that $\lim_{t\to\infty} e_i(t) = 0$ for the rest of the vehicles in the platoon. This property is strictly connected with the eigenvalues of A_e, which depend on gains k_p and k_d. To guarantee individual vehicle stability with some performance, we characterize performance requirements by introducing the set

$$\mathbb{P}(\lambda_M, \zeta_m) := \{A \in \Re^{n\times n} | \Lambda_{\max}(A) = \lambda_M,\, \zeta_{\min}(A) \geq \zeta_m\} \tag{7.12}$$

where $\lambda_M < 0$ and $\zeta_m \in (0, 1]$ are design parameters. The set $\mathbb{P}(\lambda_M, \zeta_m)$ defines constraints on the location of the eigenvalues of A_e in the complex plane.

The second property we want to guarantee is also referred to as the string stability of the vehicle platooning. It is related to the notion of $\mathcal{L}_2$-stability. In particular, concerning string stability, we refer to Definition 6.3.1 available in Section 6.3.3. It is worth mentioning that, as in Chapter 6, the analysis of string stability of the whole vehicle platooning can be analyzed by focusing on the input-output properties of the single vehicle, i.e., on the $\mathcal{L}_2$-stability of $\mathcal{H}_i^\omega$, for $i \in P_m$. String stability can be addressed from the single-vehicle viewpoint since we consider homogeneous vehicle platoons.

A critical aspect of the string stability is that it is negatively influenced by the IVC. Indeed, string stability can be degraded or compromised when network imperfections lead to prolonged unavailability of updated measurements; see [51, 60, 82, 83, 96]. Therefore, it is important to design a CACC such that the vehicle platooning maintains string stability for the largest achievable value of MANSD (identified by Δ). Furthermore, estimating Δ provides an important metric for the evaluation of the resiliency of the overall platooning concerning the DoS attacks.

The problem we solve in this chapter can now be introduced as follows.

Problem 7.3.1. *Given the platooning parameters h and τ_d, and $\mathbb{P}$ as in* (7.12)*, design gains k_p and k_d for the hybrid controller $\mathcal{K}$ such that the vehicle platooning given by* (6.2)*,* (7.1)*,* (7.3)*, and* (7.4) *satisfies the following properties with the largest achievable value of Δ:*

(P1) Individual vehicle stability with performance $\mathbb{P}$, i.e., $A_e \in \mathbb{P}$.

(P2) String stability.

7.4 Controller Design

In this section, we illustrate our approach to solve Problem 7.3.1. After describing how to meet the required performance for the individual vehicle stability, we provide sufficient conditions for $\mathcal{L}_2$-stability of $\mathcal{H}_i^\omega$, i.e., string stability of the vehicle platoon. Finally, we describe a procedure to design the controller gains to maximize the value of Δ, while satisfying the two stability properties.

7.4.1 Individual Vehicle Stability with Performance Requirements

In this section, we briefly review conditions for individual stability extensively discussed in Section 6.4.1. To this end, to ensure individual vehicle stability with satisfactorily performance, we design k_p and k_d such that $A_e \in \mathbb{P}(\lambda_M, \zeta_m)$. In particular, we aim at identifying numerical values of k_p and k_d such that for any matrix $A_e \in \mathbb{P}(\lambda_M, \zeta_m)$ one of the following conditions holds:

(C1) the real eigenvalue is equal to λ_M and, the other two eigenvalues have real part less than or equal to λ_M with damping ratio greater than ζ_m;

(C2) the spectrum of A_e is characterized by a single couple of complex eigenvalues with real part equal to λ_M and damping ratio greater than ζ_m, and the other real eigenvalue is less than λ_M.

Next, we provide necessary and sufficient conditions on k_p and k_d such that C1 or C2 hold.

Proposition 7.4.1 (N.S.C. for C1)**.** *Let k_p, $k_d \in \Re$, $\lambda_M \in \Re_{<0}$, and $\zeta_m \in \Re_{>0}$. Then, C1 is satisfied if and only if the following conditions hold:*

$$k_d = f_{C1}(k_p) := -\frac{1}{\lambda_M} k_p - \lambda_M^2 \tau_d - \lambda_M \tag{7.13a}$$

$$k_p \le \frac{|\lambda_M|(\lambda_M \tau_d + 1)^2}{4\tau_d \zeta_m^2} := \bar{k}_{pC1} \tag{7.13b}$$

$$k_p \ge 2\tau_d \lambda_M^3 + \lambda_M^2 := \underline{k}_{pC1} \tag{7.13c}$$

$$\lambda_M > -\frac{1}{3\tau_d} \tag{7.13d}$$

Now we provide necessary and sufficient conditions on the gains k_p and k_d to guarantee C2.

Proposition 7.4.2 (N.S.C. for C2)**.** *Let k_p, $k_d \in \mathfrak{R}$, $\lambda_M \in \mathfrak{R}_{<0}$, and $\zeta_m \in (0,1)$. Then, C2 holds if and only if the following conditions hold:*

$$k_d = f_{C2}(k_p) := -\frac{8\lambda_M^3\tau_d^2 + 8\lambda_M^2\tau_d + 2\lambda_M - \tau_d k_p}{2\lambda_M\tau_d + 1} \tag{7.14a}$$

$$k_p \le \frac{\lambda_M^2(2\lambda_M\tau_d + 1)}{\zeta_m^2} := \bar{k}_{pC2} \tag{7.14b}$$

$$k_p > 2\tau_d\lambda_M^3 + \lambda_M^2 := \underline{k}_{pC2} \tag{7.14c}$$

$$\lambda_M > -\frac{1}{3\tau_d} \tag{7.14d}$$

7.4.2 Sufficient Conditions for Platooning Stability

The previous subsection describes how to obtain the set of gains k_p and k_d such that the individual vehicle stability has satisfactory performance. In this subsection, we consider k_p and k_d as given, and we study the stability of $\mathcal{H}_i^\omega$, which also includes the network dynamics.

Our approach aims at formulating the control problem as a set stabilization problem. In particular, our approach consists of analyzing the stability properties of the following compact set

$$\mathcal{A} := \{0\} \times \{0\} \times [0, (\Delta + 1)T_s] \tag{7.15}$$

Definition 2.3.1 formalizes these properties. Moreover, to satisfy string stability, $\mathcal{H}_i^\omega$, $i \in P_m$, must be $\mathcal{L}_2$-stable from the input ω_{i-1} to the output ω_i with an $\mathcal{L}_2$-gain less than or equal to one. It is worth mentioning that whenever eISS and $\mathcal{L}_2$-stability are satisfied, the vehicle platooning given by (6.2), (7.1), (7.3), and (7.4) satisfies individual vehicle stability and string stability. In the following, we identify sufficient conditions to ensure those two stability properties. First, we employ Lyapunov theory for hybrid systems to provide conditions for eISS and $\mathcal{L}_2$-stability of $\mathcal{H}_i^\omega$ (Assumption 7.4.1 and Theorem 7.4.1). Then, we give sufficient conditions for eISS and $\mathcal{L}_2$-stability in the form of matrix inequalities (Theorem 7.4.2 and Lemma 7.4.1).

Consider the following assumption.

Assumption 7.4.1. *There exist two continuously differentiable functions $V_1 : \mathfrak{R}^4 \to \mathfrak{R}$, $V_2 : \mathfrak{R}^2 \to \mathfrak{R}$ and positive real numbers α_1, α_2, β_1, β_2, λ_t, and ϵ such that*

(A1) $\alpha_1|\tilde{x}_i|^2 \leq V_1(\tilde{x}_i) \leq \alpha_2|\tilde{x}_i|^2, \quad \forall x_i \in C$

(A2) $\beta_1|\eta_{i-1}|^2 \leq V_2(\eta_{i-1}, \tau_{i-1}) \leq \beta_2|\eta_{i-1}|^2, \quad \forall x_i \in C$

(A3) $V_2(0,0) \leq V_2(\eta_{i-1}, \tau_{i-1})$, $\forall \eta_{i-1} \in \mathfrak{R}$, $\tau_{i-1} \in T_s\Theta_\Delta$

(A4) the function $x_i \mapsto V(x_i) := V_1(\tilde{x}_i) + V_2(\eta_{i-1}, \tau_{i-1})$ *satisfies* $\langle \nabla V(x_i), f(x_i, \omega_{i-1})\rangle \leq -2\lambda_t V(x_i) - \omega_i^2 + \theta^2\omega_{i-1}^2$ *for each* $x_i \in C, \omega_{i-1} \in \mathfrak{R}$*, where* $\omega_i^2 = \tilde{x}_i^\top C_\omega^\top C_\omega \tilde{x}_i + \eta_{i-1}^2 + 2C_\omega\tilde{x}_i\eta_{i-1}$ *from performance output in* (7.6)*.*

Based on Assumption 7.4.1, the result given next provides sufficient conditions for eISS and $\mathcal{L}_2$-stability of $\mathcal{H}_i^\omega$.

Theorem 7.4.1. *Let Assumption 7.4.1 hold. Then:*

(i) The hybrid system $\mathcal{H}_i^\omega$ is eISS with respect to $\mathcal{A}$;

(ii) The hybrid system $\mathcal{H}_i^\omega$ is $\mathcal{L}_2$-stable from the input ω_{i-1} to the output ω_i with an $\mathcal{L}_2$-gain less than or equal to θ.

The proof is given in Appendix C.

Theorem 7.4.2. *Given the platooning parameters τ_d, h, k_p, k_d, the transmission interval T_s, the MANSD Δ, and $\theta \in \Re$, if there exist $P_1 \in \mathcal{S}_+^4$, $p_2 \in \Re_{>0}$, and $\delta \in \Re_{>0}$ such that*

$$\mathcal{M}(\tau_{i-1}) \prec 0, \, \forall \tau_{i-1} \in [0, (\Delta+1)T_s] \tag{7.16}$$

where the function $[0, (\Delta+1)T_s] \ni \tau_{i-1} \mapsto \mathcal{M}(\tau_{i-1})$ *is given by*

$$\mathcal{M}(\tau_{i-1}) = \begin{bmatrix} He(P_1 A_{xx}) + C_\omega^\top C_\omega & P_1 A_{x\eta} + C_\omega^\top + e^{-\delta\tau_{i-1}} p_2 A_{\eta x}^\top & P_1 A_{x\omega} \\ \bullet & -\delta p_2 e^{-\delta\tau_{i-1}} + 1 & -e^{-\delta\tau_{i-1}} p_2 / h \\ \bullet & \bullet & -\theta^2 \end{bmatrix} \tag{7.17}$$

Then, functions $\tilde{x}_i \mapsto V_1(\tilde{x}_i) := \tilde{x}_i^\top P_1 \tilde{x}_i$, *and* $(\eta_{i-1}, \tau_{i-1}) \mapsto V_2(\eta_{i-1}, \tau_{i-1}) := p_2 \eta_{i-1}^2 e^{-\delta\tau_{i-1}}$ *satisfy Assumption 7.4.1.*

The proof is given in Appendix C. The following lemma is employed to reduce the complexity in the use of Theorem 7.4.2.

Lemma 7.4.1. *Let $P_1 \in \mathcal{S}_+^4$, p_2, δ, τ_d, h, and T_s be given positive real number, $\Delta \in \mathfrak{N}_0$, and k_p, and k_d be given real numbers. For each $\tau_{i-1} \in [0, (\Delta+1)T_s]$, define $\mathcal{M} : \tau_{i-1} \mapsto \mathcal{M}(\tau_{i-1})$. Then, $rge\mathcal{M} = Co\{\mathcal{M}(0), \mathcal{M}((\Delta+1)T_s)\}$. Therefore,* (7.16) *holds if and only if*

$$\mathcal{M}(0) \prec 0, \quad \mathcal{M}((\Delta+1)T_s) \prec 0 \tag{7.18}$$

The proof is given in Appendix C.

The satisfaction of Theorem 7.4.2 leads to stability of $\mathcal{H}_i^\omega$ with $\mathcal{L}_2$-gain less than or equal to θ. However, notice that the requirement for string stability is $\mathcal{L}_2$-gain less than or equal to one. Moreover, consider that the individual vehicle stability leads to an $\mathcal{L}_2$-gain lower-bounded by one. Therefore, considering $\theta = 1$ would make (7.18) infeasible. For such a reason, one needs to consider a $\mathcal{L}_2$-gain less than or equal to $\theta = \sqrt{1+\epsilon}$, where ϵ is a small strictly positive value. A similar approach is employed in [23].

Remark 7.4.1. *Notice that using Lemma 7.4.1 significantly reduces the complexity of results in Theorem 7.4.2. Indeed, it allows to convert the infinite set of matrix inequalities in* (7.16) *to only two matrix inequalities in* (7.18)*.*

7.4.3 Controller Tuning Algorithm

In the following, we show how to employ Proposition 7.4.1, Proposition 7.4.2, and Theorem 7.4.2 to devise a procedure for the selection of gains k_p and k_d able to solve Problem 7.3.1.

Employing Theorem 7.4.2 and Lemma 7.4.1, one can reformulate Problem 7.3.1 as the following optimization problem:

$$\begin{aligned} &\underset{P_1,p_2,\delta,k_p,k_d}{\text{maximize}} && \Delta \\ &\text{subject to} && A_e \in \mathbb{P}, (7.18) \end{aligned} \tag{7.19}$$

Notice that the optimization problem (7.19) is nonlinear in the decision variables. For this reason, the solution to (7.19) is difficult from a numerical point of view [12]. In particular, notice that sufficient conditions (7.18) are in the form of matrix inequalities that are nonlinear in P_1, p_2, δ, k_p, and k_d. Therefore, they cannot be directly used as a computationally tractable design tool. On the other end, when δ, Δ, k_p, and k_d are fixed, (7.18) is linear in variables P_1 and p_2, hence, (7.19) becomes a semidefinite program and can be solved by using available solvers.

Our proposed strategy to obtain a suboptimal solution to (7.19) consists of operating a two-stage line search for the scalars k_p, k_d, δ, and Δ. The first stage consists of choosing values (k_p, k_d) such that $A_e \in \mathbb{P}$. The second stage considers (k_p, k_d) as given, and targets estimating the largest value of Δ by checking the feasibility of (7.18) through line searches for δ and Δ. Observe that while a line searches for δ and Δ can be easily implemented with numerical algorithms, exploring values (k_p, k_d) such that $A_e \in \mathbb{P}$ can be computationally expensive if (k_p, k_d) are not suitably selected, e.g., by using gridding techniques on both k_p and k_d. In this chapter, we choose values (k_p, k_d) by employing Propositions 7.4.1 and 7.4.2, which give upper and lower bounds on k_p and yield to obtain k_d as a function of k_p; see (7.13) and (7.14). By following this approach, k_p becomes the only parameter for the first stage of the design algorithm, which employs only a bounded line search on k_p with bounds known in advance. Hence, Propositions 7.4.1 and 7.4.2 dramatically reduce the complexity of the design procedure.

To summarize, the design procedure we propose to solve Problem 7.3.1 is outlined in Algorithms 2 and 3. In particular, Algorithm 2 provides the overall design procedure and calls Algorithm 3 for the second stage of the design strategy, i.e., estimating the value of Δ for given (kp, kd).

Algorithm 2 Tuning algorithm for performance $\mathbb{P}$, string stability, and the largest achievable Δ

Input: T_s, τ_d, h

Step 1: Explore (k_p, k_d) such that $\Lambda(A_e)$ as in C1.
  Define an array $\overrightarrow{k}_{pC1}$, with elements in $[\underline{k}_{pC1}, \bar{k}_{pC1}]$.
  For each k_p in $\overrightarrow{k}_{pC1}$:
    Feed **Algorithm 3** with $(k_p, f_{C1}(k_p))$.
    Store returned values of Δ.
  Identify k_p, k_d such that Δ is the largest.
End Step 1.
Step 2: Explore (k_p, k_d) such that $\Lambda(A_e)$ as in C2.
  Define an array $\overrightarrow{k}_{pC2}$, with elements in $(\underline{k}_{pC2}, \bar{k}_{pC2}]$.
  For each k_p in $\overrightarrow{k}_{pC2}$:
    Feed **Algorithm 3** with $(k_p, f_{C2}(k_p))$.
    Store returned values of Δ.
  Identify k_p, k_d such that Δ is the largest.
End Step 2.
Step 3: Parameters of controller $\mathcal{K}$ are assigned with values of k_p, k_d such that Δ is the largest among Step 1 and Step 2.

7.5 Numerical Results

In this section, we apply Algorithm 2 to tune the controller $\mathcal{K}$ for a homogeneous platooning of 11 vehicles. In particular, we select performance $\mathbb{P}$ from [85], and we show the outcome of tuning the controller parameters k_p, k_d by following the approach proposed

Algorithm 3 Given (k_p, k_d), estimate the largest achievable Δ

Input: T_s, τ_d, h, k_p, k_d

Initialize Δ_i, Δ, *stop* to zero.
while $stop = 0$ **do**
    line search on δ for given Δ_i such that (7.18) is feasible.
    if (line search succeeded) **then**
        $\Delta \leftarrow \Delta_i$, $\Delta_i \leftarrow \Delta_i + 1$
    else
        $stop \leftarrow 1$
    end if
end while
return Δ

in this chapter. All numerical results are obtained by using Matlab®. Semidefinite optimizations are performed by using *YALMIP* [61] with solver *SEDUMI* [102].

Numerical results are obtained by assuming a transmission rate for measurement u_{i-1} equal to 20 Hz ($T_s = 0.05\,s$), as adopted in [36]. Moreover, we select parameters $h = 0.7$, $\tau_d = 0.1$, $\lambda_M = -0.367$ from [85], and $\zeta_m = 0.7$. Let $\bar{\mathcal{K}}$ be the controller in (7.4) with gains $(k_p, k_d) = (0.2, 0.7)$, as in [85], and consider $\hat{\mathcal{K}}$ the same controller tuned with our approach. The design of $\hat{\mathcal{K}}$ through Algorithm 2 results in a final tuning characterized by $(k_p, k_d) = (0.82, 2.6)$.

To better understand the approach, consider Fig. 7.3, Fig. 7.4, and Fig. 7.5, which respectively represent the locus of $\Lambda(A_e)$ in the complex plane, the locus (k_p, k_d) such that $A_e \in \mathbb{P}$, and the locus (k_p, Δ) such that $A_e \in \mathbb{P}$ and string stability are satisfied. Notice that the tuning of $\hat{\mathcal{K}}$ aims at selecting the minimum value of k_d such that Δ is maximum. This choice allows reducing at minimum the effect of the derivative action on the controlled vehicles. By analyzing the tuning of controllers $\bar{\mathcal{K}}$ and $\hat{\mathcal{K}}$ in Fig. 7.5, one can conclude that $\hat{\mathcal{K}}$, tuned with Algorithm 2, guarantees performance $\mathbb{P}$ and string stability with higher resiliency to DoS attacks with respect to $\bar{\mathcal{K}}$. This emerges from the fact that the value of Δ obtained for $\hat{\mathcal{K}}$ is equal to 5, whereas Δ is equal to 1 for $\bar{\mathcal{K}}$. Notice that, according to the adversarial model introduced in Section 7.2.3, this means that controllers $\hat{\mathcal{K}}$ and $\bar{\mathcal{K}}$ guarantee resiliency to DoS attacks that generates, respectively, no more than 5 and

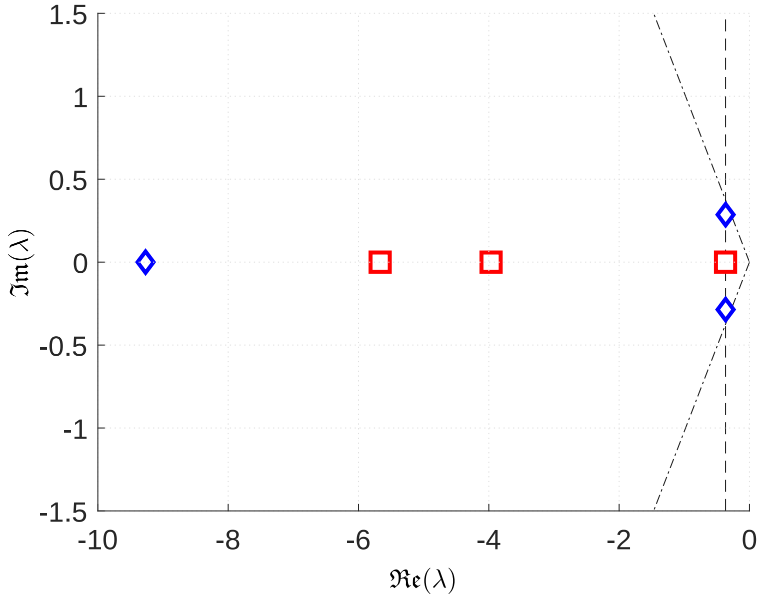

Figure 7.3: Locus of $\Lambda(A_e)$ for $\bar{\mathcal{K}}$ and $\hat{\mathcal{K}}$ in the complex plane. The blue diamond and the red square respectively identify $\Lambda(A_e)$ and (k_p, k_d) for $\bar{\mathcal{K}}$ and $\hat{\mathcal{K}}$.

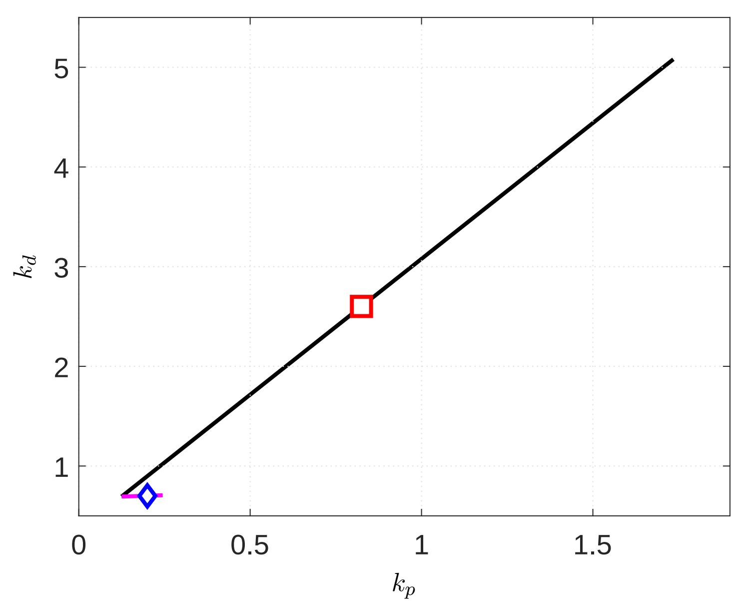

Figure 7.4: Locus of (k_p, k_d) such that Conditions C1 (black) and C2 (magenta) for $\Lambda(A_e)$ are satisfied. The blue diamond and the red square respectively identify $\Lambda(A_e)$ and (k_p, k_d) for $\bar{\mathcal{K}}$ and $\hat{\mathcal{K}}$.

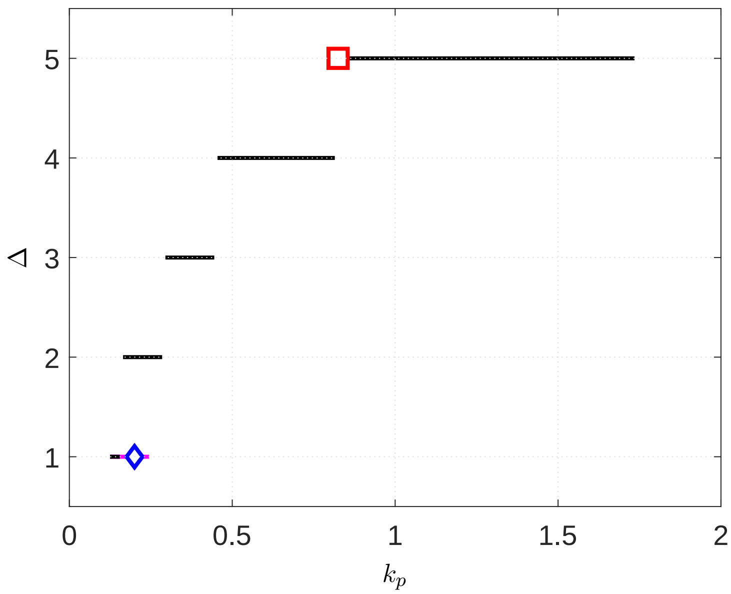

Figure 7.5: Locus of (k_p, Δ) such that Conditions C1 (black) and C2 (magenta) for $\Lambda(A_e)$ are satisfied. The blue diamond and the red square respectively identify the final tuning (k_p, Δ) for $\bar{\mathcal{K}}$ and $\hat{\mathcal{K}}$.

1 successive packet dropouts. To this end, to show how platoons controlled by $\hat{\mathcal{K}}$ and $\bar{\mathcal{K}}$ behave under attacks, we consider the worst DoS attack case scenario: We induce DoS attacks with intervals characterized by 5 consecutive packet dropouts and only 1 packet successfully delivered in between DoS intervals.

To validate our approach, we simulate a platoon of 11 vehicles where the leader performs an acceleration of $2\,m/s^2$, and a deceleration of $4\,m/s^2$. This acceleration profile is similar to that one used in [87]. Figure 7.6 and Fig. 7.7 depict velocity and distance profiles for vehicle platoons controlled by $\bar{\mathcal{K}}$ (in subplots (a)-(b)) and $\hat{\mathcal{K}}$ (in subplots (c)-(d)) respectively in case of "attack-free" IVC and IVC affected by DoS attacks. Moreover, those figures depict in red the speed of $\mathcal{V}_0$ (in subplots (a)-(c)), and the relative distance between $\mathcal{V}_0$ and $\mathcal{V}_1$ (in subplots (b)-(d)). From light grey to black are respectively depicted speeds of vehicles with indexes from 1 to 10 and relative distances of vehicles with indexes from 2 to 10.

Figures 7.6 and 7.7 show that, in case of "attack-free" IVC, the two controllers provide the same behavior. In the case of occurring DoS attacks, instead, the behavior of the vehicle platooning controlled by $\bar{\mathcal{K}}$ is degraded compared to the same controller with an "attack-free" network and compared to vehicle platoons controller by $\hat{\mathcal{K}}$ under DoS attacks. This is noticeable by the increase in overshoot for increasing vehicle index.

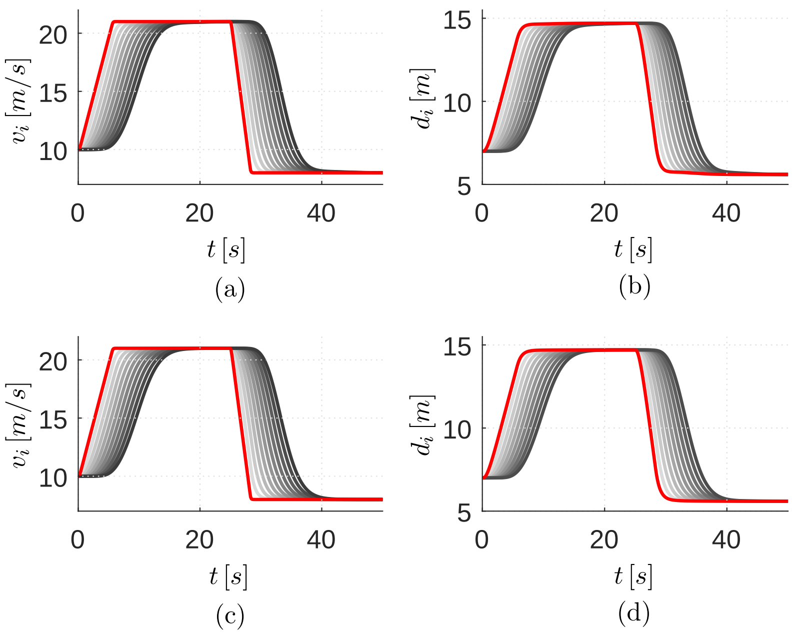

Figure 7.6: Vehicle platoons in case of "attack-free" communication network.

To conclude our numerical analysis, we gathered, in Table 7.1, the outcomes of Algorithm 2 for different values of h, the constant time gap between vehicles. It emerges that the resiliency to DoS attacks increases with h.

Table 7.1: Values of Δ and tuned parameters obtained for $\hat{\mathcal{K}}$ for different values of h by using Algorithm 2.

h [s]	0.4	0.5	0.6	0.7	0.8	0.9	1	1.1
Δ	1	2	4	5	6	7	8	9
k_p	0.5	0.5	1.05	0.82	0.69	0.59	0.52	0.46
k_d	1.73	1.73	3.23	2.6	2.25	1.97	1.78	1.62

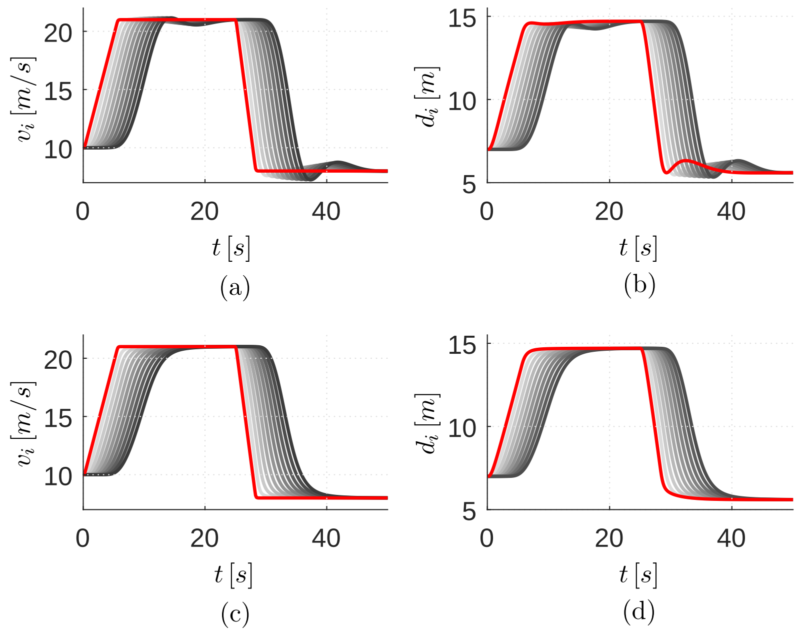

Figure 7.7: Vehicle platoons in case of communication network under DoS attacks.

7.6 Conclusion

This chapter proposes a hybrid controller for string stable homogeneous vehicle platoons. In particular, the proposed controller and tuning algorithm provides a tool to design a DoS-resilient CACC that also satisfies performance requirements. In addition, the tuning algorithm returns a metric to evaluate the resiliency of the vehicle platoon to DoS attacks. Indeed, our approach allows estimating the maximum number of consecutive packet dropouts occurring during the DoS attacks that the proposed CACC can tolerate without losing string stability of the vehicle platooning. The effectiveness of our approach is shown throughout numerical results.

Conclusion of Part II

In the second part of the dissertation, we describe tools for the design of CACC for vehicle platoons that are resilient to network unreliability and DoS attacks.

In Chapter 6, we consider the problem of designing a CACC controller with quantifiable robustness margin to variable transmission intervals and variable network delays in the presence of performance requirements. Conditions are provided to design the controller in such a way that the performance requirements and string stability are satisfied. Furthermore, we describe an algorithm tailored to this particular application, which allows solving the control problem in a computationally efficient way by employing a one parameter line search over a compact interval.

Chapter 7 proposes a hybrid controller for string stable homogeneous vehicle platoons resilient to DoS attacks. In particular, the proposed controller and tuning algorithm provides a tool to design a DoS-resilient CACC that also satisfies performance requirements. In addition, the tuning algorithm returns a metric to evaluate the resiliency of the vehicle platoon to DoS attacks. Indeed, our approach allows estimating the maximum number of consecutive packet dropouts occurring during the DoS attacks that the proposed CACC can tolerate without losing string stability of the vehicle platooning.

The effectiveness of the proposed approaches is showcased throughout numerical examples throughout this part of the dissertation. In particular, we show that the designed hybrid controllers are more resilient to network unreliability and DoS attacks compared to [85], which is designed with a continuous-time control approach.

Future directions aim at extending the proposed approach to account for:

- Heterogeneous vehicle platooning. This could lead to considering platoons where vehicles are characterized by different dynamics.

- Control input saturation, which would make the approach even more realistic from a real implementation point of view.

- Generalized holding devices, which could further increase the resiliency of the vehicle platooning by predicting or estimating the shared measurements by employing on-board sensors. This future direction aims at overcoming the limitation of ZOH holding mechanisms that keep the received measurements constant in between network updates.

- Less conservative DoS attack models; see, e.g., [21]. The proposed approach considers that DoS attacks generate packet dropouts characterized by the maximum allowable number of successive packet dropouts (MANSD). Less conservative models, e.g., [21], consider that DoS attacks lead to a pattern of packet dropouts that can be constrained in a "average" sense. This future direction considers a more authentic network behavior in the case of DoS attacks. Another way to approach this future direction is to consider the maximum number of successive packet dropouts as a stochastic variable.

- Including fuel consumption aspects in the design procedure.

- Extending the approach to vehicle platoons characterized by lateral and longitudinal dynamics.

- Extending the approach to vehicle platoons characterized by different communication topologies; see, e.g., [22, 87, 121].

- The capability of distinguishing between faults in the communication device and network unreliability.

Part III

Appendices

This page is intentionally left blank.

Appendix A

Some Useful Results

Definition A.0.1 (Congruent Matrices [12]). *Two matrices* $X, Y \in \mathcal{S}_+^n$ *are said to be congruent if there exists a nonsingular matrix* $T \in \Re^{n\times n}$ *such that* $Y = T^\top X T$.

Proposition A.0.1 (Congruence Transformation [12]). *If* X *and* Y *are congruent then* $Y \succ 0$ *if and only if* $X \succ 0$.

Lemma A.0.1 (Schur Complement [12]). *For all* $Q \in \mathcal{S}_+^n$, $R \in \mathcal{S}_+^m$, *and* $Z \in \Re^{m\times n}$. *The condition*

$$\begin{bmatrix} Q & Z^\top \\ Z & R \end{bmatrix} \succ 0 \tag{A.1}$$

is equivalent to

$$R \succ 0, \quad Q - Z^\top R^{-1} Z \succ 0 \tag{A.2}$$

Lemma A.0.2. *Let* $P_1 \in \mathcal{S}_+^{n_{x_{cl}}}$, $P_{2,0}, P_{2,1}, P_{3,0}$ *and* $P_{3,1} \in \mathcal{S}_+^{n_y}$, δ, T_2 *and* $T_{mad} \leq T_2$ *be given positive scalars. For each* $\tau \in [0, T_2], l = \{0, 1\}$ *define* $\mathcal{M} : (\tau, l) \mapsto \mathcal{M}(\tau, l)$. *Then* $rge\mathcal{M}(\tau, 1) = Co\{\mathcal{M}(0, 1), \mathcal{M}(T_{mad}, 1)\}$ *and* $rge\mathcal{M}(\tau, 0) = Co\{\mathcal{M}(T_{mad}, 0), \mathcal{M}(T_2, 0)\}$.

Proof. Let us consider the following partitioning of the matrix $\mathcal{M}(\tau, l)$ in (4.29)

$$\mathcal{M}(\tau, l) = \left[\begin{array}{c|c|c|c} \mathcal{M}_1 & \mathcal{M}_2 + e^{-\delta\tau}\mathcal{M}_{3,l} & e^{-\delta\tau}\mathcal{M}_{4,l} & \mathcal{M}_5 \\ \hline \bullet & e^{-\delta\tau}\mathcal{M}_{6,l} & e^{-\delta\tau}\mathcal{M}_{7,l} & e^{-\delta\tau}\mathcal{M}_{8,l} \\ \hline \bullet & \bullet & e^{-\delta\tau}\mathcal{M}_{9,l} & e^{-\delta\tau}\mathcal{M}_{10,l} \\ \hline \bullet & \bullet & \bullet & \mathcal{M}_{11} \end{array}\right]$$

where each block can be determined by comparison of $\mathcal{M}(\tau, l)$ in (4.29). Observe that for any $\tau \in [0, T_{mad}]$ one has:

$$e^{-\delta\tau} = \underbrace{\frac{e^{-\delta\tau} - e^{-\delta T_{mad}}}{1 - e^{-\delta T_{mad}}}}_{\lambda_{1,1}(\tau)} + \underbrace{\frac{1 - e^{-\delta\tau}}{1 - e^{-\delta T_{mad}}}}_{\lambda_{2,1}(\tau)} e^{-\delta T_{mad}} \tag{A.3}$$

and for any $\tau \in [T_{mad}, T_2]$ one has:

$$e^{-\delta\tau} = \underbrace{\frac{e^{-\delta\tau} - e^{-\delta(T_2 - T_{mad})}}{1 - e^{-\delta(T_2 - T_{mad})}}}_{\lambda_{1,0}(\tau)} + \underbrace{\frac{1 - e^{-\delta\tau}}{1 - e^{-\delta(T_2 - T_{mad})}}}_{\lambda_{2,0}(\tau)} e^{-\delta(T_2 - T_{mad})} \tag{A.4}$$

where for each $\tau \in [0, T_{mad}]$, $\lambda_{1,1}(\tau)$ and $\lambda_{2,1}(\tau)$ are nonnegative and such that $\lambda_{1,1}(\tau) + \lambda_{2,1}(\tau) = 1$. Moreover, for each $\tau \in [T_{mad}, T_2]$, $\lambda_{1,0}(\tau)$, $\lambda_{2,0}(\tau)$ are also nonnegative and such that $\lambda_{1,0}(\tau) + \lambda_{2,0}(\tau) = 1$. Therefore, for each $\tau \in [0, T_{mad}]$

$$\mathcal{M}(\tau, 1) = \lambda_{1,1}(\tau)\mathcal{M}(0, 1) + \lambda_{2,1}(\tau)\mathcal{M}(T_{mad}, 1) \tag{A.5}$$

and for each $\tau \in [T_{mad}, T_2]$

$$\mathcal{M}(\tau, 0) = \lambda_{1,0}(\tau)\mathcal{M}(T_{mad}, 0) + \lambda_{2,0}(\tau)\mathcal{M}(T_2, 0) \tag{A.6}$$

which respectively imply that $\mathrm{rge}\mathcal{M}(\tau, 1) = \mathrm{Co}\{\mathcal{M}(0, 1), \mathcal{M}(T_{mad}, 1)\}$ and $\mathrm{rge}\mathcal{M}(\tau, 0) = \mathrm{Co}\{\mathcal{M}(T_{mad}, 0), \mathcal{M}(T_2, 0)\}$. To show that $\mathrm{rge}\mathcal{M}(\tau, 1) = \mathrm{Co}\{\mathcal{M}(0, 1), \mathcal{M}(T_{mad}, 1)\}$ for each $\tau \in [0, T_{mad}]$, pick $\hat{\mathcal{M}} \in \mathrm{Co}\{\mathcal{M}(0, 1), \mathcal{M}(T_{mad}, 1)\}$, then there exists $\hat{\lambda} \in [0, 1]$ such that

$\hat{\mathcal{M}} = \hat{\lambda}\mathcal{M}(0,1) + (1-\hat{\lambda})\mathcal{M}(T_{mad},1)$. Pick

$$\hat{\tau} = -\frac{\ln\left(\hat{\lambda}(1-e^{-\delta T_{mad}}) + e^{-\delta T_{mad}}\right)}{\delta} \in [0, T_{mad}]$$

and observe that from (A.3) one has $\lambda_{1,1}(\hat{\tau}) = \hat{\lambda}$. Therefore, thanks to (A.5), one gets $\mathcal{M}(\hat{\tau},1) = \hat{\mathcal{M}}$. In the same way, to show that rge$\mathcal{M}(\tau,0) = \mathrm{Co}\{\mathcal{M}(T_{mad},0), \mathcal{M}(T_2,0)\}$ for each $\tau \in [T_{mad}, T_2]$, pick $\bar{\mathcal{M}} \in \mathrm{Co}\{\mathcal{M}(T_{mad},0), \mathcal{M}(T_2,0)\}$, then there exists $\bar{\lambda} \in [0,1]$ such that $\bar{\mathcal{M}} = \bar{\lambda}\mathcal{M}(T_{mad},0) + (1-\bar{\lambda})\mathcal{M}(T_2,0)$. Pick

$$\bar{\tau} = -\frac{\ln\left(\bar{\lambda}(1-e^{-\delta(T_2-T_{mad})}) + e^{-\delta(T_2-T_{mad})}\right)}{\delta}$$

$\bar{\tau} \in [T_{mad}, T_2]$ and observe that from (A.4) one has $\lambda_{1,0}(\bar{\tau}) = \bar{\lambda}$. Therefore, thanks to (A.6), one gets $\mathcal{M}(\bar{\tau},0) = \bar{\mathcal{M}}$. $\square$

This page is intentionally left blank.

Appendix B

Proofs of Part I

Proof of Theorem 4.3.1. Driven by the results shown in [23, 43], we consider the following positive semi-definite storage function for the hybrid system $\mathcal{H}_{cl_I}$

$$U(x_I) \coloneqq V(x_{cl}) + \gamma_l \phi_l(\tau) W^2(\eta, s, l) \tag{B.1}$$

where $V \colon \mathfrak{R}^{n_p+n_c} \mapsto \mathfrak{R}_{\geq 0}$ and ϕ_l satisfy, respectively, Assumption 4.3.1 and Assumption 4.3.2, and function W is defined as

$$W(\eta, s, l) \coloneqq \max\{\lambda^l |\eta|, |\eta + s|\} \tag{B.2}$$

where $\lambda \in (0, 1)$ is a constant. Observe that the functions V and W are semi-positive definite, and that $\phi(\tau) > 0$ for all $\tau \in \mathfrak{R}_{\geq 0}$ due to (4.9) and (4.11). Hence, the candidate storage function U is positive semidefinite. Now we show that the storage function U in (B.1) is a suitable function for the hybrid system $\mathcal{H}_{cl_I}$. First, we will show that $U(x_I^+) \leq U(x_I)$ is verified whenever $\mathcal{H}_{cl_I}$ with $\omega = 0$ experiences resets. For jumps at time $\tau \in [T_1, T_2]$, when $l = 0$, one has $x_I^+ = (x_{cl}, \eta, -\eta, 0, 1)$, $x_I = (x_{cl}, \eta, s, \tau, 0)$ and

$$W(\eta, -\eta, 1) = \max\{\lambda|\eta|, 0\} = \lambda|\eta| \leq \lambda \max\{|\eta|, |\eta + s|\} = \lambda W(\eta, s, 0) \tag{B.3}$$

which leads to

$$\begin{aligned} U(x_I^+) - U(x_I) &= \gamma_1\phi_1(0)W^2(\eta, -\eta, 1) - \gamma_0\phi_0(\tau)W^2(\eta, s, 0) \\ &\overset{(B.3)}{\leq} (\lambda^2\gamma_1\phi_1(0) - \gamma_0\phi_0(\tau))W^2(\eta, s, 0) \overset{(4.9b)}{\leq} 0 \end{aligned} \tag{B.4}$$

For jumps at time $\tau \in [0, T_{mad}]$, when $l = 1$, one has $x_I^+ = (x_{cl}, \eta + s, 0, \tau, 0)$, $x_I = (x_{cl}, \eta, s, \tau, 1)$ and

$$\begin{aligned} W(\eta + s, 0, 0) &= \max\{|\eta + s|, |\eta + s|\} = |\eta + s| \\ &\leq \max\{\lambda|\eta|, |\eta + s|\} = W(\eta, s, 1) \end{aligned} \tag{B.5}$$

which leads to

$$\begin{aligned} U(x_I^+) - U(x_I) &= \gamma_0\phi_0(\tau)W^2(\eta + s, 0, 0) - \gamma_1\phi_1(\tau)W^2(\eta, s, 1) \\ &\overset{(B.5)}{\leq} (\gamma_0\phi_0(\tau) - \gamma_1\phi_1(\tau))W^2(\eta, s, 1) \overset{(4.9a)}{\leq} 0 \end{aligned} \tag{B.6}$$

By employing an approach similar to that one presented in [23, 43], one can show that for all $\tau \in \{0, T_2\}$

$$\langle \nabla U(x_I), f_I(x_I, \omega) \rangle \leq \mu(|\omega|^2 - |y_o|^2) - (|A_{21}x_{cl} + A_{24}\omega| - \gamma_l\phi_l W(\eta, s, l))^2 \leq \mu(\gamma^2|\omega|^2 - |y_o|^2) \tag{B.7}$$

Since $\mu > 0$, we can assume, without loss of generality, that $\mu = 1$ by scaling $U(x_I)$ to $\frac{1}{\mu}U(x_I)$. Pick $\omega \in \mathcal{L}_2$, let (x_I, ω) be a maximal solution of the system $\mathcal{H}_{cl_I}$ for initial condition $x_I(0, 0)$ and input ω and pick $(t, j) \in \operatorname{dom} x_I = \cup_{j=0}^{J-1}([t_j, t_{j+1}], j)$ with $t = t_j$ and J possibly ∞ and/or $t_J = \infty$. By using the hybrid time domain $\operatorname{dom} x_I$ we can reformulate (B.4) and (B.6) and state that for each $j = 0, ..., J - 1$ one has

$$U(x_I(t_{j+1}, j + 1)) \leq U(x_I(t_{j+1}, j)) \tag{B.8}$$

and that by integration of (B.7) for each $(t',j) \in \mathrm{dom}(x_I)$ and $(t'',j) \in \mathrm{dom}(x_I)$ with $t' \le t''$ one has

$$\int_{t'}^{t''} |y_o(t)|^2 dt \le -U(x_I(t'',j)) + U(x_I(t',j)) + \gamma^2 \int_{t'}^{t''} |\omega(t)|^2 dt \tag{B.9}$$

Now, the $\mathcal{L}_2$ norm of y_o gives

$$\begin{aligned}
\|y_o\|_{\mathcal{L}_2}^2 &= \sum_{j=0}^{J-1} \int_{t_j}^{t_j+1} |y_o(t,j)|^2 dt \overset{(B.9)}{\le} \sum_{j=0}^{J-1} \Big[-U(x_I(t_{j+1},j)) + U(x_I(t_j,j)) + \gamma^2 \int_{t'}^{t''} |\omega(t)|^2 dt \Big] \\
&= U(x_I(0,0)) - U(x_I(t_J, J-1)) + \gamma^2 \|\omega\|_{\mathcal{L}_2}^2 + \sum_{j=0}^{J-2} \Big[U(x_I(t_{j+1}, j+1)) - U(x_I(t_{j+1}, j)) \Big] \\
&\overset{(B.8)}{\le} U(x_I(0,0)) + \gamma^2 \|\omega\|_{\mathcal{L}_2}^2 \le (U(x_I(0,0))^{\frac{1}{2}} + \gamma \|\omega\|_{\mathcal{L}_2})^2
\end{aligned} \tag{B.10}$$

which leads to have $\|y_o\|_{\mathcal{L}_2} \le U(x_I(0,0))^{\frac{1}{2}} + \gamma \|\omega\|_{\mathcal{L}_2}$; hence, equation (2.10) holds with $\beta(|x_I(0,0)|) = U(x_I(0,0))^{\frac{1}{2}}$. The latter shows that the hybrid system $\mathcal{H}_{cl_I}$ is $\mathcal{L}_2$-stable from the input ω to the output y_o with an $\mathcal{L}_2$-gain less than or equal to γ; hence, it concludes the proof. □

Proof of Theorem 4.4.1. Consider the following Lyapunov function candidate $V(x) := V_1(x_{cl}) + V_2(\eta, \tau, l) + V_3(\sigma, \tau, l)$ for the hybrid system (3.6) defined for every $x \in \mathfrak{R}^{n_x}$. We prove (i) first. By setting $\rho_1 = \min\{\alpha_1, \beta_1, \theta_1\}$, $\rho_2 = \max\{\alpha_2, \beta_2, \theta_2\}$ and in view of the definition of the set $\mathcal{A}$ in (4.23) one gets

$$\rho_1 |x|_{\mathcal{A}}^2 \le V(x) \le \rho_2 |x|_{\mathcal{A}}^2 \qquad \forall x \in C \cup D \tag{B.11}$$

Moreover, from Assumption 4.4.1 item (A6) one has that $\forall x \in C, \omega \in \mathfrak{R}^{n_\omega}$

$$\langle \nabla V(x), f(x,\omega) \rangle \le -2\lambda_t V(x) + \gamma^2 \omega^\top \omega \tag{B.12}$$

and from Assumption 4.4.1 items (A4) and (A5), one has that for all $x \in D$

$$V(g(x)) \le V(x) \tag{B.13}$$

Let (ϕ, ω) be a maximal solution pair to (3.6). Following the same steps as in [28, proof of Theorem 1], using (B.11), (B.12) and (B.13), for all $(t, j) \in \mathrm{dom}\phi$ one has

$$|\phi(t,j)|_{\mathcal{A}} \leq \max\left\{2\sqrt{\frac{\rho_2}{\rho_1}}e^{-\lambda_t t}|\phi(0,0)|_{\mathcal{A}}, \frac{2\gamma}{\sqrt{2\lambda_t\rho_1}}\|\omega\|_\infty\right\} \tag{B.14}$$

This shows that (2.8) holds with $\kappa = 2\sqrt{\rho_2/\rho_1}$, $\lambda = \lambda_t$ and $r \mapsto p(r) := (2\gamma/\sqrt{2\lambda_t\rho_1})r$. Hence, since every maximal solution pair to $\mathcal{H}_{cl_D}$ is complete, (i) is established. To conclude, let (ϕ, ω) be a maximal solution pair to $\mathcal{H}_{cl_D}$ and pick $t > 0$. Again, by using the same approach as in [28, proof of Theorem 1], thanks to Assumption 4.4.1 items (A4) and (A5), since V is nonincreasing at jumps, one gets

$$\int_{\mathcal{I}(t)} x_{cl}(r,j(r))^\top \bar{C}_o^\top \bar{C}_o x_{cl}(r,j(r))dr \leq V(\phi(0,0)) + \gamma^2\int_{\mathcal{I}(t)} |\omega(r,j(r))|^2 dr \tag{B.15}$$

where $\mathcal{I}(t) := [0,t] \cap \mathrm{dom}_t\phi$. Therefore, by taking the limit for t approaching $\sup_t \mathrm{dom}\phi$, thanks to (B.11), one gets (ii) with $\alpha = \rho_2$. Hence, the result is established. $\square$

Proof of Theorem 4.4.2. Let V_1, V_2 and V_3 be defined as in (4.26). By selecting

$$\begin{aligned}
\alpha_1 = \lambda_{\min}(P_1), \quad \alpha_2 = \lambda_{\max}(P_1)\\
\beta_1 = \min\{\lambda_{\min}(P_{2,0})e^{-\delta T_2}, \lambda_{\min}(P_{2,1})e^{-\delta T_{mad}}\}\\
\beta_2 = \max\{\lambda_{\max}(P_{2,0}), \lambda_{\max}(P_{2,1})\}\\
\theta_1 = \min\{\lambda_{\min}(P_{3,0})e^{-\delta T_2}, \lambda_{\min}(P_{3,1})e^{-\delta T_{mad}}\}\\
\theta_2 = \max\{\lambda_{\max}(P_{3,0}), \lambda_{\max}(P_{3,1})\}
\end{aligned} \tag{B.16}$$

items (A1), (A2) and (A3) of the Assumption 4.4.1 are satisfied. By using (4.27a), and (4.27b) one can show that items (A4) and (A5) hold. Regarding item (A4), one has that, for all $x \in D$ with $l = 0$,

$$V_2(\eta,0,1) + V_3(0,0,1) - V_2(\eta,\tau,0) - V_3(\sigma,\tau,0) \leq \eta^\top\left(P_{2,1} - e^{-\delta\tau}P_{2,0}\right)\eta \tag{B.17}$$

Notice that, since $\delta > 0$, for all $\tau \in [T_1, T_2]$,

$$P_{2,1} - e^{-\delta\tau} P_{2,0} \preceq P_{2,1} - e^{-\delta T_2} P_{2,0} \tag{B.18}$$

Therefore, the satisfaction of (4.27a) implies

$$P_{2,1} - e^{-\delta\tau} P_{2,0} \preceq 0 \quad \forall \tau \in [T_1, T_2] \tag{B.19}$$

which shows that (A4) holds. For item (A5), one has that for all $x \in D$ with $l = 1$ due to (4.27b), it follows that

$$V_2(\sigma,\tau,0) + V_3(\sigma,\tau,0) - V_2(\eta,\tau,1) - V_3(\sigma,\tau,1) \leq e^{-\delta\tau}\sigma^\top \left(P_{2,0} + P_{3,0} - P_{3,1}\right)\sigma \leq 0 \tag{B.20}$$

which shows that (A5) holds because of (4.27b). Regarding item (A6) of Assumption 4.4.1, let

$$V(x) = V_1(x_{cl}) + V_2(\eta,\tau,l) + V_3(\sigma,\tau,l) \tag{B.21}$$

Then, from the definition of the flow map in (3.7), for each $x \in C$, $\omega \in \mathfrak{R}^{n_\omega}$ one can define

$$\Omega(x,\omega) \coloneqq \langle \nabla V(x), f(x,\omega)\rangle + x_{cl}^\top \bar{C}_o^\top \bar{C}_o x_{cl} - \gamma^2 \omega^\top \omega \tag{B.22}$$

Therefore, by defining $\Psi(x,\omega) := (x_{cl}, \eta, \sigma, \omega)$, for each $x \in C$ and $\omega \in \mathfrak{R}^{n_\omega}$, one has $\Omega(x,\omega) = \Psi(x,\omega)^\top \mathcal{M}(\tau,l)\Psi(x,\omega)$ where the symmetric matrix $\mathcal{M}$ is given in (4.29). Furthermore, by employing Lemma A.0.2 in Appendix A, it is straightforward to show that there exists $\hat{\lambda} : [0,\tau] \mapsto [0,1]$ such that for each $\tau \in [0, T_{mad}]$

$$\mathcal{M}(\tau,1) = \hat{\lambda}(\tau)\mathcal{M}(0,1) + (1 - \hat{\lambda}(\tau))\mathcal{M}(T_{mad},1) \tag{B.23}$$

and there exists $\bar{\lambda} : [0,\tau] \mapsto [0,1]$ such that for each $\tau \in [T_{mad}, T_2]$

$$\mathcal{M}(\tau,0) = \bar{\lambda}(\tau)\mathcal{M}(T_{mad},0) + (1 - \bar{\lambda}(\tau))\mathcal{M}((\Delta+1)T_s,0) \tag{B.24}$$

Therefore, one has that the satisfaction of (4.28) implies

$$\mathcal{M}(\tau,l) \prec 0,\ \forall(\tau,l) \in [0,T_2]\times\{0,1\} \tag{B.25}$$

which lead to

$$\overline{\varsigma} := \max_{(\tau,l)\in[0,T_2]\times\{0,1\}} \lambda_{\max}(\mathcal{M}(\tau,l)) < 0 \tag{B.26}$$

Observe that the above quantity is well defined, $(\tau,l) \mapsto \mathcal{M}(\tau,l)$ being continuous on $[0,T_2]\times\{0,1\}$. Therefore, one has that

$$\Omega(x,\omega) \leq -\overline{\varsigma} x_{cl}^\top x_{cl} = -\overline{\varsigma}|x|_{\mathcal{A}}^2, \quad \forall x \in C, \omega \in \mathfrak{R}^{n_\omega} \tag{B.27}$$

Defining $\rho_2 = \max\{\alpha_2,\beta_2,\theta_2\}$, using (B.11) and the definition of Ω, one finally gets

$$\langle\nabla V(x), f(x,\omega)\rangle \leq -\frac{\overline{\varsigma}}{\rho_2}V(x) - x_{cl}^\top \bar{C}_o^\top \bar{C}_o x_{cl} + \gamma^2\omega^\top\omega, \quad \forall x \in C, \omega \in \mathfrak{R}^{n_\omega} \tag{B.28}$$

which reads as (A6). Hence, the result is established. $\square$

Proof of Theorem 5.3.1. For all $x \in \mathcal{X}$, define $V(x) := V_1(x_{cl}) + V_2(\eta,\tau)$. We prove (i) first. Select

$$\begin{aligned} \chi_1 &:= \min\{\underline{c}_{v_1}, \underline{c}_{v_2}\} \\ \chi_2 &:= \max\{\overline{c}_{v_1}, \overline{c}_{v_2}\} \end{aligned} \tag{B.29}$$

Then, using (5.18a) and (5.18b) for all $x \in \mathcal{C}$, one gets

$$\chi_1|x|_{\mathcal{A}}^2 \leq V(x) \leq \chi_2|x|_{\mathcal{A}}^2 \qquad \forall x \in \mathcal{C} \cup \mathcal{D} \cup G(\mathcal{D}) \tag{B.30}$$

Moreover, by using (5.18b), for each $\bar{g} = (x_{cl}, 0, z) \in G(x)$, $x = (x_{cl},\eta,\tau) \in \mathcal{D}$ one has

$$V(g) - V(x) = V_2(0,z) - V_2(\eta,0) \leq -\overline{c}_{v_2}|\eta|^2 \leq 0 \tag{B.31}$$

Now observe that, from (5.18c) and (5.18d), for all $x \in \mathcal{C}$, $\omega \in \mathfrak{R}^{n_\omega}$

$$
\begin{aligned}
\langle \nabla V(x), f(x) \rangle &= \langle \nabla V_1(x_{cl}), \mathbb{A}x_{cl} + \mathbb{B}\eta + \mathbb{V}\omega \rangle + \langle \nabla V_2(\eta,\tau), H\eta + \mathbb{J}x_{cl} + \mathbb{W}\omega \rangle \\
&\overset{(5.18c),(5.18d)}{\leq} -\rho_1(x_{cl}) + \rho_2(\eta) - \sigma_1(\eta) + \sigma_2(x_{cl}) + \rho_3(x_{cl},\omega) + \sigma_3(\omega) \\
&\overset{(5.18e),(5.18f),(5.18g)}{\leq} -k_{v_1}|x_{cl}|^2 - k_{v_2}|\eta|^2 - x_{cl}^\top \bar{C}_o^\top \bar{C}_o x_{cl} + \gamma^2 \omega^\top \omega
\end{aligned}
\tag{B.32}
$$

which gives for all $x \in \mathcal{C}$, $\omega \in \mathfrak{R}^{n_\omega}$

$$
\langle \nabla V(x), f(x) \rangle \leq -\underbrace{\min\{k_{v_1}, k_{v_2}\}}_{\chi_3} |x|_{\mathcal{A}}^2 - x_{cl}^\top \bar{C}_o^\top \bar{C}_o x_{cl} + \gamma^2 \omega^\top \omega \tag{B.33}
$$

Using (B.30), the above relationship yields for all $x \in \mathcal{C}$, $\omega \in \mathfrak{R}^{n_\omega}$

$$
\langle \nabla V(x), f(x) \rangle \leq -2\lambda_t V(x) - x_{cl}^\top \bar{C}_o^\top \bar{C}_o x_{cl} + \gamma^2 \omega^\top \omega \tag{B.34}
$$

where $\lambda_t := \frac{\chi_3}{2\chi_2}$. Let (ϕ, ω) be a maximal solution pair to $\mathcal{H}_{cl}$. Following the same steps as in [28, proof of Theorem 1], using (B.30), (B.31), and (B.34), for all $(t,j) \in \operatorname{dom} \phi$ one has

$$
|\phi(t,j)|_{\mathcal{A}} \leq \max\left\{ 2\sqrt{\frac{\chi_2}{\chi_1}} e^{-\lambda_t t} |\phi(0,0)|_{\mathcal{A}}, \frac{2\gamma}{\sqrt{2\lambda_t \chi_1}} \|\omega\|_\infty \right\} \tag{B.35}
$$

This shows that (2.8) holds with $\kappa = 2\sqrt{\chi_2/\chi_1}$, $\lambda = \lambda_t$ and $r \mapsto p(r) := (2\gamma/\sqrt{2\lambda_t\chi_1})r$. Hence, since every maximal solution pair to $\mathcal{H}_{cl}$ is complete, (i) is established. To conclude, let (ϕ, ω) be a maximal solution pair to $\mathcal{H}_{cl}$ and pick $t > 0$. Again, by using the same approach as in [28, proof of Theorem 1], thanks to (B.31), since V is nonincreasing at jumps, one gets

$$
\int_{\mathcal{I}(t)} x_{cl}(r, j(r))^\top \bar{C}_o^\top \bar{C}_o x_{cl}(r, j(r)) dr \leq V(\phi(0,0)) + \gamma^2 \int_{\mathcal{I}(t)} |\omega(r, j(r))|^2 dr \tag{B.36}
$$

where $\mathcal{I}(t) := [0,t] \cap \operatorname{dom}_t \phi$. Therefore, by taking the limit for t approaching $\sup_t \operatorname{dom}\phi$, thanks to (B.11), one gets (ii) with $\alpha = \chi_2$. Hence, the result is established. □

Proof of Proposition 5.3.1. Let V_1 and V_2 be as defined in (5.20),

$$\rho_1(x_{cl}) \coloneqq x_{cl}^\top S x_{cl}, \quad \rho_2(\eta) \coloneqq \eta^\top Q \eta, \quad \rho_3(x_{cl}, \omega) \coloneqq -x_{cl}^\top \bar{C}_o^\top \bar{C}_o x_{cl} + \gamma_1 \omega^\top \omega \tag{B.37a}$$

$$\sigma_1(\eta) \coloneqq \eta^\top T \eta, \quad \sigma_2(x_{cl}) \coloneqq x_{cl}^\top R x_{cl}, \quad \sigma_3(\omega) \coloneqq \gamma_2 \omega^\top \omega \tag{B.37b}$$

By selecting

$$\underline{c}_{v_1} = \lambda_{\min}(P_1), \quad \overline{c}_{v_1} = \lambda_{\max}(P_1), \quad \underline{c}_{v_2} = \lambda_{\min}(P_2), \quad \overline{c}_{v_2} = \lambda_{\max}(P_2) e^{\delta T_2} \tag{B.38}$$

conditions (5.18a) and (5.18b) are respectively satisfied. Regarding condition (5.18c) of Property 5.3.1, from the definition of the flow map in (5.11), for each $x \in \mathcal{C}, \omega \in \mathfrak{R}^{n_\omega}$, one can define

$$\begin{aligned} \Omega_1(x_{cl}, \eta, \omega) &\coloneqq \langle \nabla V_1(x_{cl}), \mathbb{A} x_{cl} + \mathbb{B}\eta + \mathbb{V}\omega \rangle + x_{cl}^\top (S + \bar{C}_o{}^\top \bar{C}_o) x_{cl} - \eta^\top Q \eta - \gamma_1 \omega^\top \omega \\ &= (x_{cl}, \eta, \omega)^\top \mathcal{M}_1 (x_{cl}, \eta, \omega) \end{aligned} \tag{B.39}$$

where the symmetric matrix $\mathcal{M}_1$ is given in (5.21c). Therefore, the satisfaction of (5.21c) implies (5.18c). Concerning condition (5.18d) of Property 5.3.1, observe that from the definition of the flow map in (5.11), for each $x \in \mathcal{C}$, $\omega \in \mathfrak{R}^{n_\omega}$, one can define

$$\begin{aligned} \Omega_2(x_{cl}, \eta, \tau, \omega) &\coloneqq \langle \nabla W_2(x_{cl}), \widehat{H}\eta + \mathbb{J} x_{cl} + \mathbb{W}\omega \rangle + \eta^\top T \eta - x_{cl}^\top R x_{cl} - \gamma_2 \omega^\top \omega \\ &= (\eta, x_{cl}, \omega)^\top \mathcal{M}_2(\tau)(\eta, x_{cl}\omega) \end{aligned} \tag{B.40}$$

where the symmetric matrix $\mathcal{M}_2(\tau)$ is given in (5.22) for all $\tau \in [0, T_2]$. Furthermore, notice that it is straightforward to show that there exists $\lambda : [0, \tau] \mapsto [0, 1]$ such that for each $\tau \in [0, T_2]$, $\mathcal{M}_2(\tau) = \lambda(\tau)\mathcal{M}(0) + (1 - \lambda(\tau))\mathcal{M}_2(T_2)$; see [30] for further details. Therefore, one has that the satisfaction of (5.21d) implies $\mathcal{M}_2(\tau) \preceq 0$, $\forall \tau \in [0, T_2]$, hence

(5.18d). Concerning conditions (5.18e) and (5.18f), select

$$k_{w_1} = -\lambda_{\max}(R - S), \quad k_{w_2} = -\lambda_{\max}(Q - T) \tag{B.41}$$

and observe that these quantities are strictly positive due to (5.21b) and (5.21a). Hence, one has

$$x_{cl}^\top (R - S) x_{cl} \leq -k_{w_1} |x_{cl}|^2, \quad \eta^\top (Q - T)\eta \leq -k_{w_2} |\eta|^2 \tag{B.42}$$

which respectively read as (5.18e) and (5.18f). To conclude, observe that, due to (5.21e), for all $x_{cl} \in \mathfrak{R}^{n_p+n_c}$, $\omega \in \mathfrak{R}^{n_\omega}$ one gets

$$\rho_3(x_{cl}, \omega) + \sigma_3(\omega) = -x_{cl}^\top \bar{C}_o^\top \bar{C}_o x_{cl} + (\gamma_1 + \gamma_2)\omega^\top \omega \leq -x_{cl}^\top \bar{C}_o^\top \bar{C}_o x_{cl} + \gamma^2 \omega^\top \omega \tag{B.43}$$

which reads as (5.18g), and concludes the proof. □

Proof of Lemma 5.4.1. Since $F \in \mathcal{S}_+^n$, for any $\alpha \in \mathfrak{R}$ one has

$$(F^{-1} - \alpha \mathbf{I})^\top F (F^{-1} - \alpha \mathbf{I}) \succeq 0 \tag{B.44}$$

Expanding the above expression yields (5.23). Therefore, the result is established. □

Proof of Theorem 5.4.1. Nonsingularity of $\mathbf{I} - XY$ follows from (5.24a). Indeed, from [9, Proposition 2.8.3, page 116]

$$\det \Theta = \det(Y) \det(X - Y^{-1}) \tag{B.45}$$

which by using the symmetry of X and Y, via some simple algebra, yields

$$\det \Theta = \det(YX - \mathbf{I}) = (-1)^{n_p} \det(\mathbf{I} - XY) \tag{B.46}$$

The remainder of the proof aims at showing that the hypotheses of the theorem imply all the conditions in the Proposition 5.3.1. Notice that conditions (5.21a) and (5.24b) are unchanged. After a preliminary step, other conditions are shown below.

Preliminary step. Next, we select

$$P_1 = \begin{bmatrix} X & U \\ U^\top & -V^{-1}(Y - YXY)V^{-\top} \end{bmatrix} \tag{B.47}$$

$$S = F^{-1} \tag{B.48}$$

Proof of $P_1 \succ 0$*.* Pick P_1 as in (B.47), and notice that matrix Φ in (5.26) is nonsingular because V is nonsingular. Using (5.28), it can be shown that $\Theta = \Phi^\top P_1 \Phi$. Hence, (5.24a) implies $P_1 \succ 0$.

Proof of (5.21b)*.* From Lemma 5.4.1, it follows that

$$-F^{-1} + 2\alpha\mathbf{I} - \alpha^2 F \preceq 0 \tag{B.49}$$

Hence, by using (5.24c), one has

$$R - F^{-1} \prec 0 \tag{B.50}$$

which reads as (5.21b) with $S = F^{-1}$.

Proof of (5.21c)*.* By following an approach similar to [95], we show that (5.24d) is equivalent to (5.21c) for the proposed selection of the controller parameters and of the variables P_1 and S. By Schur complement (see Lemma A.0.1), (5.21c) is equivalent to

$$\overline{\mathcal{M}}_1 := \begin{bmatrix} \mathrm{He}(P_1\mathbb{A}) & P_1\mathbb{B} & P_1\mathbb{V} & \mathbf{I} & \bar{C}_o^\top \\ \bullet & -Q & 0 & 0 & 0 \\ \bullet & \bullet & -\gamma_1\mathbf{I} & 0 & 0 \\ \bullet & \bullet & \bullet & -F & 0 \\ \bullet & \bullet & \bullet & \bullet & -\mathbf{I} \end{bmatrix} \preceq 0 \tag{B.51}$$

Now let us perform the following congruence transformation (see Proposition A.0.1)

$$
\begin{aligned}
\widetilde{\mathcal{M}_1} &:= \operatorname{diag}\{\Phi^\top, \mathbf{I}, \mathbf{I}, \mathbf{I}, \mathbf{I}\}\overline{\mathcal{M}}_1 \operatorname{diag}\{\Phi, \mathbf{I}, \mathbf{I}, \mathbf{I}, \mathbf{I}\} \\
&= \begin{bmatrix} \mathrm{He}(\Phi^\top P_1 \mathbb{A}\Phi) & \Phi^\top P_1 \mathbb{B} & \Phi^\top P_1 \mathbb{V} & \Phi^\top & \Phi^\top \bar{C}_o^\top \\ \bullet & -Q & 0 & 0 & 0 \\ \bullet & \bullet & -\gamma_1 \mathbf{I} & 0 & 0 \\ \bullet & \bullet & \bullet & -F & 0 \\ \bullet & \bullet & \bullet & \bullet & -\mathbf{I} \end{bmatrix}
\end{aligned} \tag{B.52}
$$

Notice that $\widetilde{\mathcal{M}_1}$ differs from $\widehat{\mathcal{M}_1}$ in (5.24d) only in the entries $(1,1)$, $(1,2)$, $(1,3)$, and their transposed $(2,1)$ and $(3,1)$. Before showing that $\Lambda = \Phi^\top P_1 \mathbb{A}\Phi$, $\Pi = \Phi^\top P_1 \mathbb{B}$, and $\Xi = \Phi^\top P_1 \mathbb{V}$, we first invert the left equation in (5.29) as

$$
\left[\begin{array}{c|c} K - XA_pY & L \\ \hline M & N \end{array}\right] = \begin{bmatrix} U & XB_p \\ 0 & \mathbf{I} \end{bmatrix} \left[\begin{array}{c|c} A_c & B_c \\ \hline C_c & D_c \end{array}\right] \begin{bmatrix} V^\top & 0 \\ C_pY & \mathbf{I} \end{bmatrix} \tag{B.53}
$$

Using (5.28), by straightforward calculations one can obtain:

$$
\Phi^\top P_1 \mathbb{A}\Phi = \begin{bmatrix} A_pY + B_p(D_cC_pY + C_cV^\top) & A_p + B_pD_cC_p \\ \Gamma & XA_p + (XB_pD_c + UB_c)C_p \end{bmatrix} \tag{B.54a}
$$

$$
\Phi^\top P_1 \mathbb{B} = -\begin{bmatrix} B_pD_c \\ XB_pD_c + UB_c \end{bmatrix} \tag{B.54b}
$$

$$
\Phi^\top P_1 \mathbb{V} = -\begin{bmatrix} W \\ XW \end{bmatrix} \tag{B.54c}
$$

where $\Gamma := X(A_p + B_pD_cC_p)Y + U(B_cC_pY + A_kV^\top) + XB_pC_cV^\top$. By employing (B.53), equations (B.54a), (B.54b) and (B.54c) read as, respectively, Λ, Π, and Ξ in (5.27). This shows that (5.24d) is equivalent to (5.21c) for the proposed selection of the controller parameters and variables P_1 and S.

Proof of (5.21d). By setting $\widehat{H} = P_2^{-1} J$ and $\widehat{E} = P_2^{-1} Z$ in (5.22) yields (5.25). This shows that the satisfaction of (5.25) is equivalent to the satisfaction of (5.22). Hence, (5.24e) is equivalent to (5.21d).

To conclude the proof, notice that conditions (5.24f) and (5.21e) are the same. $\square$

Appendix C

Proofs of Part II

Proof of Proposition 6.4.1. Sufficiency: Assume that (6.18) hold and let

$$rho(s; k_p, k_d) := \det(sI - A_e) = \frac{k_p}{\tau_d} + \frac{k_d}{\tau_d}s + \frac{1}{\tau_d}s^2 + s^3 \tag{C.1}$$

be the characteristic polynomial of A_e. By replacing the expression of k_d in (6.18a), one gets

$$\rho(s; k_p) := \rho_1(s; k_p)(s - \lambda_M) \tag{C.2}$$

where

$$\rho_1(s; k_p) := s^2 + \frac{\lambda_M \tau_d + 1}{\tau_d}s - \frac{k_p}{\lambda_M \tau_d} \tag{C.3}$$

This shows that λ_M is an eigenvalue of A_e. Now, observe that

$$\zeta(\rho_1(s; k_p)) = (\lambda_M \tau_d + 1)/(2\tau_d \sqrt{-\frac{k_p}{\lambda_M \tau_d}}) \tag{C.4}$$

hence, from (6.18b) it follows that $\zeta(\rho_1(s; k_p)) \geq \zeta_m$. To conclude, it suffices to observe that, thanks to the Routh-Hurwitz criterion, (6.18c) and (6.18d) ensure that the real part of the eigenvalues of $\rho_1(s; k_p)$ is less than or equal to λ_M. Hence, (6.18) implies C1. This concludes the proof of sufficiency.

Necessity: Assume that C1 holds. Then, it follows that $\rho(s; k_p, k_d)$ can be factorized as follows

$$\rho(s;k_p,k_d) = (s-\lambda_M)\rho_1(s;k_p,k_d) \tag{C.5}$$

and ρ_1 is such that $\zeta(\rho_1(s;k_p,k_d)) \geq \zeta_m$ and $\mathfrak{Re}(\rho_1(s;k_p,k_d)) \leq \lambda_M$. Straightforward calculations yields

$$\rho_1(s;k_p,k_d) = s^2 + \frac{\lambda_M\tau_d+1}{\tau_d}s + \frac{\lambda_M^2\tau_d+\lambda_M+k_d}{\tau_d} \tag{C.6}$$

which, in turn, shows that $\zeta(\rho_1(s;k_p,k_d)) \geq \zeta_m$ and $\Lambda_{\max}(\rho_1(s;k_p,k_d)) \leq \lambda_M$ implies (6.18). This concludes the proof of necessity. □

Proof of Proposition 6.4.2. Sufficiency: Assume that (6.19) hold and let $\rho(s;k_p,k_d)$ be the characteristic polynomial of A_e. By using the expression of k_d in (6.19a), one gets

$$\rho(s;k_p) = \underbrace{\left(s+\frac{2\lambda_M\tau_d+1}{\tau_d}\right)}_{\rho_1(s;k_p)}\underbrace{\left(s^2-2\lambda_M s+\frac{k_p}{2\lambda_M\tau_d+1}\right)}_{\rho_2(s;k_p)} \tag{C.7}$$

At this stage, notice that (6.19d) implies that the unique root of ρ_1 is smaller than λ_M. To conclude, we analyze the roots of ρ_2. Specifically, from the definition of ρ_2 it turns out that

$$\zeta(\rho_2(s;k_p)) = -\lambda_M/(\sqrt{\frac{k_p}{2\lambda_M\tau_d+1}}) \tag{C.8}$$

which from (6.19b)-(6.19c) gives $1 > \zeta(\rho_2(s;k_p)) \geq \zeta_m$; this ensures that $\mathfrak{Im}(\rho_2(s;k_p)) \neq 0$. Moreover, straightforward calculations show that $\Lambda_{\max}(\rho_2(s;k_p)) = \lambda_M$. Thus, C2 holds and this concludes the proof of sufficiency.

Necessity: Assume that C2 holds. Then, it follows that $\rho(s;k_p,k_d)$ can be factorized as follows

$$\rho(s;k_p,k_d) = (s-\lambda)\underbrace{(s-\lambda_M+j\omega)(s-\lambda_M-j\omega)}_{\rho_3(s;k_p,k_d)} \tag{C.9}$$

with $\lambda \leq \lambda_M$, $\omega > 0$, and ρ_3 is such that $1 > \zeta(\rho_3(s;k_p,k_d)) \geq \zeta_m$. By solving the system of equation $\mathfrak{Re}(\rho(\lambda_M+j\omega;k_p,k_d)) = 0$ and $\mathfrak{Im}(\rho(\lambda_M+j\omega;k_p,k_d)) = 0$ in the variables k_p

and ω one obtains (6.19a). By replacing (6.19a) in ρ_3 one gets

$$\rho_3(s;k_p) := s^2 - 2s\lambda_M + \frac{k_p}{2\lambda_M\tau_d + 1} \tag{C.10}$$

At this stage, straightforward calculations yield $1 > \zeta(\rho_3(s;k_p)) \geq \zeta_m$ and $\Lambda_{\max}(\rho_3(s;k_p)) = \lambda_M$, which, in turn, implies, respectively, (6.19b) and (6.19c). Moreover, from $\rho(s;k_p, f_{C2}(k_p))$, one has that

$$\lambda := -\frac{2\lambda_M\tau_d + 1}{\tau_d} \tag{C.11}$$

and since $\lambda \leq \lambda_M$, (6.19d) holds. This concludes the proof of necessity. □

Proof of Theorem 7.4.1. Let $V(x_i) := V_1(\tilde{x}_i) + V_2(\eta_{i-1}, \tau_{i-1})$ be the Lyapunov function candidate for the hybrid system $\mathcal{H}_i^\omega$, which is defined for every $x_i \in \mathfrak{R}^6$. We prove (i) first. Select $\rho_1 = \min\{\alpha_1, \beta_1\}$, $\rho_2 = \max\{\alpha_2, \beta_2\}$. By considering the definition of the set $\mathcal{A}$ in (7.15), one obtains

$$\rho_1|x_i|_{\mathcal{A}}^2 \leq V(x_i) \leq \rho_2|x_i|_{\mathcal{A}}^2 \qquad \forall x_i \in C \cup D \tag{C.12}$$

Moreover, from Assumption 7.4.1 item (A4) one has that $\forall x_i \in C, \omega_{i-1} \in \mathfrak{R}$

$$\langle \nabla V(x_i), f(x_i, \omega_{i-1})\rangle \leq -2\lambda_t V(x_i) + \theta^2\omega_{i-1}^2 \tag{C.13}$$

and from Assumption 7.4.1 item (A3), one has that for all $x_i \in D$

$$V(g(x_i)) \leq V(x_i) \tag{C.14}$$

Let (ϕ_i, ω_{i-1}) be a maximal solution pair to $\mathcal{H}_i^\omega$. By using (C.12), (C.13), and (C.14) through the same steps in [28, proof of Theorem 1], one obtains that for all $(t,j) \in \operatorname{dom}\phi_i$

$$|\phi_i(t,j)|_{\mathcal{A}} \leq \max\left\{2\sqrt{\frac{\rho_2}{\rho_1}}e^{-\lambda_t t}|\phi_i(0,0)|_{\mathcal{A}}, \frac{2\theta}{\sqrt{2\lambda_t\rho_1}}\|\omega_{i-1}\|_\infty\right\} \tag{C.15}$$

which reads as (2.3.1) with $\kappa = 2\sqrt{\frac{\rho_2}{\rho_1}}$, $\lambda = \lambda_t$ and $r \mapsto p(r) := (2\theta/\sqrt{2\lambda_t\rho_1})r$. Hence, since every maximal solution pair to $\mathcal{H}_i^\omega$ is complete, (i) is established. Now we prove (ii). Let (ϕ_i, ω_{i-1}) be a maximal solution pair to $\mathcal{H}_i^\omega$ and select $t > 0$. Notice that because of Assumption 7.4.1 item (A3) V is nonincreasing at jumps. Therefore, by following the same approach in [28, proof of Theorem 1], one obtains

$$\int_{\mathcal{I}(t)} \omega_i(r, j(r))^2 dr \leq V(\phi_i(0,0)) + \theta^2 \int_{\mathcal{I}(t)} \omega_{i-1}(r, j(r))^2 dr \tag{C.16}$$

where $\mathcal{I}(t) := [0, t] \cap \operatorname{dom}_t \phi_i$. To conclude, one can take the limit for t approaching $\sup_t \operatorname{dom} \phi_i$, and by considering (C.12), one obtains (2.3.3) with $\beta(x_i(0,0)) = \rho_2 |x_i(0,0)|_{\mathcal{A}}$. Hence, the result (ii) is established. □

Proof of Theorem 7.4.2. Consider the functions $\tilde{x}_i \mapsto V_1(\tilde{x}_i) := \tilde{x}_i^\top P_1 \tilde{x}_i$, and $(\eta_{i-1}, \tau_{i-1}) \mapsto V_2(\eta_{i-1}, \tau_{i-1}) := p_2 \eta_{i-1}^2 e^{-\delta \tau_{i-1}}$. By choosing $\alpha_1 = \lambda_{\min}(P_1)$, $\alpha_2 = \lambda_{\max}(P_1)$, $\beta_1 = p_2 e^{-\delta(\Delta+1)T_s}$, $\beta_2 = p_2$ turns out that items (A1) and (A2) of the Assumption 7.4.1 hold. To show that item (A3) holds, notice that, by employing the jump map of $\mathcal{H}_i^\omega$, for all $\eta_{i-1} \in \mathfrak{R}$ and for all $\tau_{i-1} \in T_s \Theta_\Delta$ one has that

$$V_2(0,0) - V_2(\eta, \tau_{i-1}) = -p_2 \eta_{i-1}^2 e^{-\delta \tau_{i-1}} \leq 0 \tag{C.17}$$

Regarding item (A4) of Assumption 7.4.1, let $V(x_i) = V_1(\tilde{x}_i) + V_2(\eta_{i-1}, \tau_{i-1})$. Then, from the definition of the flow map in (7.7), for each $x_i \in C$, $\omega_{i-1} \in \mathfrak{R}$ one can define

$$\Omega(x_i, \omega_{i-1}) := \langle \nabla V(x_i), f(x_i, \omega_{u-1}) \rangle + \tilde{x}_i^\top C_\omega^\top C_\omega \tilde{x}_i + \eta_{i-1}^2 + 2 C_\omega \tilde{x}_i \eta_{i-1} - \theta^2 \omega_{i-1}^2 \tag{C.18}$$

Therefore, by defining $\Psi(x_i, \omega_{i-1}) := (\tilde{x}_i, \eta_{i-1}, \omega_{i-1})$, for each $x_i \in C$ and $\omega_{i-1} \in \mathfrak{R}$, one has

$$\Omega(x_i, \omega_{i-1}) := \Psi(x_i, \omega_{i-1})^\top \mathcal{M}(\tau_{i-1}) \Psi(x_i, \omega_{i-1}) \tag{C.19}$$

where the symmetric matrix $\mathcal{M}(\tau_{i-1})$ is given in (7.17). The satisfaction of

$$\mathcal{M}(\tau_{i-1}) \prec 0, \, \forall \tau_{i-1} \in [0, (\Delta+1)T_s] \tag{C.20}$$

leads to

$$\overline{\varsigma} \coloneqq \max_{\tau_{i-1} \in [0,(\Delta+1)T_s]} \lambda_{\max}(\mathcal{M}(\tau_{i-1})) < 0 \tag{C.21}$$

Observe that, since $\tau_{i-1} \mapsto \mathcal{M}(\tau_{i-1})$ is continuous on $[0, (\Delta+1)T_s]$, $\overline{\varsigma}$ is well defined. Therefore, one has that for all $x_i \in C$, $\omega_{i-1} \in \mathfrak{R}$

$$\Omega(x_i, \omega_{i-1}) \leq -\overline{\varsigma}\tilde{x}_i^\top \tilde{x}_i = -\overline{\varsigma}|x_i|^2_{\mathcal{A}} \tag{C.22}$$

To conclude, let $\rho_2 = \max\{\alpha_2, \beta_2\}$, and use (C.12) and the definition of Ω. Then, for all $x_i \in C$, $\omega_{i-1} \in \mathfrak{R}$

$$\langle \nabla V(x_i), f(x_i, \omega_{i-1}) \rangle \leq -\frac{\overline{\varsigma}}{\rho_2} V(x_i) - \tilde{x}_i^\top C_\omega^\top C_\omega \tilde{x}_i - \eta_{i-1}^2 - 2C_\omega \tilde{x}_i \eta_{i-1} + \theta^2 \omega_{i-1}^2 \tag{C.23}$$

which reads as (A4). Hence, item (A4) holds. □

Proof of Lemma 7.4.1. Following same steps as in Lemma A.0.2, it is straightforward to show that there exists $\lambda : [0, \tau_{i-1}] \mapsto [0, 1]$ such that for each $\tau_{i-1} \in [0, (\Delta+1)T_s]$,

$$\mathcal{M}(\tau_{i-1}) = \lambda(\tau_{i-1})\mathcal{M}(0) + (1 - \lambda(\tau_{i-1}))\mathcal{M}((\Delta+1)T_s) \tag{C.24}$$

Therefore, one has that the satisfaction of (7.18) implies

$$\mathcal{M}(\tau_{i-1}) \prec 0, \, \forall \tau_{i-1} \in [0, (\Delta+1)T_s] \tag{C.25}$$

which concludes the proof. □

This page is intentionally left blank.

Bibliography

[1] Internet of things forecast. `https://www.ericsson.com/en/mobility-report/internet-of-things-forecast`.

[2] Smart city challenge. `https://www.transportation.gov/sites/dot.gov/files/docs/Smart%20City%20Challenge%20Lessons%20Learned.pdf`.

[3] F. Acciani, P. Frasca, A. Stoorvogel, E. Semsar-Kazerooni, and G. Heijenk. Cooperative adaptive cruise control over unreliable networks: an observer-based approach to increase robustness to packet loss. In *2018 European Control Conference (ECC)*, pages 1399–1404. IEEE, 2018.

[4] A. Alipour-Fanid, M. Dabaghchian, H. Zhang, and K. Zeng. String stability analysis of cooperative adaptive cruise control under jamming attacks. In *Proceedings of the 18th IEEE International Symposium on High Assurance Systems Engineering (HASE)*, pages 157–162, 2017.

[5] S. Amin, A. Cárdenas, and S. Sastry. Safe and secure networked control systems under denial-of-service attacks. In *International Workshop on Hybrid Systems: Computation and Control*, pages 31–45. Springer, 2009.

[6] M. Amoozadeh, A. Raghuramu, C. Chuah, D. Ghosal, H. Zhang, J. Rowe, and K. Levitt. Security vulnerabilities of connected vehicle streams and their impact on cooperative driving. *IEEE Communications Magazine*, 53(6):126–132, 2015.

[7] D. Antunes, J. P. Hespanha, and C. Silvestre. Control of impulsive renewal systems: Application to direct design in networked control. In *Proceedings of the 48h IEEE Conference on Decision and Control (CDC) held jointly with 2009 28th Chinese Control Conference*, pages 6882–6887. IEEE, 2009.

[8] N. Bauer, M. Donkers, N. Van de Wouw, and M. Heemels. Decentralized observer-based control via networked communication. *Automatica*, 49(7):2074–2086, 2013.

[9] D. S. Bernstein. *Matrix mathematics: Theory, facts, and formulas with application to linear systems theory*. Princeton university press, 2005.

[10] Z. A. Biron, S. Dey, and P. Pisu. Resilient control strategy under denial of service in connected vehicles. In *Proceedings of the American Control Conference (ACC)*, pages 4971–4976. IEEE, 2017.

[11] Z. A. Biron, S. Dey, and P. Pisu. Real-time detection and estimation of denial of service attack in connected vehicle systems. *IEEE Transactions on Intelligent Transportation Systems*, (99):1–10, 2018.

[12] S. Boyd, L. El Ghaoui, E. Feron, and V. Balakrishnan. *Linear matrix inequalities in system and control theory*, volume 15. SIAM, 1994.

[13] S. Boyd and L. Vandenberghe. *Convex optimization*. Cambridge University press, 2004.

[14] C. Briat. Spectral necessary and sufficient conditions for sampling-period-independent stabilisation of periodic and aperiodic sampled-data systems using a class of generalised sampled-data hold functions. *International Journal of Control*, 87(3):612–621, 2014.

[15] C. Cai and A. Teel. Characterizations of input-to-state stability for hybrid systems. *Systems & Control Letters*, 58(1):47–53, 2009.

[16] D. Carnevale, A. Teel, and D. Nešić. A Lyapunov proof of an improved maximum allowable transfer interval for networked control systems. *IEEE Transactions on Automatic Control*, 52(5):892–897, 2007.

[17] M. Cloosterman, N. Van de Wouw, M. Heemels, and H. Nijmeijer. Stability of networked control systems with uncertain time-varying delays. *IEEE Transactions on Automatic Control*, 54(7):1575–1580, 2009.

[18] M. B. G. Cloosterman, L. Hetel, N. van de Wouw, M. Heemels, J. Daafouz, and H. Nijmeijer. Controller synthesis for networked control systems. *Automatica*, 46(10):1584–1594, 2010.

[19] D. Dačić and D. Nešić. Quadratic stabilization of linear networked control systems via simultaneous protocol and controller design. *Automatica*, 43(7):1145–1155, 2007.

[20] S. Dadras, R. Gerdes, and R. Sharma. Vehicular platooning in an adversarial environment. In *Proceedings of the 10th ACM Symposium on Information, Computer and Communications Security*, pages 167–178, 2015.

[21] C. De Persis and P. Tesi. A comparison among deterministic packet-dropouts models in networked control systems. *IEEE Control Systems Letters*, 2(1):109–114, 2018.

[22] M. Di Bernardo, A. Salvi, and S. Santini. Distributed consensus strategy for platooning of vehicles in the presence of time-varying heterogeneous communication delays. *IEEE Transactions on Intelligent Transportation Systems*, 16(1):102–112, 2014.

[23] V. Dolk, J. Ploeg, and M. Heemels. Event-triggered control for string-stable vehicle platooning. *IEEE Transactions on Intelligent Transportation Systems*, 18(12):3486–3500, 2017.

[24] V. Dolk, P. Tesi, C. De Persis, and M. Heemels. Event-triggered control systems under denial-of-service attacks. *IEEE Transactions on Control of Network Systems*, 4(1):93–105, 2017.

[25] M. Donkers, J. Daafouz, and M. Heemels. Output-based controller synthesis for networked control systems with periodic protocols and time-varying transmission intervals and delays. *IFAC Proceedings Volumes*, 47(3):6478–6483, 2014.

[26] Z. Du, D. Yue, and S. Hu. $\mathcal{H}_\infty$ stabilization for singular networked cascade control systems with state delay and disturbance. *IEEE Transactions on Industrial Informatics*, 10(2):882–894, 2014.

[27] S. Feng and P Tesi. Resilient control under denial-of-service: Robust design. *Automatica*, 79:42–51, 2017.

[28] F. Ferrante, F. Gouaisbaut, R. Sanfelice, and S. Tarbouriech. A hybrid observer with a continuous intersample injection in the presence of sporadic measurements. In *Proceedings of the 54th Annual Conference on Decision and Control*, pages 5654–5659, 2015.

[29] F. Ferrante, F. Gouaisbaut, R. Sanfelice, and S. Tarbouriech. Observer-based control design for linear systems in the presence of limited measurement streams and intermittent input access. In *2015 American Control Conference (ACC)*, pages 4689–4694. IEEE, 2015.

[30] F. Ferrante, F. Gouaisbaut, R. Sanfelice, and S. Tarbouriech. $\mathcal{L}_2$ state estimation with guaranteed convergence speed in the presence of sporadic measurements. *IEEE Transactions on Automatic Control*, 64(8):3362–3369, 2019.

[31] A. Festag. Cooperative intelligent transport systems standards in europe. *IEEE Communications Magazine*, 52(12):166–172, 2014.

[32] E. Fridman. A refined input delay approach to sampled-data control. *Automatica*, 46(2):421–427, 2010.

[33] E. Fridman, A. Seuret, and J. Richard. Robust sampled-data stabilization of linear systems: an input delay approach. *Automatica*, 40(8):1441–1446, 2004.

[34] E. Fridman, U. Shaked, and V. Suplin. Input/output delay approach to robust sampled-data $\mathcal{H}_\infty$ control. *Systems & Control Letters*, 54(3):271–282, 2005.

[35] H. Gao and T. Chen. Network-based $\mathcal{H}_\infty$ output tracking control. *IEEE Transactions on Automatic control*, 53(3):655–667, 2008.

[36] S. Gao, A. Lim, and D. Bevly. An empirical study of DSRC V2V performance in truck platooning scenarios. *Digital Communications and Networks*, 2(4):233–244, 2016.

[37] R. Goebel, R. Sanfelice, and Andrew R. Teel. *Hybrid Dynamical Systems: Modeling, Stability, and Robustness*. Princeton University Press, 2012.

[38] J. Gong, Y. Zhao, and Z. Lu. Sampled-data vehicular platoon control with communication delay. *In Proceedings of the Institution of Mechanical Engineers, Part I: Journal of Systems and Control Engineering*, 232(1):39–49, 2018.

[39] L. Guzzella and A. Sciarretta. *Vehicle propulsion systems*, volume 1. Springer, 2007.

[40] A. Hamieh, J. Ben-Othman, and L. Mokdad. Detection of radio interference attacks in VANET. In *Global Telecommunications Conference*, pages 1–5. IEEE, 2009.

[41] Y. Harfouch, S. Yuan, and S. Baldi. An adaptive switched control approach to heterogeneous platooning with intervehicle communication losses. *IEEE Transactions on Control of Network Systems*, 5(3):1434–1444, 2017.

[42] J. K. Hedrick, M. Tomizuka, and P. Varaiya. Control issues in automated highway systems. *IEEE Control Systems*, 14(6):21–32, 1994.

[43] M. Heemels, A. Teel, N. Van de Wouw, and D. Nešić. Networked control systems with communication constraints: Tradeoffs between transmission intervals, delays and performance. *IEEE Transactions on Automatic Control*, 55(8):1781–1796, 2010.

[44] J. Hespanha, P. Naghshtabrizi, and Y. Xu. A survey of recent results in networked control systems. *Proceedings of the IEEE*, 95(1):138–162, 2007.

[45] L. Hetel, J. Daafouz, and C. Iung. Analysis and control of lti and switched systems in digital loops via an event-based modelling. *International Journal of Control*, 81(7):1125–1138, 2008.

[46] L. Hetel, C. Fiter, H. Omran, A. Seuret, E. Fridman, J. Richard, and S. Niculescu. Recent developments on the stability of systems with aperiodic sampling: An overview. *Automatica*, 76:309–335, 2017.

[47] M. Huang and S. Dey. Stability of kalman filtering with markovian packet losses. *Automatica*, 43(4):598–607, 2007.

[48] H. Ito, R. Freeman, and A Chaillet. Revisiting the IISS small-gain theorem through transient plus ISS small-gain regulation. *Asian Journal of Control*, 15(1):11–19, 2013.

[49] X. Jiang, Q. Han, S. Liu, and A. Xue. A new $\mathcal{H}_\infty$ stabilization criterion for networked control systems. *IEEE Transactions on Automatic Control*, 53(4):1025–1032, 2008.

[50] P. Kabamba. Control of linear systems using generalized sampled-data hold functions. *IEEE transactions on Automatic Control*, 32(9):772–783, 1987.

[51] L. Kester, W. van Willigen, and J. De Jongh. Critical headway estimation under uncertainty and non-ideal communication conditions. In *Proceedings of the 17th IEEE International Conference on Intelligent Transportation Systems (ITSC)*, pages 320–327, 2014.

[52] F. Lamnabhi-Lagarrigue, A. Annaswamy, S. Engell, A. Isaksson, P. Khargonekar, R. Murray, H. Nijmeijer, T. Samad, D. Tilbury, and P. Van den Hof. Systems & control for the future of humanity, research agenda: Current and future roles, impact and grand challenges. *Annual Reviews in Control*, 43:1–64, 2017.

[53] D. Lawrence. On output feedback stabilization for linear impulsive systems. In *2012 American Control Conference (ACC)*, pages 5936–5941. IEEE, 2012.

[54] C. Lee, S. Lee, M. Park, and O. Kwon. Stability and stabilization criteria for sampled-data control system via augmented Lyapunov-Krasovskii functionals. *International Journal of Control, Automation and Systems*, 16(5):2290–2302, 2018.

[55] J. Li, H. Yu, W. Liang, P. Zeng, and M. Yuan. A survey of packet disordering existing in networked control systems. In *2015 IEEE International Conference on Cyber Technology in Automation, Control, and Intelligent Systems (CYBER)*, pages 1797–1801, 2015.

[56] J. Li, Q. Zhang, and M. Cai. Modelling and robust stability of networked control systems with packet reordering and long delay. *International Journal of Control*, 82(10):1773–1785, 2009.

[57] S. Li, Y. Zheng, K. Li, and J. Wang. An overview of vehicular platoon control under the four-component framework. In *Proceedings of the IEEE Intelligent Vehicles Symposium*, pages 286–291, 2015.

[58] Y.J. Li. An overview of the DSRC/WAVE technology. In *International Conference on Heterogeneous Networking for Quality, Reliability, Security and Robustness*, pages 544–558. Springer, 2010.

[59] Z. Li, B. Hu, M. Li, and G. Luo. String stability analysis for vehicle platooning under unreliable communication links with event-triggered strategy. *IEEE Transactions on Vehicular Technology*, 68(3):2152–2164, 2019.

[60] X. Liu, A. Goldsmith, S. Mahal, and J. Hedrick. Effects of communication delay on string stability in vehicle platoons. In *Proceedings of the IEEE Intelligent Transportation Systems*, pages 625–630, 2001.

[61] J. Lofberg. Yalmip: A toolbox for modeling and optimization in Matlab. In *International Symposium on Computer Aided Control Systems Design*, pages 284–289. IEEE, 2004.

[62] N. Lu, N. Cheng, N. Zhang, X. Shen, and J. Mark. Connected vehicles: Solutions and challenges. *IEEE Internet of Things Journal*, 1(4):289–299, 2014.

[63] M. Mahmoud. Networked control systems analysis and design: An overview. *Arabian Journal for Science and Engineering*, 41(3):711–758, 2016.

[64] M. Mahmoud, S.Z. Selim, P. Shi, and M.H. Baig. New results on networked control systems with non-stationary packet dropouts. *IET Control Theory & Applications*, 6(15):2442–2452, 2012.

[65] E. Medina and D. Lawrence. Output feedback stabilization for linear impulsive systems. In *Proceedings of the 2010 American Control Conference*, pages 4211–4216. IEEE, 2010.

[66] R. Merco, F. Ferrante, and P. Pisu. DoS-resilient hybrid controller for string-stable connected vehicles. In *Proceedings of the IEEE Intelligent Vehicles Symposium*, 2019.

[67] R. Merco, F. Ferrante, and P. Pisu. Network aware control design for string stabilization in vehicle platoons: An LMI approach. In *Proceedings of the American Control Conference (ACC)*, 2019.

[68] R. Merco, F. Ferrante, and P. Pisu. On DoS resiliency analysis of networked control systems: Trade-off between jamming actions and network delays. *IEEE Control Systems Letters*, 3(3):559–564, 2019.

[69] Z. Mir and F. Filali. LTE and IEEE 802.11p for vehicular networking: a performance evaluation. *EURASIP Journal on Wireless Communications and Networking*, 2014(1):89, 2014.

[70] L. Mirkin. Intermittent redesign of analog controllers via the Youla parameter. *IEEE Transactions on Automatic Control*, 62(4):1838–1851, 2016.

[71] L. Mirkin, H. Rotstein, and Z. Palmor. H^2 and H^∞ design of sampled-data systems using lifting. Part I: General framework and solutions. *SIAM Journal on Control and Optimization*, 38(1):175–196, 1999.

[72] R. Murray, K. Astrom, S. Boyd, R. Brockett, and G. Stein. Future directions in control in an information-rich world. *IEEE Control Systems*, 23(2):20–33, 2003.

[73] X. Na, Y. Zhan, Y. Xia, and J. Dong. Control of networked systems with packet loss and channel uncertainty. *IET Control Theory & Applications*, 10(17):2251–2259, 2016.

[74] P. Naghshtabrizi and J. Hespanha. Stability of networked control systems with variable sampling and delay. In *Proceedings of the Annual Allerton Conference on Communication, Control, and Computing*, 2006.

[75] P. Naghshtabrizi, J. Hespanha, and A. Teel. Exponential stability of impulsive systems with application to uncertain sampled-data systems. *Systems & Control Letters*, 57(5):378–385, 2008.

[76] N. Nahi. Optimal recursive estimation with uncertain observation. *IEEE Transactions on Information Theory*, 15(4):457–462, 1969.

[77] G. Naus, R. Vugts, J. Ploeg, M. Van de Molengraft, and M. Steinbuch. String-stable CACC design and experimental validation: A frequency-domain approach. *IEEE Transactions on Vehicular Technology*, 59(9):4268–4279, 2010.

[78] D. Nešić and A. Teel. Input-output stability properties of networked control systems. *IEEE Transactions on Automatic Control*, 49(10):1650–1667, 2004.

[79] D. Nešić, A. Teel, and D. Carnevale. Explicit computation of the sampling period in emulation of controllers for nonlinear sampled-data systems. *IEEE Transactions on Automatic Control*, 54(3):619–624, 2009.

[80] D. Nešić, A. Teel, G. Valmorbida, and L. Zaccarian. Finite-gain $\mathcal{L}_p$ stability for hybrid dynamical systems. *Automatica*, 49(8):2384–2396, 2013.

[81] S. Noei, A. Sargolzaei, A. Abbaspour, and K. Yen. A decision support system for improving resiliency of cooperative adaptive cruise control systems. *Procedia Computer Science*, 95:489–496, 2016.

[82] S. Öncü, J. Ploeg, N. Van de Wouw, and H. Nijmeijer. Cooperative adaptive cruise control: Network-aware analysis of string stability. *IEEE Transactions on Intelligent Transportation Systems*, 15(4):1527–1537, 2014.

[83] S. Öncü, N. Van de Wouw, M. Heemels, and H. Nijmeijer. String stability of interconnected vehicles under communication constraints. In *Proceedings of the 51st IEEE Conference on Decision and Control (CDC)*, pages 2459–2464, 2012.

[84] F. Pasqualetti, F. Dörfler, and F. Bullo. Attack detection and identification in cyber-physical systems. *IEEE Transactions on Automatic Control*, 58(11):2715–2729, 2013.

[85] J. Ploeg, B. Scheepers, E. Van Nunen, N. Van de Wouw, and H. Nijmeijer. Design and experimental evaluation of cooperative adaptive cruise control. In *Proceedings of the 14th IEEE International Conference on Intelligent Transportation Systems*, pages 260–265, 2011.

[86] J. Ploeg, E. Semsar-Kazerooni, G. Lijster, N. van de Wouw, and H. Nijmeijer. Graceful degradation of cooperative adaptive cruise control. *IEEE Transactions on Intelligent Transportation Systems*, 16(1):488–497, 2014.

[87] J. Ploeg, D. Shukla, N. Van de Wouw, and H. Nijmeijer. Controller synthesis for string stability of vehicle platoons. *IEEE Transactions Intelligent Transportation Systems*, 15(2):854–865, 2014.

[88] J. Ploeg, N. Van De Wouw, and H. Nijmeijer. $\mathcal{L}_p$ string stability of cascaded systems: Application to vehicle platooning. *IEEE Transactions on Control Systems Technology*, 22(2):786–793, 2014.

[89] R. Poisel. *Modern Communications Jamming: Principles and Techniques*. Artech House, 2011.

[90] A. Rayamajhi, Z. A. Biron, R. Merco, P. Pisu, J. M. Westall, and J. Martin. The impact of dedicated short range communication on cooperative adaptive cruise control. In *International Conference on Communications (ICC)*, pages 1–7. IEEE, 2018.

[91] H. Ríos, L. Hetel, and D. Efimov. Robust output-feedback control for uncertain linear sampled-data systems: A 2D impulsive system approach. *Nonlinear Analysis: Hybrid Systems*, 32:177–201, 2019.

[92] A. Sala. Improving performance under sampling-rate variations via generalized hold functions. *IEEE transactions on control systems technology*, 15(4):794–797, 2007.

[93] R. Sanfelice, D. Copp, and P. Nanez. A toolbox for simulation of hybrid systems in Matlab/Simulink: Hybrid equations (HyEQ) toolbox. In *Proceedings of the 16th International Conference on Hybrid Systems:Computation and Control*, pages 101–106. ACM, 2013.

[94] G. Savaia, Z. A. Biron, and P. Pisu. A receding horizon switching control resilient to communication failures for connected vehicles. In *ASME 2017 Dynamic Systems and Control Conference*. American Society of Mechanical Engineers, 2017.

[95] C. Scherer, P. Gahinet, and M. Chilali. Multiobjective output-feedback control via LMI optimization. *IEEE Transactions on Automatic Control*, 42(7):896–911, 1997.

[96] P. Seiler and R. Sengupta. Analysis of communication losses in vehicle control problems. In *Proceedings of the American Control Conference*, volume 2, pages 1491–1496, 2001.

[97] Y. Shen, D. Zhang, and X. Xia. Continuous output feedback stabilization for nonlinear systems based on sampled and delayed output measurements. *International Journal of Robust and Nonlinear Control*, 26(14):3075–3087, 2016.

[98] Y. Shi and B. Yu. Robust mixed $\mathcal{H}_2/\mathcal{H}_\infty$ control of networked control systems with random time delays in both forward and backward communication links. *Automatica*, 47(4):754–760, 2011.

[99] S. Shladover. Automated vehicles for highway operations (automated highway systems). *in Proceedings of the Institution of Mechanical Engineers, Part I: Journal of Systems and Control Engineering*, 219(1):53–75, 2005.

[100] B. Sinopoli, L. Schenato, M. Franceschetti, K. Poolla, M. Jordan, and S. Sastry. Kalman filtering with intermittent observations. *IEEE Transactions on Automatic Control*, 49(9):1453–1464, 2004.

[101] S. Stankovic, M. Stanojevic, and D. Siljak. Decentralized overlapping control of a platoon of vehicles. *IEEE Transactions on Control Systems Technology*, 8(5):816–832, 2000.

[102] J. Sturm. Using SeDuMi 1.02, a Matlab toolbox for optimization over symmetric cones. *Optimization Methods and Software*, 11(1-4):625–653, 1999.

[103] T. Tamba and Y. Nazaruddin. Distributed resilient tracking control of a vehicle platoon under communication imperfection. In *4th International Conference on Electric Vehicular Technology (ICEVT)*, pages 18–23. IEEE, 2017.

[104] R. Tütüncü, K. Toh, and M. Todd. Solving semidefinite-quadratic-linear programs using SDPT3. *Mathematical Programming*, 95(2):189–217, 2003.

[105] B. Van Arem, C. Van Driel, and R. Visser. The impact of cooperative adaptive cruise control on traffic-flow characteristics. *IEEE Transactions on Intelligent Transportation Systems*, 7(4):429–436, 2006.

[106] N. van de Wouw, P. Naghshtabrizi, M. Cloosterman, and J. Hespanha. Tracking control for sampled-data systems with uncertain time-varying sampling intervals and delays. *International Journal of Robust and Nonlinear Control: IFAC-Affiliated Journal*, 20(4):387–411, 2010.

[107] G. Walsh, H. Ye, and L. Bushnell. Stability analysis of networked control systems. *IEEE Transactions On Control Systems Technology*, 10(3):438–446, 2002.

[108] Y. Wang and Q. Han. Modelling and controller design for discrete-time networked control systems with limited channels and data drift. *Information Sciences*, 269:332–348, 2014.

[109] Z. Wang, F. Yang, D. Ho, and X. Liu. Robust $\mathcal{H}_\infty$ control for networked systems with random packet losses. *IEEE Transactions on Systems, Man, and Cybernetics, Part B (Cybernetics)*, 37(4):916–924, 2007.

[110] M. Webb et al. Smart 2020: Enabling the low carbon economy in the information age. *The Climate Group. London*, 1(1):1–1, 2008.

[111] C. Wu, Y. Lin, and A. Eskandarian. Cooperative adaptive cruise control with adaptive kalman filter subject to temporary communication loss. *IEEE Access*, 7:93558–93568, 2019.

[112] Y. Xia, Y. Gao, L. Yan, and M. Fu. Recent progress in networked control systems—a survey. *International Journal of Automation and Computing*, 12(4):343–367, 2015.

[113] W. Xu, K. Ma, W. Trappe, and Y. Zhang. Jamming sensor networks: attack and defense strategies. *IEEE Network*, 20(3):41–47, 2006.

[114] Y. Yuan, Q. Zhu, F. Sun, Q. Wang, and T. Başar. Resilient control of cyber-physical systems against denial-of-service attacks. In *6th International Symposium on Resilient Control Systems (ISRCS)*, pages 54–59, 2013.

[115] D. Yue, Q. Han, and J. Lam. Network-based robust H_∞ control of systems with uncertainty. *Automatica*, 41(6):999–1007, 2005.

[116] D. Yue, Q. Han, and C. Peng. State feedback controller design of networked control systems. In *Proceedings of the 2004 IEEE International Conference on Control Applications*, volume 1, pages 242–247. IEEE, 2004.

[117] L. Zhang, H. Gao, and O. Kaynak. Network-induced constraints in networked control systems—a survey. *IEEE Transactions on Industrial Informatics*, 9(1):403–416, 2013.

[118] L. Zhang, Y. Shi, T. Chen, and B. Huang. A new method for stabilization of networked control systems with random delays. *IEEE Transactions on Automatic Control*, 50(8):1177–1181, 2005.

[119] X. Zhang and Q. Han. Network-based $\mathcal{H}_\infty$ filtering for discrete-time systems. *IEEE Transactions on Signal Processing*, 60(2):956–961, 2012.

[120] X. Zhang, Q. Han, and X. Yu. Survey on recent advances in networked control systems. *IEEE Transactions on Industrial Informatics*, 12(5):1740–1752, 2016.

[121] Y. Zheng, S. E. Li, J. Wang, L. Y. Wang, and K. Li. Influence of information flow topology on closed-loop stability of vehicle platoon with rigid formation. In *17th International IEEE Conference on Intelligent Transportation Systems (ITSC)*, pages 2094–2100. IEEE, 2014.

[122] Y. Zhou, J. Li, L. Lamont, and C. Rabbath. Modeling of packet dropout for UAV wireless communications. In *Computing, Networking and Communications (ICNC), 2012 International Conference on*, pages 677–682. IEEE, 2012.